The ADAP/SKAP55-Module Regulates F-Actin Cytoskeleton Reorganization Through the Interaction with Ena/VASP Proteins in T cells

Dissertation

zur Erlangung des akademischen Grades

doctor rerum naturalium (Dr. rer. nat.)

genehmigt durch die Fakultät für Naturwissenschaften
der Otto-von-Guericke-Universität Magdeburg

von Diplom-Biochemikerin Janine Degen

geb. am 08. August 1984 in Magdeburg

Gutachter: Dr. Stefanie Kliche
Prof. Dr. Theresia Stradal

eingereicht am: 11. Mai 2020
verteidigt am: 03. Dezember 2020

Table of Contents

Summary

The integrin leukocyte function associated antigen (LFA-1) mediates chemokine C-C motif ligand 21 (CCL21)-induced adhesion and migration of T cells on entry into secondary lymphoid organs (SLOs). Within the SLOs, LFA-1 mediates the interaction of T cells with antigen-presenting cells (APCs). These processes are essential for the participation of T cells in the adaptive immune response. T-cell receptor (TCR) and chemokine triggering lead to the activation of signaling pathways termed '*inside-out*' *signaling,* which induce changes in the conformation of integrins. This enables LFA-1 to bind its respective ligand, the intercellular adhesion molecule-1 (ICAM-1) (affinity regulation). The activation of LFA-1 leads to the formation of integrin clusters (avidity regulation), which are probably regulated by the actin cytoskeleton. The ADAP/SKAP55-module plays a key role in LFA-1 activation, T-cell adhesion, and migration in response to chemokine and TCR stimuli *ex vivo*. In the first part of my thesis, I analyzed whether the ADAP/SKAP55-module is required for T-cell adhesion and migration *in vivo*. The results obtained show that the ADAP/SKAP55- module is crucial for T-cell homing and the stable interaction of T cells with the endothelium of blood venules. The analysis of ADAP$^{-/-}$ T cells on primary endothelial cells under shear flow *ex vivo* revealed an attenuated detachment and crawling on the endothelium. Moreover, ADAP$^{-/-}$ T cells are less polarized, which correlates with a reduced F-actin polymerization and enhanced F-actin depolymerization during chemokine stimulation, indicating that this module regulates F-actin cytoskeleton remodeling. These defects may explain the reduced homing capacity of ADAP$^{-/-}$ T cells to SLOs. The molecular basis of how the ADAP/SKAP55-module modulates the F-actin cytoskeleton is not fully understood, and this question is addressed in the second part of my thesis. T cells express two of the three members of the Ena/VASP proteins, Evl-I and VASP, which are both regulators of the actin cytoskeleton. These Ena/VASP proteins are known to interact with ADAP and RIAM, the interaction partners of SKAP55. Immunoprecipitation studies confirmed that ADAP and RIAM are linked to Ena/VASP proteins. To analyze the functional relevance of Evl-I and VASP, I established a shRNA-mediated knockdown in Jurkat T cells. Here, I found that both Evl-I and VASP are responsible for TCR-mediated F-actin polymerization and lamellipodia formation. The absence of Ena/VASP proteins led to increase LFA-1-mediated adhesion upon TCR stimulation, although the interaction of T-cell/APC was diminished, indicating an integrin-independent but more actin cytoskeleton-dependent function of these proteins for T-cell conjugation with APCs. In contrast to the TCR-mediated function, chemokine-mediated F-actin remodeling was reduced, while chemokine-mediated adhesion and migration were not impaired. This suggests different functional properties of Ena/VASP proteins in TCR- and chemokine-mediated signaling processes.

Zusammenfassung

Für die Teilnahme von T-Zellen an der adaptiven Immunantwort reguliert das Integrin *leukocyte function associated antigen* (LFA-1) die über das Chemokin C-C motif ligand 21 (CCL21)-vermittelte Adhäsion und Migration von Lymphozyten. Dies ermöglicht ihnen die Einwanderung in die sekundären lymphatischen Organe wie der Milz oder den Lymphknoten. In der Milz und im Lymphknoten reguliert LFA-1 die Interaktion von T-Zellen mit antigenpräsentierenden Zellen (APZ). Die Stimulation von T-Zellen über den T-Zell-Rezeptor (TZR) und Chemokinrezeptor bewirkt die Aktivierung von Signalwegen, die eine Veränderung der Integrinkonformation hervorrufen (*inside-out signaling*). Dadurch kann LFA-1 an seinem Liganden das *intercellular adhesion molecule-1* (ICAM-1) binden (Affinitätsregulierung). Nach der Aktivierung kommt es zur Bildung von Integrinclustern (Aviditätsregulierung), welche vermutlich über das Aktinzytoskelett reguliert werden. Nach Stimulation des TZRs sowie des Chemokinrezeptors CCR7 spielt das ADAP/SKAP55-Modul eine entscheidende Rolle bei der Aktivierung von LFA-1 und ist an Adhäsions- und Migrationsprozessen in T-Zellen *ex vivo* beteiligt. Im ersten Teil meiner Arbeit untersuchte ich die funktionelle Relevanz des ADAP/SKAP55-Moduls bei der Adhäsion und Migration von T-Zellen *in vivo*. ADAP$^{-/-}$ T-Zellen zeigten eine verminderte Wanderung in die sekundären lymphatischen Organe. Mit Hilfe der 2-Photon-Mikroskopie konnte gezeigt werden, dass das ADAP/SKAP55-Modul für die stabile Interaktion der T-Zelle mit dem Blutgefäßendothel verantwortlich ist. In *ex vivo* Experimenten zeigten ADAP$^{-/-}$ T-Zellen ein vermehrtes Ablösen und ein gestörtes Laufverhalten auf primären murinen Endothelzellen unter Durchflussbedingungen. Ferner wurde beobachtet, dass ADAP$^{-/-}$ T-Zellen weniger polarisiert sind, was vermutlich darauf zurückzuführen ist, dass das ADAP/SKAP55-Modul das Aktinzytoskelett beeinflusst. Weitere Untersuchungen ergaben, dass der Verlust von ADAP nach Chemokinstimulation zu einer verminderten F-Aktin-Polymerisierung bzw. zu einer verstärkten Depolymerisierung führte. Diese Defekte sind vermutlich dafür verantwortlich, dass ADAP$^{-/-}$ T-Zellen mit einer zeitlichen Verzögerung in Milz und Lymphknoten einwandern.

Die molekularen Mechanismen wie das ADAP/SKAP55-Modul das F-Aktinzytoskelett moduliert sind unklar und wurden im zweiten Teil meiner Dissertation untersucht. In T-Zellen werden zwei der drei Mitglieder der Ena/VASP-Familie exprimiert, Evl-I und VASP. Ena/VASP-Proteine sind dafür bekannt, dass sie das Aktinzytoskelett modulieren. Ebenfalls konnte gezeigt werden, dass Evl-I und VASP mit ADAP und RIAM, dem Interaktionspartner von SKAP55, interagieren. In Immunpräzipitationsstudien konnte die Bindung von ADAP und RIAM an Evl-I und VASP verifiziert werden. Um die funktionellen Konsequenzen von Evl-I und VASP in Jurkat T-Zellen zu analysieren, etablierte ich eine shRNA-vermittelte Reduktion der Expression dieser Proteine. Mit Hilfe dieses shRNA basierten *knockdowns* von Evl-I und

VASP konnte ich zeigen, dass diese Proteine an der TZR-vermittelte F-Aktin-Polymerisierung und Lamellipodiaformation beteiligt sind. Darüber hinaus führte die Reduktion der Expression von Ena/VASP-Proteinen zu einer gesteigerten LFA-1-vermittelten Adhäsion nach TZR Stimulation. Im Gegensatz zur erhöhten TZR-vermittelten Adhäsion war die Interaktion der Ena/VASP-defizienten Jurkat T-Zellen mit Superantigen-beladenen Raji B-Zellen stark vermindert, was auf eine Integrin-unabhängige, aber Aktin-regulierende Funktion dieser Proteine bei der Interaktion von T-Zellen mit B Zellen hindeutet. Ebenso konnte eine verminderte F-Aktin-Polymerisierung nach Chemokinstimulation nachgewiesen werden, wohingegen die Chemokin-vermittelte Adhäsion und Migration nicht beeinflusst war. Diese Ergebnisse lassen vermuten, dass Ena/VASP-Proteine verschiedene Funktionen bei Signalwegen der TZR- und Chemokin-vermittelten Adhäsion und Migration ausüben.

1 Introduction

1.1 The Immune System

The main function of the immune system is to protect mammalian organisms against the invasion of pathogens such as toxins, bacteria, fungi, or viruses from the environment and against infected or tumor cells inside of the body. During evolution, the innate and adaptive immune systems developed various humoral and cellular components. The innate immunity begins to fight pathogens immediately after pathogen entry into the body. During the innate immune response, cell components like macrophages engulf and digest the pathogens and present foreign antigens on their cell surface. They also release cytokines and chemokines to attract and activate monocytes and neutrophils to fight the pathogens. In addition, complement factors help to combat the pathogens. If the innate immune response does not succeed in eliminating the pathogens, the second line of defense – the adaptive immunity – is activated and specifically recognizes the pathogens. Moreover, the adaptive immunity provides improved protection against reinfection through the formation of an immunological memory. Humoral and cellular components of the adaptive immunity include antibodies, chemokines, and cytokines released by B and T lymphocytes. T-cell activation occurs in secondary lymphoid organs (SLOs), like the spleen and lymph nodes. Thereby, dendritic cells (DCs) capture, process, and present antigens to T cells, leading to effector cell differentiation of T cells (Chaplin, 2006; Griffiths, 1995).

1.2 T Lymphocyte

Before T cells fulfill their effector functions, they mature in the thymus from precursor cells that migrate from the bone marrow through the blood into the thymus (Ward and Marelli-Berg, 2009). After their thymic selection and maturation (Germain, 2002; Starr et al., 2003), naïve (has not encountered cognate peptide) single-positive ($CD4^+$ or $CD8^+$) T cells leave the thymus and navigate into SLOs, such as lymph nodes or the spleen. Here $CD4^+$ T cells recognize foreign peptides presented by major histocompatibility complex (MHC) class II molecules expressed on antigen-presenting cells (APCs), like DCs. Depending on the cytokine milieu, $CD4^+$ T cells can differentiate into several subsets of helper T (TH) lymphocytes, like TH1, TH2, TH17, or regulatory T cells (Tregs) (Zhu and Paul, 2010; Zhu et al., 2010). TH1 cells, which express interferon-γ (IFN-γ), are essential in protecting the organism against intracellular viruses and bacteria. TH2 cells are important for the defense against extracellular pathogens (e.g. helminths) and produce Interleukin 4 (IL-4), IL-5, and IL-13. TH17 cells are characterized by the production of IL-17 and control extracellular bacteria and fungi. The fourth T cell subtypes, Tregs can either differentiate from peripheral

naïve $CD4^+$ T cells (induced Treg; iTreg) or develop in the thymus (thymic derived Treg; tTreg). In contrast to other TH subtypes, which promote immune responses, Tregs are immune suppressive (von Boehmer, 2005; Ohkura et al., 2013). In contrast to $CD4^+$ T cells, $CD8^+$ cytotoxic T cells recognize antigens presented by MHC class I molecules, which are expressed by all nucleated cells. These cells possess cytotoxic activity and directly kill infected cells through the release of soluble factors such as perforin and granzyme B. These factors form pores in the plasma membrane and induce apoptosis of targeted cells (Griffiths, 1995).

1.2.1 T-lymphocyte homing into secondary lymphoid organs

To enter the lymph node, T cells must pass through high endothelial venules (HEVs), which are abundant in lymph nodes with the exception of the spleen (Girard and Springer, 1995). The first contact between a T cell and the vascular endothelium is facilitated by selectins such as CD62L that bind to glycoproteins (peripheral lymph node addressin (PNAd) expressed on endothelial cells. This interaction induces tethering and rolling via the endothelium (**Fig. 1, Step I**) (Lawrence et al., 1997). Thus, T cells become slower and adhere firmly to the endothelium through the interaction of integrins (leukocyte function associated antigen-1 (LFA-1)) with extracellular matrix adhesion molecules (intercellular adhesion molecule-1 (ICAM-1)) (**Fig. 1, Step II**) (Hogg et al., 2011). Segregation of the chemokine C-C motif ligand 21 (CCL21) by the endothelium initiates the G-protein-coupled receptor-mediated integrin activation of T cells (Hogg et al., 2011; Schmidt et al., 2012). Thereby, CCL21 binds to the C-C chemokine receptor type 7 (CCR7), which facilitates polarization and migration of T cells on the endothelial surface and transmigration through the endothelium (Schmidt et al., 2012). This transmigration depends on LFA-1-mediated interaction with the endothelium and the actin cytoskeleton reorganization regulating the T-cell shape (**Fig. 1, Steps III and IV**) (Burkhardt et al., 2008; Hogg et al., 2011). The migration of T cells into the underlying tissue requires the remodeling of the actin cytoskeleton to form a uropod and a leading edge (**Fig. 1, Step V**) (Burkhardt et al., 2008). After entry into the lymph node, T cells predominantly located in the T-cell zone (Worbs et al., 2008). The interaction with APCs leads to the formation of a narrow contact zone between T cell and APC, which is mediated by actin cytoskeleton reorganization and LFA-1 activation (**Fig. 1, Step VI**). This structure is called immunological synapse (IS) (Burkhardt et al., 2008; Hogg et al., 2011).

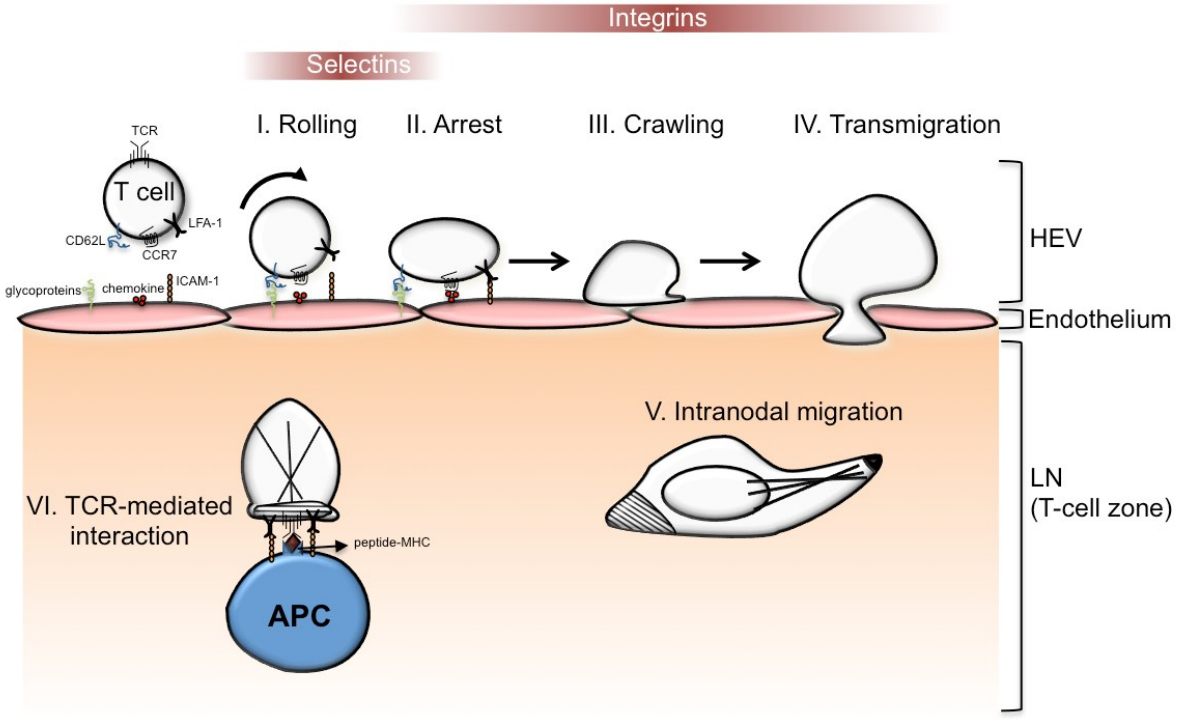

Figure 1: T-cell extravasation into secondary lymphoid organs (SLOs). Naïve T cells express several molecules required for the homing of lymphocytes into secondary lymphoid organs (SLOs), such as the chemokine receptor CCR7, the leukocyte function-associated antigen-1 (LFA-1), and L-selectin (CD62L). The interaction of CD62L with its ligands expressed on the high endothelial venules (HEVs) induces rolling of the T cells (**Step I**). This process slows down the T cell, enabling activation of the C-C chemokine receptor type 7 (CCR7) by chemokines presented on the endothelium. The chemokine-bound CCR7 induces the activation of the integrin LFA-1 to mediate interaction with its ligand the intercellular adhesion molecule-1 (ICAM-1). This interaction allows the T cell to firmly adhere (**Step II**) and to polarize on the endothelium (**Step III**). The T cell forms actin-based structures like a leading edge and a uropod that mediate T-cell crawling (**Step III**) and transmigration through the endothelium (**Step IV**). After migration into the T-cell zone of the lymph node, the T cell starts screening for antigen-presenting cells (APCs) (**Step V**). The firm contact of the T cell with an APC is mediated by the interaction of the T-cell receptor (TCR) with the peptide-bound major histocompatibility complex (TCR-pMHC) and LFA-1 with ICAM-1. These interactions lead to the formation of the immunological synapse (IS) and recruitment of actin and LFA-1 into IS (**Step VI**) (Burkhardt et al., 2008; Hogg et al., 2011; Schmidt et al., 2012).

1.3 Cytoskeletal Remodeling and Integrins

T-cell homing and activation require coordinated cellular processes that lead to adhesion, polarization, crawling, migration, and interaction with APCs. These processes crucially depend on the actin cytoskeleton and integrins (Burkhardt et al., 2008; Hogg et al., 2011).

1.3.1 Cytoskeletal remodeling

TCR and chemokine receptor initiate cytoskeleton remodeling, which induces morphologic cues crucial for T-cell migration and the formation of the IS. The forward protrusion of the cell front is the first step in T-cell crawling. T cells form a leading edge, the front of a crawling T cell, and a uropod that trails behind (**Fig. 2A**). The leading edge is a highly dynamic, actin-rich structure of a thin-layer membrane protrusion called lamellipodium. Due to their high dynamics, lamellipodia adhere weakly to the substratum, allowing the T cell to change its

direction of movement quickly. Lamellipodial structures have also been involved in stable interactions like the IS, the interface between a T cell and an APC (Chhabra and Higgs, 2007). The accumulation of actin filaments in the IS supports further TCR-pMHC interactions and adhesion mediated by the integrin LFA-1. The IS has a bulls-eye structure with a central, peripheral, and distal supramolecular activation cluster (cSMAC, pSMAC, dSMAC) (**Fig. 2B**). The dSMAC is where proteins with large ectodomains are located, like the tyrosine-protein phosphatase CD45. The components of the cSMAC are key molecules for T-cell signaling, such as the TCR. In contrast, the pSMAC consists of actin and the integrin LFA-1 (Gomez and Billadeau, 2008; Yokosuka and Saito, 2010) (**Fig. 2B**). Actin filaments help to shape the IS and maintain the final bulls-eye structure of the IS. The centripetally retrograde flow is initiated by actin polymerization at the rim below the plasma membrane. Newly synthesized actin filaments shuttle signaling molecules such as the TCR to the center of the actin-depleted cSMAC, whereas LFA-1 moves to the edge of the cSMAC (Kaizuka et al., 2007).

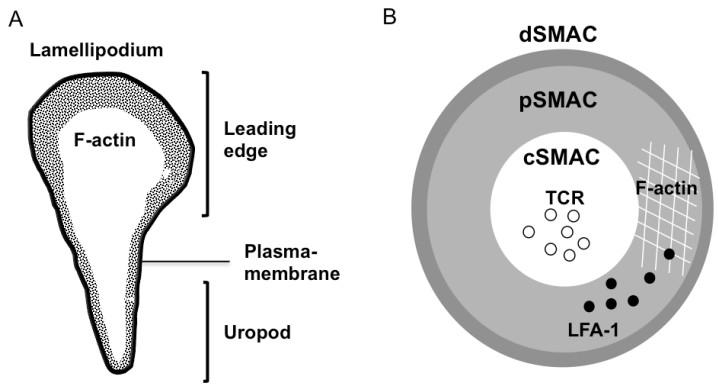

Figure 2: Schematic representation of a polarized T cell and an immunological synapse. **(A)** The leading edge with the actin-rich lamellipodium lies in front of a migrating T cell, whereas the uropod trails behind. **(B)** Front view of the immunological synapse with the typical bullseye structure. The central supramolecular activation cluster (cSMAC) is enriched with signaling molecules such as the T cell receptor (TCR). In contrast, leukocyte function associated antigen 1 (LFA-1) and actin filaments are localized in the peripheral SMAC (pSMAC). The distal supramolecular activation cluster (dSMAC) contains the tyrosine-protein phosphatase CD45. Adapted and modified from Stradal et al., 2006.

The actin cytoskeleton regulates cell morphology by forming highly dynamic actin filaments. Actin exists in two forms, (1) globular, monomeric (G) actin and (2) filamentous, polymeric (F) actin. Actin filaments are characterized by a fast-growing barbed end (+ end), which ATP-bound G-actin associates, and a pointed end (- end) that is relatively inert and slow-growing. Various actin-binding proteins control F-actin polymerization or depolymerization, branch formation, anchoring to membranes and membrane proteins, and cell protrusions such as lamellipodia and filopodia (Winder and Ayscough, 2005).

Signaling processes, which mediate F-actin polymerization or depolymerization are regulated by actin-severing (e.g. cofilin), actin-capping (e.g. gelsolin), actin-regulatory (e.g. Wiskott-

Aldrich syndrome protein (WASP) and WASP verprolin homologous (WAVE)) and actin-nucleating proteins (e.g. actin-related protein 2/3 (Arp2/3) complex). Actin severing proteins cleave F-actin, thereby providing G-actin for new F-actin filament growth. Actin-capping proteins bind to the barbed end of F-actin to prevent actin polymerization. Actin-regulatory proteins modulate actin dynamics through their association with F-actin. Actin-nucleating proteins facilitate actin nucleation through binding either the barbed or pointed end of F-actin in combination with their binding to G-actin or G-actin/profilin complexes (Burkhardt et al., 2008; Dupré et al., 2015; Samstag et al., 2003).

1.3.2 Integrins

Integrins are heterodimeric transmembrane receptors consisting of a α-subunit and a β-subunit. Mammals express 18 α-subunits and eight β-subunits and allow the formation of at least 25 integrins (**Fig. 3**) (Hogg et al., 2011).

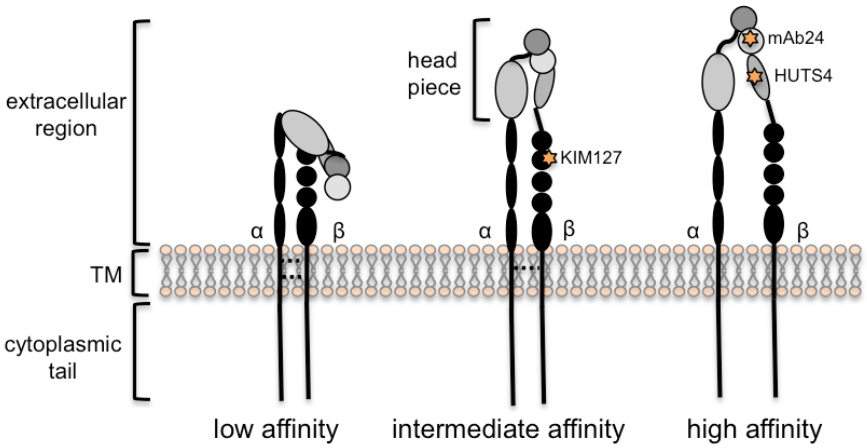

Figure 3: Different conformations of integrins. Three different conformations of integrins can be distinguished by their binding affinity for their ligands. On resting T cells, integrins like leukocyte function-associated antigen-1 (LFA-1) and very late antigen-4 (VLA-4) are in a bent conformation with low affinity to their ligands. The headpiece is near the plasma membrane, and the cytoplasmic tails are close to each other (**left**). *Inside-out signaling* induces a conformational change of the headpiece to mediate the intermediate affinities for their ligands (**center)**. The fully activated integrin has an open headpiece to allow high affinity binding to its ligand (**right**). The cytoplasmic tails and the transmembrane domain (TM) with inner and outer membrane clasps' (dotted lines) are close together in the low-affinity form of the integrin **(left**). While the inner 'membrane clasp' is interrupted in the intermediate-affinity form of the integrin (**middle**), both 'membrane clasps' are broken in the high-affinity form of the integrin (**right**). The two subunits can separate from each other, and the β-subunit is angled. The different integrin conformations are recognized by monoclonal antibodies (mAbs). The LFA-1-specific mAb KIM127 detects the intermediate conformation of the human β2-chain (**center**). In contrast, mAb24 and HUTS4 detect epitopes only accessible in the high-affinity status of LFA-1 and VLA-4 (**right**). The positions of LFA-1 and VLA-4 conformation-sensitive epitopes for KIM127, mAb24, and HUTS4 are indicated by stars. Adapted and modified from Hogg et al., 2011.

T cells express LFA-1 (αLβ2 or CD11a/CD18) and the very late antigen-4 (VLA-4, α4β1 or CD49d/CD29) (Kinashi, 2005). The intercellular adhesion molecule-1, -2, -3, -4 and -5 (ICAM-1-5) (Tan, 2012) are the ligands of LFA-1. Binding of LFA-1 to its ligands is necessary for T-cell adhesion on HEVs, crawling, migration into LNs and T-cell interactions with APCs. The vascular cell adhesion molecule-1 (VCAM-1) and the extracellular matrix protein

fibronectin are bound by VLA-4 (Kinashi 2005). Ligand binding by VLA-4 is required for T-cell adhesion to the extracellular matrix and migration of T cells to sites of inflammation (Yang and Hagmann, 2003; Zhang and Wang, 2012).

On resting T cells, both LFA-1 and VLA-4 are expressed in a bent conformation with the headpieces close to the plasma membrane and the cytoplasmic tails near each other. In this conformation, the affinity to its ligands is low (**Fig. 3, left**). Stimulation of chemokine receptors (e.g., CXCR4 or CCR7) or engagement of the TCR by peptide/MHC I or II induces a switch from an inactive to an active integrin conformation ('*inside-out signaling'* (Kinashi, 2005)). The interaction of various adapter proteins with the cytoplasmic tail of integrins leads to an extended conformation with close headpiece for intermediate ligand affinity (**Fig. 3, center**) (Hogg et al., 2011). Binding of the ligand to the intermediate affinity state induces the fully activated integrin with an open headpiece and comparatively distant cytoplasmic tails, which represents the high affinity state (**Fig. 3, right**) (Hogg et al., 2011; Tan, 2012).

Monoclonal antibodies (mAbs) have been generated to investigate the conformational changes of human LFA-1. KIM127 identifies a β2-epitope that is exposed when LFA-1 extends, whereas mAb24 recognizes an epitope in the headpiece that is only accessible when LFA-1 is in the high-affinity conformation (Hogg et al., 2011). The mAb HUTS4 recognizes an epitope similar to mAb24 when the human VLA-4 is in its activated conformation (**Fig. 2, right**) (Mould et al., 2003).

Furthermore, integrins form clusters (avidity regulation) probably due to their lateral mobility, which is believed to depend on the remodeling of the actin cytoskeleton (Kinashi, 2005). The avidity regulation of integrins increases ligand binding and strengthens the attachment of T cells to the endothelium or with APCs (Hogg et al., 2011; Zhang and Wang, 2012)**.** Ligand bound integrins promote co-stimulatory signals into the cell (termed '*outside-in signaling*') to induce adhesion, polarization, migration, survival, differentiation, and proliferation of T cells (Hynes, 2002; Kinashi, 2005; Tan, 2012). By the conversion of intracellular (from TCR or chemokine receptors) and extracellular (from ligand binding) stimuli, integrins facilitate bi-directional signaling, which is required for T-cell activation (Hynes, 2002).

Mutations in the human LFA-1 gene are associated with a rare human immunodeficiency termed leukocyte adhesion deficiency type I (LAD-I). These mutations lead to a reduction or complete absence of LFA-1 expression on leukocytes, which cause recurrent severe bacterial and fungal infections and impaired wound healing. Due to the impaired LFA-1 expression, leukocytes do not migrate from the blood into inflamed tissue, which is a crucial

event during host defense against foreign pathogens (Hanna and Etzioni, 2012). To date, two anti-integrin antibodies are used as therapeutics to block either the α-subunit (CD11a) of LFA-1 (Efalizumab) or the α-subunit (CD49d) of VLA-4 (Natalizumab). Efalizumab and Natalizumab are used for the treatment of psoriasis and multiple sclerosis, respectively (Kitchens et al., 2011). Given the importance of integrins for T cell function, I will subsequently describe the molecular events that occur during LFA-1 activation.

1.3.3 Integrin activation

Key molecules in LFA-1 activation upon TCR or chemokine receptor stimulation are Talin1, Kindlin-3, the GTPase Ras proximity 1 (Rap1), Rap1 interacting adapter molecule (RIAM), regulator for cell adhesion and polarization enriched in lymphoid tissues (RAPL), and mammalian sterile20-like kinase 1 (Mst1) (Hogg et al., 2011; Kinashi, 2005).

FERM domain-containing proteins: Talin and Kindlin-3

The FERM (4.1 protein, ezrin, radixin, moesin) domain-containing protein Talin exists in vertebrates in two isoforms termed Talin1 and Talin2 (Monkley et al., 2001). Talin1 is expressed ubiquitously and Talin2 is highly expressed in the brain and striated muscle (Monkley et al., 2001). Talin1 consists of an N-terminal head domain and a C-terminal flexible rod domain. The N-terminal FERM domain binds to the cytoplasmic domain of the integrin β-chain and actin. However, the rod domain interacts with RIAM, and contains two additional integrin-binding site for the cytoplasmic domain of the β-chain (Klapholz and Brown, 2017) (**Fig. 4A**). In addition, the C-terminal I/LWEQ motif of Talin1 mediates dimerization and represents a direct binding site to F-actin (Senetar et al., 2004; Smith & McCann, 2007) (**Fig. 4A**). In T lymphocytes, Talin1 is required for TCR-mediated adhesion, LFA-1 and VLA-4 affinity and clustering, T-cell interaction with APCs, and F-actin stabilization at the IS (Alon et al., 2005; Manevich et al., 2007; Simonson et al., 2006; Wernimont et al., 2011). In addition Talin1 deficiency in T cells leads to impaired homing into lymph nodes *in vivo* and random migration on ICAM-1 *ex vivo* (Smith et al., 2005).

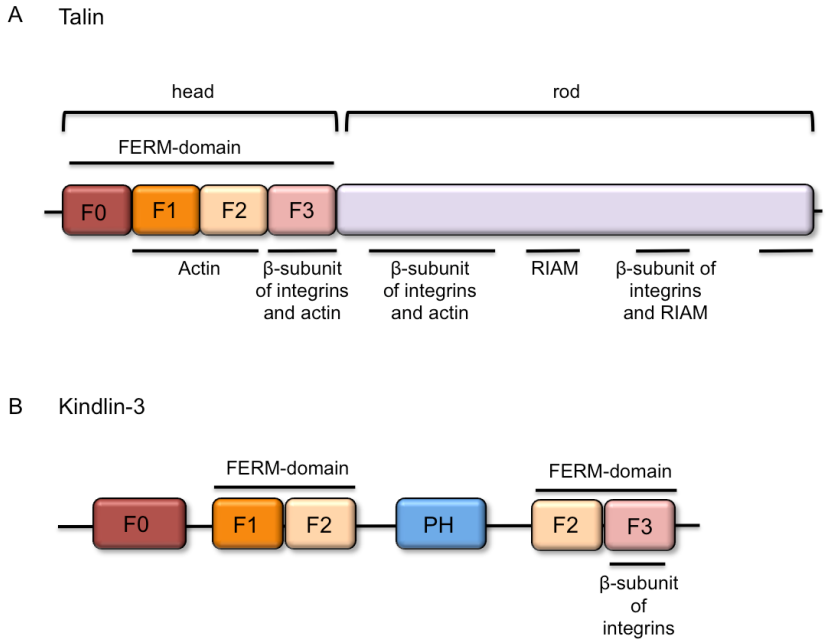

Figure 4: Structure of Talin and Kindlin-3. (A) The FERM (4.1 protein, ezrin, radixin, moesin) domain-containing protein Talin consists of an N-terminal head and a C-terminal rod. The head contains the FERM domain, which is devidid into four subdomains F0, F1, F2, and F3. The F1, F2, and F3 domains bind to actin. The F3 domain has an additional binding site for the cytoplasmic domain of the β-subunit of integrins. The rod contains additional binding site for the β-subunit of integrins, RIAM and F-actin. (**B**) Kindlin-3 possesses a FERM domain. A pleckstrin homology (PH) domain is inserted into the F2 and F3 subdomains. The F3 domain contains the binding site for the cytoplasmic domain of the β-subunit of integrins. (Calderwood et al., 2013; Critchley and Gingras, 2008; Karaköse et al., 2010; Malinin et al., 2010).

The second FERM domain-containing protein is Kindlin. It is named after the gene mutated in the Kindler syndrome, a rare skin blistering disease (Kindler, 1954). Three Kindlin isoforms are expressed in mammals: Kindlin-1 (epithelial cells), Kindlin-2 (most tissues, high in smooth and skeletal muscle) and Kindlin-3 (hematopoietic cells) (Jobard et al., 2003; Siegel et al., 2003; Ussar et al., 2006). Kindlin-3 possesses a FERM domain that is disrupted by a pleckstrin-homology (PH) domain. This PH domain is required for lipid binding at the plasma membrane (Malinin et al., 2010; Hart et al., 2013) (**Fig. 4B**). The F3 domain contains the binding site for the cytoplasmic domain of the β-subunit of integrins. Kindlin-3 interacts directly with the β1-, β2- and β3-subunit of integrins, facilitating the conformational induced shift of integrins from the low- to the high-affinity state (Kloeker et al., 2004; Moser et al., 2008, 2009). Harburger and colleagues showed that Kindlin-3 is required for Talin-integrin interaction, which induces integrin activation. It is based on the finding that overexpression of the Talin head domain and simultaneous knockdown of Kindlin-3 failed to increase integrin affinity (Harburger et al., 2009). In contrast, Lefort and colleagues showed that Talin1 is required for LFA-1 extension, leading to the intermediate affinity conformation of LFA-1, while both Talin1 and Kindlin-3 are required for the induction of the high-affinity conformation of LFA-1 (Lefort et al., 2012). However, whether Kindlin-3 and Talin bind simultaneously or

sequentially to the β2-subunit of LFA-1 to promote its activation clearly requires further investigations.

Mutations in *Kindlin3* lead to leukocyte adhesion deficiency type III (LAD-III). Patients suffering from LAD-III have severe defects in integrin activation of leukocytes and platelets. These defects in integrin activation leads to a strong bleeding tendency, poor wound healing, and recurrent infections similar to patients with LAD-I (Kuijpers et al., 2007, 2009; Malinin et al., 2009; Mory et al., 2008; Svensson et al., 2009).

The GTPase Rap1 and Rap1 effector proteins

Research over the last ten years has shown that Rap1 is mandatory for the activation of integrins upon TCR and chemokine receptor stimulation (Katagiri et al., 2002; Shimonaka et al., 2003; Bos et al., 2003). Rap1 is a Ras-related small GTPase that alternates between an inactive GDP-bound and an active GTP-bound form (Bos 2005). In resting T cells Rap1 co-localizes with endomembranes. Upon TCR stimulation Rap1 is transported to the plasma membrane to promote T-cell adhesion (Bivona et al*.,* 2004). Rap1 regulates LFA-1 and VLA-4 affinity and avidity regulation (Bertoni et al., 2002; Sebzda et al., 2002). In primary T lymphocytes, overexpression of constitutive active Rap1 (Rap1V12) increases the adhesion of LFA-1 and VLA-4 and spontaneous LFA-1 clustering (Sebzda et al., 2002). The analysis of dominant-negative Rap1 (Rap1N17) confirmed that Rap1 is mandatory for integrin activation in T cells. Rap1N17 expression in T cells blocks LFA-1 activation and abrogates LFA-1-ICAM-1-mediated interactions with antigen-pulsed APCs (Katagiri et al., 2000, 2002). In addition to TCR signaling, lymphocytes expressing Rap1V12 showed increased random migration on ICAM-1- and VCAM-1-coated cover slides and migrate through endothelial cells under shear flow in the absence of chemokines *ex vivo* (Shimonaka et al., 2003). Moreover, T cells from $Rap1^{-/-}$ mice show a diminished adhesive capacity for ICAM-1 and fibronectin *ex vivo* (Duchniewicz et al., 2006; Su et al., 2015) and reduced T-cell homing *in vivo* (Ishihara et al., 2015)

The molecular mechanisms by which Rap1 regulates the processes described above in T lymphocytes are not fully understood. Several years ago, studies identified two effector molecules that bind to GTP-loaded Rap1, namely RAPL and RIAM (Katagiri et al., 2003; Lafuente et al., 2004).

RAPL and RIAM

RAPL is predominantly expressed in lymphoid tissue and contains a central Rap1-binding domain (RBD) (**Fig. 5A**). Katagiri *et al.* showed that RAPL directly binds to the α-subunit of

LFA-1 (Katagiri et al., 2003). Gain-of-function and loss-of-function analysis revealed that RAPL is required for targeting activated Rap1 to the plasma membrane (Katagiri et al., 2003, 2006) to regulate TCR-mediated LFA-1 activation (Katagiri et al., 2006, 2009; Zhou et al., 2008). In addition to TCR signaling RAPL$^{-/-}$ T cells exhibit impaired chemokine-mediated adhesion to ICAM-1 and VCAM-1 as well as reduced polarization and motility *ex vivo* (Katagiri and Kinashi, 2011; Katagiri et al., 2003, 2004). The defects in chemokine-induced adhesion of RAPL$^{-/-}$ T cells might account for the impaired homing of RAPL$^{-/-}$ T lymphocytes to the spleen and lymph nodes *in vivo* (Katagiri et al., 2004).

RAPL interacts with the mammalian Ste20-like kinase 1 (Mst1) in T cells. Mst1 suppression or overexpression in T cells showed that Mst1 is required for TCR and chemokine-mediated adhesion and T-cell polarization *ex vivo* (Katagiri et al., 2006, 2009). The defective phenotype of integrin activation of RAPL$^{-/-}$ in T cells is comparable with Mst1 deficiency in T cells. Kinashi and colleagues showed that Mst1$^{-/-}$ T cells attenuate homing to the spleen and lymph nodes *in vivo*. These cells display reduced chemokine-mediated adhesion to ICAM-1 and VCAM-1, and reduced chemokine-mediated LFA-1 clustering *ex vivo* (Katagiri et al., 2006, 2009).

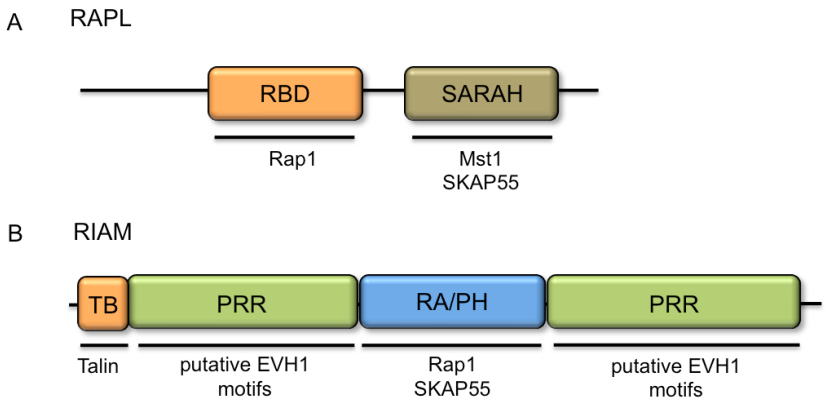

Figure 5: Structure of RAPL and RIAM. (A) RAPL comprises an N-terminal Ras-binding domain (RBD) that mediates the binding to Rap1. The C-terminal Sav/Rassf/Hpo domain (SARAH) binds to Mst1 and the Src kinase-associated adapter protein of 55 kDa (SKAP55) (Katagiri et al., 2003; Raab et al., 2010). (**B**) RIAM contains an N- and C-terminal proline-rich domain (PRR), an N-terminal Talin-binding (TB) site, and a Ras-association-domain/pleckstrin homology (RA/PH) tandem. The PRR domain at the N- and C-terminus comprises putative Ena/VASP-homology 1 (EVH1)-binding sites. In addition, the C-terminal PRR domain binds to Profilin. The RA/PH domain interacts with activated Rap1 (GTP-loaded) and SKAP55 (Coló et al., 2012).

RIAM includes a Ras-association-domain/pleckstrin-homology-domain tandem (RA/PH tandem) flanked by N- and C-terminal proline-rich regions (PRR) (Coló et al., 2012). It has been shown that the RA/PH tandem interacts with activated Rap1 and the Src kinase-associated adapter protein of 55 kDa (SKAP55) (Lafuente et al., 2004; Ménasché et al., 2007). The N-terminal proline-rich region (PRR) comprises a Talin-binding (TB) region and two putative Ena-VASP-homology 1 (EVH1)-binding sites whereas the C-terminal PRR

contains five EVH1-binding sites and five profilin-binding regions (Coló et al., 2012; Lee et al., 2009) (**Fig. 5B**).

Suppression and overexpression studies showed that RIAM regulates TCR-mediated LFA-1 and VLA-4 activation in Jurkat T cells. Overexpression studies of RIAM demonstrated that this Rap1 interacting adapter molecule (like RAPL) facilitates the transport of Rap1 to the plasma membrane (Lafuente et al., 2004). $RIAM^{-/-}$ T cells showed reduced TCR- and chemokine-mediated adhesion to ICAM-1 and VCAM in a static and shear flow adhesion assay *ex vivo* (Klapproth et al., 2015). Similar to $RAPL^{-/-}$ T cells, the homing of $RIAM^{-/-}$ T cells is dramatically reduced in lymph nodes, but in contrast to $RAPL^{-/-}$ T cells not in the spleen (Klapproth et al., 2015).

Next to the Rap1 effector proteins, the adapter protein: adhesion and degranulation adapter protein (ADAP), plays a crucial role in integrin activation in T cells (Ménasché et al., 2007; Witte et al., 2012). The functional relevance of this adapter protein will be discussed in the following section.

1.4 Cytosolic Adapter Protein ADAP

Adapter proteins lack enzymatic or transcriptional activity and are composed of protein-protein and protein-lipid interaction domains. Adapter proteins are divided into two groups: transmembrane adapter proteins and cytosolic adapter proteins (Horejsí et al., 2004; Jordan et al., 2003; Togni et al., 2004). The cytosolic adapter protein ADAP mediates the formation of macromolecular complexes that are responsible for signal transduction, like T-cell or integrin activation (Ménasché et al., 2007; Witte et al., 2012).

Expression, structural and functional features of ADAP

ADAP has been identified as interaction partners of the Src kinase feline yes-related protein (Fyn) and the cytosolic adapter protein Src homology 2 domain containing leukocyte protein of 76 kDa (SLP76) (Marie-Cardine et al., 1998a; Raab et al., 1999; da Silva et al., 1997). ADAP is expressed in the hematopoietic system comprising platelets, mast cells, myeloid cells, natural killer (NK) cells, neutrophils, dendritic cells, and T cells, with the exception of mature B cells (Dluzniewska et al., 2007; Musci et al., 1997; Veale et al., 1999).

In human patients two studies identified nonsense mutations in the *FYB* gene, which encodes ADAP (Hamamy et al., 2014; Levin et al., 2015). These mutations result in premature stop codons and these translational terminations presumably lead to a truncated

version of ADAP. These patients showed an autosomal recessive small-platelet thrombocytopenia (Hamamy et al., 2014; Levin et al., 2013, 2015) and an increased tendency to bleed, but they did not developed immune defects or showed signs of recurrent infections (Hamamy et al., 2014; Levin et al., 2015).

As a typical adapter protein, ADAP hosts various protein-interacting domains: a PRR domain, multiple tyrosine-based signaling motifs (TBSMs), an EVH1 binding region, and two unique helical Src homology 3 (hSH3) domains (Heuer et al., 2004, 2005; Krause et al., 2000; Liu et al., 1998; Marie-Cardine et al., 1998a; Raab et al., 1999) (**Fig. 6**).

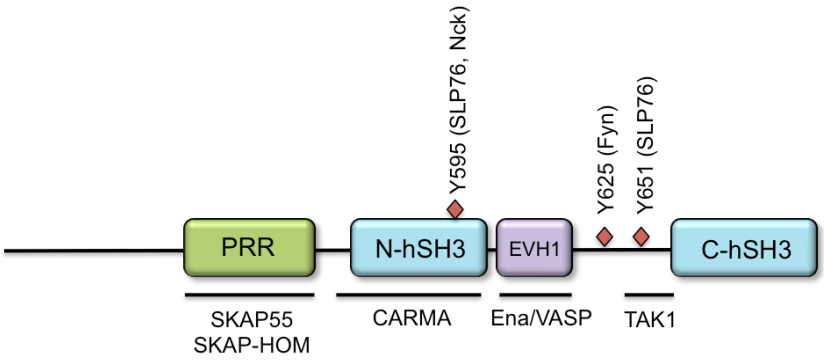

Figure 6: Structure of ADAP. ADAP contains an N-terminal proline-rich domain (PRR), several tyrosine-based signaling motifs (indicated as red squares), two helical extended SH3 domains, an Ena/VASP homology 1 (EVH1)-binding site and interaction sites for caspase recruitment domain containing membrane-associated guanylate kinase protein-1 (CARMA-1) and transforming growth factor β-activated kinase (TAK1). The amino acid stretch 340-364 of ADAP (within the PRR) interacts with the SH3 domain of SKAP55. Adapted and modified from Witte et al., 2012.

In comparison to other SH3 domains, these hSH3 domains of ADAP (**Fig. 6**) contain a unique N-terminal α-helical extension, which folds back to the peptide-binding pocket. These hSH3 domains do not bind proline-rich sequences (Heuer et al., 2004). The N-terminal α-helical extension displays several positively charged amino acid side chains that mediate lipid binding *in vitro* and might be important for plasma membrane targeting (Heuer et al., 2004, 2005). Deletion of the N-terminal α-helical extension of both hSH3 domains attenuates TCR-mediated adhesion and chemokine-induced migration of Jurkat T cells (Heuer et al., 2006).

The EVH1-binding site (FPPPPDDDI motif, amino acid (aa) 616-624) represents the binding motif for proteins of the Ena/VASP family (**Fig. 6**) (Krause et al., 2000). These proteins are regulator of the actin cytoskeleton and will be described in section 1.6 (Burkhardt et al., 2008; Dupré et al., 2015; Samstag et al., 2003).

As depicted in **Figure 6**, the best characterized tyrosine phosphorylation sites Y595, Y625 and Y651 are localized in the unstructured region between two hSH3 domains of ADAP

(**Fig. 6**). Upon TCR stimulation, ADAP becomes tyrosine-phosphorylated by the Src kinase Fyn (Geng et al., 1999; Sylvester et al., 2010) and serves as a hub for Src homology 2 (SH2) domain-containing effector proteins, including Fyn, Non-catalytic region of tyrosine kinase (Nck), and SLP76. The SH2 domain of Fyn interacts with the phosphorylated Y625 of ADAP. The inducible Fyn-ADAP binding is necessary for the TCR-induced release of IL-2 (da Silva et al., 1997). The inducible interaction of Nck with ADAP is mediated via phosphorylated Y595 and Y651. The inducible Nck-ADAP interaction connects ADAP with the actin cytoskeleton to integrins (Lettau et al., 2014; Pauker et al., 2011). The cytosolic adaptor protein SLP76 binds to two phosphorylated tyrosine residues of ADAP, namely Y595 and Y651, thereby recruiting ADAP into a macromolecular complex the LAT-Gads-SLP76 signalosome (Geng et al., 1999; Horn et al., 2009; da Silva et al., 1997). The inducible association of SLP76-ADAP promotes plasma membrane recruitment of ADAP and TCR-mediated activation as well as integrin regulation (Geng et al., 1999; Horn et al., 2009; da Silva et al., 1997; Wang et al., 2004, 2009).

Previous studies have shown that ADAP interacts constitutively with the two cytosolic adapter proteins Src kinase-associated adapter protein of 55 kDa (SKAP55) and SKAP-Homologue (SKAP-HOM). Here, the PRR of ADAP (aa 340-364) binds to the SH3 domain of SKAP55 and SKAP-HOM (Kliche et al., 2006; Liu et al., 1998; Marie-Cardine et al., 1998a) (**Fig. 6**). This constitutive association between ADAP and SKAP proteins facilitates the stable protein expression of both SKAP55 and SKAP-HOM proteins by protecting them from degradation (Burbach et al., 2008, 2011; Huang et al., 2005; Kliche et al., 2006; Marie-Cardine et al., 1998b; Wang et al., 2007). In Jurkat T cells (that only express SKAP55 (Kliche et al., 2006)), the interaction of ADAP with SKAP55 is crucial for TCR-mediated integrin function. ADAP mutants, lacking the entire PRR or 24 aa within the PRR, failed to increase TCR-mediated adhesion to ICAM-1/fibronectin and T-cell interaction with APCs (Burbach et al., 2008, 2011; Kliche et al., 2006)**.** Both of these ADAP mutants lack the expression of SKAP55 (Kliche et al., 2006). Complementary, SKAP55 mutants that lack the entire SH3 domain or carry a W333K point mutation within the same domain (both mutants cannot bind to ADAP) failed to increase TCR-mediated adhesion and T-cell interaction with APCs (Burbach et al., 2008, 2011; Kliche et al., 2006)**.** These findings suggest that the interaction of ADAP with SKAP55 is crucial for TCR-mediated integrin activation. For T cells this functional signaling unit for integrin activation was termed the ADAP/SKAP55-module.

Two pools of ADAP were identified in T cells: 70% of ADAP molecules are bound to SKAP55 (Marie-Cardine et al., 1998a) and modulate integrin function. 30% of ADAP molecules are not associated to SKAP55 and regulate nuclear factor kappa B (NF-κB) signaling via an

inducible association of caspase recruitment domain containing membrane-associated guanylate kinase protein-1 (CARMA-1) and transforming growth factor β-activated kinase (TAK1) upon TCR/CD28 stimulation (Burbach et al., 2008, 2011; Medeiros et al., 2007; Srivastava et al., 2010). These two interactions partners of ADAP regulate IL-2 production and proliferation (Medeiros et al., 2007; Srivastava et al., 2010).

ADAP$^{-/-}$ mice

Two independent groups generated ADAP$^{-/-}$ mice (Griffiths et al., 2001; Peterson et al., 2001). These mice show a defect in T-cell development (Wu et al., 2006). Isolated peripheral T cells from these mice lack the expression of SKAP55 and SKAP-HOM (triple knockout mice for ADAP, SKAP55, and SKAP-HOM) (Kliche et al., 2006). The analysis of peripheral CD4^{+} and CD8^{+} T cells showed that ADAP$^{-/-}$ mice have a reduced total T-cell count, but the frequency of CD4^{+} or CD8^{+} T cells is comparable to WT mice (Peterson et al., 2001). Peripheral ADAP$^{-/-}$ T cells showed an impaired proliferation, a reduced CD69 and CD25 expression, and attenuated cytokine production (IL-2 and IFN-γ) upon CD3/CD28 stimulation (Griffiths et al., 2001; Peterson et al., 2001; Mueller et al., 2007). In addition, ADAP deficiency in peripheral T cells leads to defective T-cell adhesion mediated by β1 and β2 integrins, reduced clustering of LFA-1 and attenuated interactions of T cells with APCs (Burbach et al., 2008, 2011; Griffiths et al., 2001; Mueller et al., 2007; Peterson et al., 2001). Moreover, chemokine-induced migration and adhesion to ICAM-1/VCAM-1 is attenuated in peripheral ADAP$^{-/-}$ T cells *ex vivo* (Kliche et al., 2006; Parzmair et al., 2017).

In contrast to T cells from ADAP$^{-/-}$ mice, which lack the expression of SKAP55 and SKAP-HOM (Kliche et al., 2006), individual SKAP55$^{-/-}$ or SKAP-HOM$^{-/-}$ mice express normal ADAP protein levels (Togni et al., 2005; Wang et al., 2007). These mice show no alterations in the T-cell development (Togni et al., 2005; Wang et al., 2007). SKAP55$^{-/-}$ T cells show a decreased proliferation, impaired IL-2 and IFN-γ production, decreased CD69/CD25 upregulation, attenuated adhesion to ICAM-1/fibronectin and LFA-1-clustering upon TCR stimulation, but not as pronounced as ADAP$^{-/-}$ T cells (Wang et al., 2007). In contrast to ADAP$^{-/-}$ and SKAP55$^{-/-}$ T cells, SKAP-HOM$^{-/-}$ T cells have no functional defects in T-cell activation and adhesion (Togni et al., 2005). In contrast to ADAP$^{-/-}$ T cells, individual SKAP55- and SKAP-HOM-deficient T cells show normal chemokine-mediated migration *ex vivo* (Kliche et al., 2012; Wang et al., 2010). This indicates that the individual SKAP proteins might compensate for each other in T cells.

1.5. Integrin Activation and Actin Remodeling by the ADAP/SKAP55-module

Chemokine-mediated integrin regulation by the ADAP/SKAP55-module

The ADAP/SKAP55-module is involved in chemokine-mediated integrin activation in T cells. It regulates CCL21-mediated T-cell adhesion and migration by controlling LFA-1 affinity and clustering *ex vivo* (Horn et al., 2009; Kliche et al., 2012). The molecular basis how the ADAP/SKAP55-module regulates integrin activation in T cells was assessed in two recent studies. These studies showed that the two Rap1 effector proteins, RIAM and RAPL, are constitutively associated with SKAP55 within the ADAP/SKAP55-module (**Fig. 7**) (Ménasché et al., 2007; Raab et al., 2010). Since the ADAP/SKAP55-module can be associated with RIAM or RAPL, it was important to address whether RIAM and RAPL bind independently or together to the ADAP/SKAP55-complex. For this reason, we conducted immunoprecipitation studies and identified two distinct ADAP/SKAP55-complexes constitutively linked either to RIAM or to RAPL in T cells. The ADAPSKAP55-module associated with RIAM additionally contains Mst1, Rap1, Talin, and Kindlin-3. The second complex includes ADAP, SKAP55, RAPL, Mst1, and Rap1 (Kliche et al., 2012). Since it was reported that RAPL is linked to the α-subunit of LFA-1, we performed a Glutathione-S-Transferase (GST) pull-down assay using the cytoplasmic tail of the α-subunit of LFA-1. Here we identified an inducible association of ADAP, SKAP55, RAPL, Mst1, and Rap1 to this chain upon CCL21-stimulation in primary human T cells. In addition, pulldown studies with a GST-coupled cytoplasmic part of the β-chain of LFA-1 revealed that the ADAP/SKAP55/RIAM/Mst1/Rap1/Talin/Kindlin-3-module is associated with the β-subunit of LFA-1 in CCL21-stimulated T cells. Importantly, the presence of the ADAP/SKAP55-module is required for CCL21-mediated recruitment of both signaling complexes to LFA-1 at the plasma membrane (Kliche et al., 2012) (**Fig. 7, left**).

Despite the function of the ADAP/SKAP55-module for chemokine-mediated LFA-1 regulation, Dios-Esponera and colleagues have shown that ADAP is also required for VLA-4-mediated static adhesion and stable arrest to VCAM-1 under shear flow during chemokine stimulation (Dios-Esponera et al., 2015). T cells lacking ADAP expression showed lower resistant to higher shear than control cells (Dios-Esponera et al., 2015). However, the expression of CD29 (β1-subunit) of VLA-4 and its affinity for VCAM-1-binding were not affected in the absence of ADAP (Dios-Esponera et al., 2015).

TCR-mediated integrin regulation by the ADAP/SKAP55-module

Two studies had indicated that the two of the ADAP/SKAP55-modules, either linked to RIAM or RAPL, not only regulate chemokine signaling, but are also involved in TCR-mediated integrin activation (**Fig. 7 right**). Our group have shown that disruption of the interaction

between SKAP55 and RIAM attenuates TCR-mediated adhesion and T-cell interaction with APCs (Kliche et al., 2006; Ménasché et al., 2007). In addition, we showed that loss of the ADAP/SKAP55 proteins attenuated plasma membrane targeting of both RIAM and Rap1 (Ménasché et al., 2007). Moreover, others have demonstrated that disruption of the interaction between SKAP55 and RAPL (or loss SKAP55) impairs the binding of RAPL/Rap1 to LFA-1 and subsequently attenuates TCR-mediated adhesion and T-cell-APC interaction (Raab et al., 2010). Since our group identified a constitutive interaction of the ADAP/SKAP55-module with RAPL/Mst1 or RIAM/Mst1/Kindlin-3 in resting primary human T cells, we speculate that both complexes are associated with LFA-1 upon TCR stimulation (**Fig. 7 right**). In summary, these data show that the associations of RAPL and RIAM with the ADAP/SKAP55-module are crucial for T-cell adhesion and T-cell interaction with APCs.

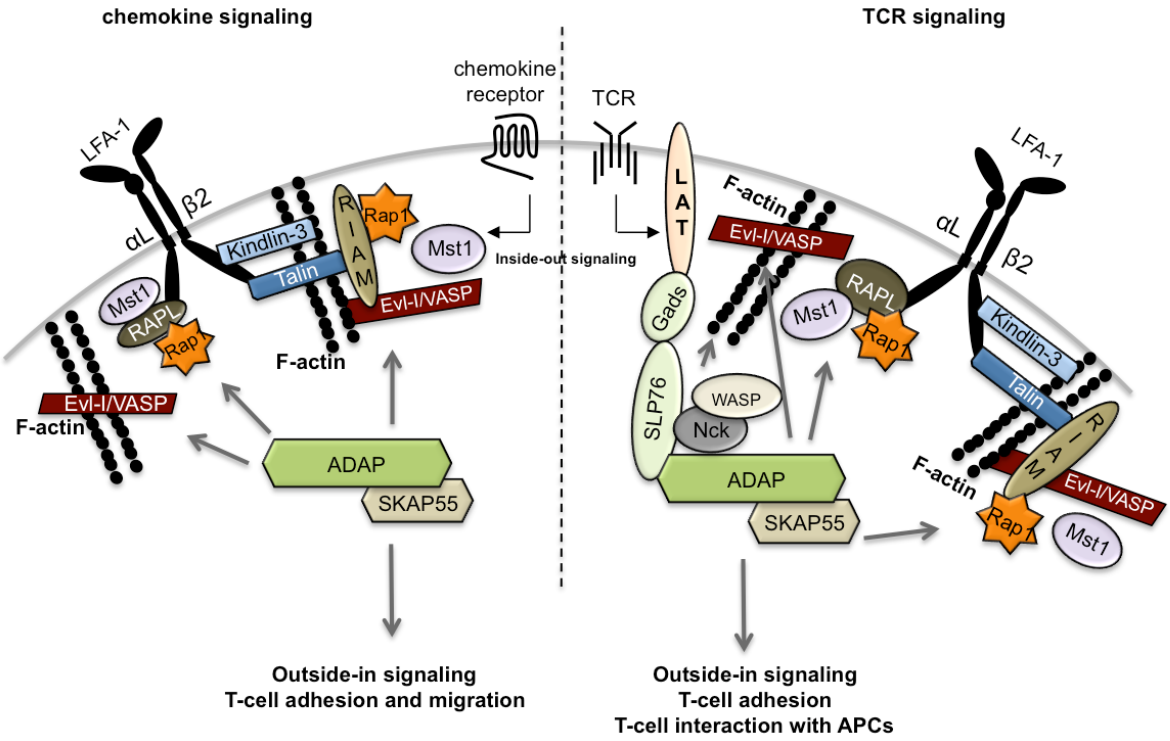

Figure 7: TCR and chemokine signaling mediates LFA-1 activation and F-actin reorganization by the cytosolic adapter proteins ADAP and SKAP55. The ADAP/SKAP55-module provides a platform for different signaling molecules that affect F-actin reorganization and integrin activation. Stimulation of chemokine receptors leads to the independently occurring association of the ADAP/SKAP55-module with the RAPL/Mst1/Rap1 linked to the α-chain of LFA-1 and RIAM/Rap1/Mst1/Kindlin-3/Talin binding to the β-chain of LFA-1. The association of the ADAP/SKAP55-module with either Ena/VASP proteins or Kindlin-3/Talin offers two possibilities for interaction with the actin cytoskeleton (left). After TCR engagement, a LAT-Gads-SLP76 signalosome is assembled and associates with the ADAP/SKAP55-module through the SLP76-ADAP interaction. In addition to this interaction, both SLP76 and ADAP interact with Nck, which associates with WASP (or probably WAVE), or with Evl/VASP to regulate F-actin remodeling (right). Both chemokine receptor and TCR stimulation facilitate ADAP/SKAP55-module-mediated *inside-out/outside-in signaling* to promote the adhesion and migration of T cells. Adapted and modified from Witte et al., 2012.

The ADAP/SKAP55-module and actin cytoskeleton rearrangement

In addition to its association with SKAP55, ADAP is connected to the actin cytoskeleton through interaction with either the Nck-WASP complex or Ena/VASP proteins (**Fig. 7**; Krause et al., 2000; Lehmann et al., 2009; Lettau et al., 2010; Pauker et al., 2011; Sylvester et al., 2010). The group of Barda-Saad proposed that the TCR-mediated interaction of Nck and ADAP facilitates the association between SLP76 and WASP. T cells lacking both ADAP and Nck show severe defects in F-actin polymerization and lamellipodia formation (Pauker et al., 2011).

It has also been reported that ADAP interacts with VASP and Evl in T cells (Krause et al., 2000; Lehmann et al., 2009) (**Fig. 7**). Biochemical approaches showed that VASP constitutively binds to the FPPPPDDDI motif of ADAP (Krause et al., 2000). ADAP together with VASP and Evl co-localize with F-actin at the interface between a T cell and an anti-CD3 antibody-coated bead (Krause et al., 2000).

Moreover, Lafuente and colleagues showed that the SKAP55 interaction partner RIAM interacts with Ena/VASP proteins (Lafuente et al., 2004) (**Fig. 7**). Overexpression of RIAM enhanced TCR-mediated spreading and increased F-actin polymerization in Jurkat T cells. In contrast, suppression of RIAM expression attenuated the F-actin content in activated T cells (Lafuente et al., 2004). Whether and how Evl and/or VASP regulate actin reorganization and thereby modulate integrin function for adhesion and migration in T cells has not been elucidated.

1.6 The Ena/VASP Family

General overview of the family

Members of the Ena/VASP protein family play a key role in remodeling the actin cytoskeleton. The first member, VASP (vasodilator-stimulated phosphoprotein), was identified in platelets as a substrate of cGMP- and cAMP-dependent kinases (Butt et al., 1994; Halbrügge et al., 1990; Reinhard et al., 1992). Later, a screening for orthologs of Drosophila enabled (Ena) in mice identified mammalian Ena (Mena), Ena-VASP-like (Evl) (Gertler et al., 1996) and the splice variant of Evl, termed Evl-I (Lambrechts et al., 2000).

The Ena/VASP family shares a conserved domain structure including an N-terminal EVH1 domain, an integrated PRR domain, and a C-terminal EVH2 domain (Kwiatkowski et al., 2003) (**Fig. 8**). Evl-I differs from Evl by an exon that encodes a 21 amino acid insertion in the EVH2 domain (Lambrechts et al., 2000). The EVH1 domain interacts with the specific

proline-rich motif F/Y/LWPPPP (Gertler et al., 1996; Niebuhr et al., 1997) as found in ADAP (Krause et al., 2000; Obergfell et al., 2001; Lehmann et al., 2009) and RIAM (Lafuente et al., 2004). Ena/VASP proteins interact via the PRR motif with profilin (Reinhard et al., 1995; Gertler et al., 1996; Ahern-Djamali et al., 1998; Ahern-Djamali et al., 1999; Lambrechts et al., 2000). EVH2 harbors a G-actin-binding region (GAB), a F-actin-binding region (FAB) (Harbeck et al., 2000), and a coiled-coil region (CC). The coiled-coil region in Ena/VASP proteins leads to tetramerization and is required for the oligomerization of Ena/VASP proteins (Bachmann et al., 1999; Carl et al., 1999; Riquelme et al., 2015) (**Fig. 8**).

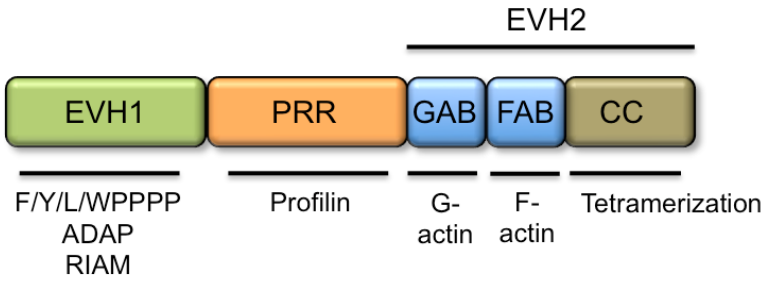

Figure 8: Structure of Ena/VASP proteins. Members of Ena/VASP proteins share a common domain structure. The N-terminal Ena/VASP-homology domain 1 (EVH1) recognizes the F/Y/L/WPPPP motif found in ADAP and RIAM. The central proline-rich region (PRR) binds to profilin. The C-terminal EVH2 domain contains a G-actin-binding region (GAB) and a F-actin-binding region (FAB). The coiled-coil region (CC) domain within the EVH2 domain facilitates the tetramerization of Ena/VASP proteins (Krause et al., 2003; Reinhard et al., 2001).

Function of Ena/VASP proteins

Ena/VASP proteins bind directly to G- and F-actin. *In vitro* studies have shown that Ena/VASP proteins serve as anti-capping factors, promote actin nucleation and elongation as well as F-actin bundling (Barzik et al., 2005; Bear et al., 2002; Breitsprecher et al., 2011; Harbeck et al., 2000; Lambrechts et al., 2000; Walders-Harbeck et al., 2002). Several studies demonstrated that Ena/VASP proteins are localized at the rim of lamellipodia or within these F-actin rich structures, stress fibers, focal adhesions, and at tips of filopodia of various cell types (Bear et al., 2000; Bear et al., 2002; Lambrechts et al., 2000; Lanier et al., 1999; Reinhard et al., 1992; Rottner et al., 2001). Depending on their localization, they are involved in actin-based processes such as cell-cell adhesion, cell-matrix adhesion, cell motility, and integrin regulation in fibroblasts, endothelial cells, neutrophils, and platelets.

The role of Ena/VASP proteins in adhesion and migration in immune cells, like VASP, remains controversial. Platelets of VASP$^{-/-}$ mice show enhanced adhesion to the blood vessel wall *in vivo* (Massberg et al., 2004) and increased spreading on fibrinogen under shear flow *ex vivo* (Kasirer-Friede et al., 2010). Moreover, it has been shown that platelets lacking VASP have increased β3 integrin-mediated binding to collagen and aggregation (Aszódi et al., 1999). In contrast to VASP$^{-/-}$ platelets, VASP-deficiency in neutrophils showed diminished

migration and attenuated adhesion to fibrinogen the ligand of α5β1integrin *ex vivo* (Deevi et al., 2010).

A recent report demonstrated that Mena interacts directly with α5-subunits of $\alpha5\beta1$ integrin and modulates the formation of focal adhesions, cell spreading and cell migration in fibroblasts (Gupton et al., 2012). However, it is unknown whether Ena/VASP proteins interact with other subunits of integrins like LFA-1 or VLA-4.

It has been shown that Evl and VASP localize in the contact site between T cells and CD3-coated beads (Krause et al., 2000). Furthermore, both Evl and VASP are found in F-actin-rich structures and at the distal tips of microspikes and lamellipodia in T cells plated on CD3-coated coverslips (Gomez et al., 2007; Lambrechts et al., 2000). This indicates that Ena/VASP proteins may play a role in IS formation/stabilization and migratory processes in T cells.

1.7 Aims of This Work

We showed that ADAP/SKAP55$^{-/-}$ T cells have a defect in CCL21-mediated migration *ex vivo* (Kliche et al., 2012). Since CCL21 is crucial for T-cell homing into SLOs, I first wanted to investigate whether ADAP deficiency in T cells alters their homing into the spleen and lymph nodes *in vivo*. The extravasation of T cells into SLOs is a multi-stage process regulated by the interplay of integrin activation and actin remodeling. In this context, my aim was to dissect which of these steps are controlled by the ADAP/SKAP55-module. For this, I wanted to analyze the adhesion of WT and ADAP$^{-/-}$ T cells to HEVs using 2-photon microscopy *in vivo*. Using a parallel flow chamber under physiological shear flow *ex vivo*, I further investigated the role of the ADAP/SKAP55-module in T-cell attachment, polarization, and crawling on an endothelia monolayer.

The second aim of my thesis was based on the reported interaction of ADAP and/or RIAM with Evl and VASP. This leads to the hypothesis that the ADAP/SKAP55-module is involved in the regulation of actin cytoskeleton remodeling, which will be investigated here. Furthermore, the role of Ena/VASP proteins to facilitate cell migration and their possible interplay with integrins is controversial. Since data on the function of Ena/VASP proteins in T cells are scarce, I wanted to analyze whether Evl and/or VASP are required for TCR- and chemokine receptor-mediated processes to regulate T-cell adhesion and migration.

2 Materials and Methods

2.1 Materials

2.1.1 Instruments

Microscope	
Fluorescence microscope *Leica DMIL*	Leica Microsystems
Inverted microscope *AxioObserver Z1*	Zeiss
Laser-scanning confocal microscope *Leica TCS SP2*	Leica Microsystems
Light microscope *Axiovert 25*	Zeiss
Two-Photon microscope *Zeiss LSM 710 with MaiTai DeepSee 2-Photon-Laser*	Zeiss, Spectra-Physics
Centrifuge	
Centrifuge *5415R*	Eppendorf
Centrifuge *5415D*	Eppendorf
Multifuge *1 S-R Centrifuge*	Heraeus
Flow cytometer	
FACSCalibur	BD Bioscience
FACSFortessa	BD Bioscience
Gel electrophorese/Western Blot	
Bio-Rad Mini DNA system	Bio-Rad
Bio-Rad Mini protein system *Mini-PROTEAN System*	Bio-Rad
Documentation station *UV-Transilluminator*	Herolab GmbH
Power PAC 200/300/3000	Bio-Rad
Western Blot Transfer *Multiphor II*	Amersham
Cell/bacteria incubator and working station	
Incubator *C200*	Labotect
Bench Heraeus LaminAir HB 2472	DJB Labcare Ltd
Bench Safe 2020	Thermo Scientific
Bench Antares	Biohit
Incubator for bacteria	Binder
Incubation-shaking cabinet for bacteria	Edmund Bühler, GFL
Glass slides	
12 spot slides (pre-coated with poly-L-Lysine)	Marienfeld
Coverslip (for Neubauer counting chamber)	Roth
Coverslips 24x50 mm (for immunofluorescence)	Roth

Glass slides super frost	Roth
Neubauer counting chamber	Marienfeld
Others	
AutoMACS Separator	Miltenyi Biotec
Automated syringe pump	Harvard Apparatus
AxioExaminer upright stage with a 20x, NA 1.0	Zeiss
Electroporation machine *Bio-Rad GenePulser II*	Bio-Rad
ELISA reader *Dynatech MR 5000*	DPC Biermann GmbH
Oximeter O2C	LEA
Pasteur pipette	Roth
PCR machine *DNA engine PTC 200*	Bio-Rad
pH meter	inoLab
Pipette *Accu-jet pro*	Brand
Quartz cell for UV range	VWR
Rotator *Intelli-Mixer*	Neolab
Thermomixer compact	Eppendorf
UV-spectrometer *Ultraspec 3000*	Pharmacia Biotech
Wheel shaker *Duomax 1030*	Heidolph
X-ray cassette *X-omatic*	Kodak
X-ray film processing machine *Cawomat 2000 IR*	Fischer-Peinemann

2.1.2 Plastic ware

100 mm cell culture dishes	BD Bioscience
15 mL and 50 mL tubes	Greiner
6, 24, 96 well cell culture plates	Costar
70 µm pore size cell strainer	BD Bioscience
Acus Omnifix-F	B. Braun
Bacteria culture tubes (14 mL)	BD Bioscience
Cell culture flasks (25 cm^2, 75 cm^2 175 cm^2)	Corning
Cell scrapers	TPP
Electroporation cuvette BTX	Harvard Apparatus
Eppendorf tips (10 µL, 200 µL, 1 mL)	Eppendorf
Eppendorf tubes (0.5 mL, 1.5 mL, 2.0 mL)	Eppendorf
FACS tubes	Falcon
Pap pen for immunostaining	Sigma

PCR soft tubes	Biozym
Plastic pipettes (5 mL, 10 mL, 25 mL, 50 mL)	Costar
Syringes (1mL, 2 mL, 5 mL, 20 mL)	BD Bioscience
Western Blot membrane Hybond-C Extra	GE Healthcare
X-ray film Hyperfilm MP	GE Healthcare
µ-dish 35 mm low	Ibidi

2.1.3 Reagents

100 bp and 250 bp DNA Ladder	Roth
2-mercaptoethanol (99% v/v)	Roth
2-propanol	Roth
Acetic acid (96% v/v)	Roth
Acrylamide/bis-acrylamide (30% w/v), ratio: 37.5:1	Serva
Agar-agar	Roth
Alkaline phosphatase	New England Biolabs
Ammonium persulfate (APS)	Roth
Ampicillin	Roth
Bovine Serum Albumin (BSA)	Sigma
Bromophenol Blue	Roth
Buffer S1, S2, and S3 from the NucleoBond Xtra Maxi Kit	Macherey-Nagel
Calcium chloride ($CaCl_2$)	Merck
CellTrace Far Red DDAO-SE	Invitrogen
CellTracker blue CMAC (7-Amino-4-Chloromethylcoumarin)	Invitrogen
CellTracker Orange CMTMR (5-(and-6)-(((4-Chloromethyl)Benzoyl)Amino)Tetramethylrhodamine)	Invitrogen
CFSE (5-(and-6) Carboxyfluorescein Diacetate, Succinimidyl Ester)	Invitrogen
Ciprobay (2 mg/mL)	Bayer
Desoxynucleotide triphosphate (dNTP)	Fermentas
Dextran (conjugated with FITC, Rhodamine)	Sigma
Dimethyl sulfoxide (DMSO)	Roth
Endonuclease dilution buffer 10x (A, B, C)	New England Biolabs
Endonuclease specific buffer 10x (A, B, H, M)	Roche
Endonucleases: *BamHI, NheI, BglII, HindIII, SalI, XbaI, MluI, NotI*	New England Biolabs
Ethanol (99% v/v)	Roth

Ethidium bromide (10 mg/mL in water)	Roth
Ethylenediaminetetraacetic acid (EDTA)	Sigma
Fetal Calf Serum (FCS)	Pan Biotech GmbH
Fibronectin	Roche
Glucose	Roth
Glycerol	Roth
Glycine	Roth
Heparin (5000 U/mL)	Biochrom AG
HEPES (4-(2-hydroxyethyl)-piperazineethanesulfonic acid)	Roth
Horse serum	Biochrom AG
Human CXCL12	Tebu-bio
Human Fc-ICAM-1	R&D Systems
Hydrogen chloride (37% v/v) (HCl)	Roth
Igepal CA-630 (Nonidet P-40 (NP-40))	Sigma
Immersion liquid Type F	Leica Microsystems
Kanamycin	Roth
Ketamine	Inresa
Lauryl maltoside / n-Dodecyl-β-D-maltoside (LM)	Calbiochem
Liquid nitrogen	Air Liquid Medical
Magnesium sulfate heptahydrate ($MgSO_4$x7 H_2O)	Roth
Manganese chloride ($MnCl_2$)	Roth
Methanol (99.9% v/v)	Roth
Milk powder (fat-free blotting grade)	Roth
Murine CCL21	R&D Systems
Mowiol 4-88	Calbiochem
Murine Fc-ICAM-1	R&D Systems
Oxygen isoflurane	DeltaSelect
PageRuler prestained protein ladder	Fermentas
Paraformaldehyde (PFA)	Merck
Pefabloc SC (PEFA)	Roth
Penicillin/Streptomycin 10000 U/10000 µg/mL	Biochrom AG
Peptone/Tryptone	Roth
PeqGOLD universal agarose	PeqLab
Pfu DNA Polymerase	Fermentas
Pfu-DNA Polymerase Puffer 10x with $MgSO_4$	Fermentas

Phalloidin (coupled with Alexa633, Fluorescein isothiocyanate (FITC), Tetramethylrhodamine B isothiocyanate (TRITC)	Invitrogen, Sigma
Phenol-Chloroform-Isoamyl Alcohol (25:24:1)	Roth
Phenylmethylsulfonyl fluoride (PMSF)	Sigma
Phorbol myristate acetate (PMA)	Calbiochem
Ponceau S	Roth
Potassium acetate (KCH_3COO)	Roth
Potassium chloride (KCl)	Roth
Protein A and G agarose beads	Santa Cruz
Roti Lumin 1 and 2 solutions	Roth
Roti Nanoquant reagent	Roth
Sodium azide (NaN_3)	Roth
Sodium chloride (NaCl)	Roth
Sodium dodecyl sulfate (SDS)	Roth
Sodium fluoride (NaF)	Sigma
Sodium hydrogen carbonate ($NaHCO_3$)	Roth
Sodium hydroxide (NaOH)	Roth
Sodium orthovanadate (Na_4VO_3)	Sigma
Staphylococcus enterotoxin A, C, E	Toxin Technology
Taq-Polymerase	Invitek
T4 DNA Ligase	New England Biolabs
T4 DNA Ligase buffer 10x	New England Biolabs
Tetramethylethylenediamine (TEMED)	Roth
TNF-α mouse, recombinant (*E. coli*)	PromoKine
Tris (hydroxymethyl)-aminomethane	Roth
Triton X-100	Sigma
Trypan blue solution 0.4% in 0.81% sodium chloride and 0.06% potassium phosphate	Sigma
Tween 20	Roth
Xylazine	Bayer Health Care
Xylenexylanol	Roth
Yeast extract	Roth

2.1.4 General buffers, cell culture, and bacteria media

2.1.4.1 Buffers

Hank's balanced salt solution (HBSS)	Biochrom AG
Phosphate-buffered saline (PBS) with Ca^{2+} and Mg^{2+}	Biochrom AG
Phosphate-buffered saline (PBS) without Ca^{2+} and Mg^{2+}	Biochrom AG
Trypsin (0.05% w/v) / EDTA (0.02% w/v) solution	Biochrom AG
Biocoll separating solution (Ficoll, density 1.077 g/mL)	Biochrom AG

2.1.4.2 Cell culture media

Dulbecco's modified eagle's medium (DMEM) with high glucose, pyruvate	Gibco
Dulbecco's modified eagle's medium (DMEM) without Na-pyruvate and L-glutamine, with 3.7 g/L $NaHCO_3$, 4.5 g/L D-glucose	Biochrom AG
RPMI 1640 medium with stable glutamine, 2 g/L sodium hydrogen carbonate ($NaHCO_3$)	Biochrom AG
Dulbecco's modified eagle's medium (DMEM), 5% FCS, 25 mM HEPES, 2% L-glutamine, without phenol red	Gibco

2.1.4.3 Bacteria media

SOC medium	2% (w/v) tryptone peptone, 0.5% (w/v) yeast extract, 100 mM NaCl, 2.5 mM KCl, 900 mL dd H_2O, autoclaved and after cooling down, supplemented with 10 mM $MgCl_2$-6xH_2O (sterile filtrated) and 20 mM glucose (sterile filtrated)
TYM medium	2% (w/v) tryptone peptone, 0.5% (w/v) yeast extract, 100 mM NaCl, 10 mM $MgSO_4$
Luria Broth (LB) medium	1% (w/v) tryptone peptone, 0.5% (w/v) yeast extract, 85 mM NaCl
LB agar	LB medium, 1.5% (w/v) Agar-Agar
1% PFA	1% (w/v) PFA in PBS
2% PFA	2% (w/v) PFA in PBS
3.5% PFA	3.5% (w/v) PFA in PBS

2.1.5 Antibodies

2.1.5.1 Primary antibodies

2.1.5.1.1 Antibodies for stimulation

Table 1: Antibodies for stimulation

Antibody	Species	Antigen	Source	Application
W6/32	mouse	HLA class I	ATCC	Spreading assay
CD3	mouse	CD3 ε-chain human (clone OKT3)	eBioscience	WB
CD3	mouse	CD3 ε-chain human (clone OKT3)	ATCC	Spreading assay, F-actin polymerization adhesion assay

WB: Western blot

2.1.5.1.2 Antibodies for flow cytometry

Table 2: Antibodies for flow cytometry

Antibody	Species	Antigen	Conjugate	Source/ provided by
CD11a	rat	αL-integrin, mouse (clone M17/4)	Biotin	eBioscience
CD18	mouse	β2-integrin, human (clone MEM48)		V. Horejsi
CD18	rat	β2-integrin, mouse (clone M18/2)	Biotin	eBioscience
CD184	mouse	CXCR4, human		BD Bioscience
CD197	rat	CCR7, mouse (clone 4B12)	APC	eBioscience
CD29	mouse	β1-integrin, human (clone MEM101A)		V. Horejsi
CD3	mouse	CD3 ε-chain human (clone OKT3)		ATCC
CD4	rat	CD4 mouse (clone GK1.5)	APC	BioLegend
CD62L	rat	CD62L mouse (clone MEL-14)	APC	eBioscience
CD69	mouse	CD69 human (clone FN50)	APC	BioLegend

Antibody	Species	Antigen	Conjugate	Source/ provided by
CD8	rat	CD8α mouse (clone 53-6.7)	APC	BioLegend
CD8	rat	CD8α mouse (clone 53-6.7)	FITC	BioLegend
Isotype control	Armenian hamster		FITC	BioLegend
Isotype control	rat		APC	BioLegend
Isotype control	rat		FITC	BioLegend
Isotype control	Armenian hamster		APC	BioLegend

APC: Allophycocyanin; FITC: Fluorescein isothiocyanate

2.1.5.1.3 Antibodies for Western blotting and immunoprecipitation

Table 3: Antibodies for Western blotting and immunoprecipitation

Antibody	Species	Antigen	Source/ provided by
ADAP	sheep	ADAP human	G. Koretzky
ADAP	mouse	FYB/SLAP-130 human	BD Bioscience
Evl-I	mouse	Evl/Evl-I human, mouse (clone 84H1)	T. Stradal
Evl-I	rabbit	Evl/Evl-I human, mouse	J. van Lint
Flag	mouse	clone M2	Sigma-Aldrich
GFP	mouse	GFP	Santa Cruz
Kindlin-3	rabbit	Kindlin-3 human, mouse	M. Moser
Mena	mouse	Mena mouse	BD Bioscience
Mst1	rabbit	Mst1 human	Cell signaling
Mst1	mouse	Mst1 human	BD Bioscience
Rap1	mouse	Rap1 human, mouse	BD Bioscience
RAPL	rat	RAPL human, mouse (clone 104B4G12)	S. Kliche
RAPL	rabbit	RAPL human	S. Kliche
RIAM	rat	RIAM human, mouse (clone 15B7E8)	S. Kliche
RIAM	rabbit	RIAM human	T. Stradal
SKAP55	rat	SKAP55 human, mouse (clone 13B6B7)	S. Kliche
SKAP55	mouse	SKAP55 human	BD Bioscience

Antibody	Species	Antigen	Source/ provided by
VASP	mouse	VASP human, mouse (clone IF297)	T. Stradal
VASP	rabbit	VASP human, mouse (clone 9A2)	Cell signaling
β-Actin	mouse	β-Actin (clone AC-15)	Sigma-Aldrich

2.1.5.1.4 Antibodies for immunofluorescence

Table 4: Antibodies for immunofluorescence

Antibody	Species	Antigen	provided by
ADAP	rat	ADAP human (clone 92B2)	S. Kliche
Evl-I	mouse	Evl/Evl-I human, mouse (clone 84H1)	T. Stradal
RIAM	rat	RIAM human, mouse (clone 15B7E8)	S. Kliche
SKAP55	rat	SKAP55 human, mouse (clone 13B6F2)	S. Kliche
VASP	mouse	VASP human, mouse (clone IF297)	T. Stradal

2.1.5.2 Secondary Antibodies

Table 5: Secondary Antibodies

Antibody	Conjugated with	Application, dilution	Order number
Goat anti-mouse IgG	Horseradish peroxidase (HRP)	WB, 1:10000	# 115-035-068
Donkey anti-mouse IgG	DyLight649	IF, 1:100	# 715-495-151
Donkey anti-mouse IgG	FITC	IF, FACS, 1:100	# 715-095-150
Donkey anti-mouse IgG	Cyanine 5 (Cy5), Cyanine 3 (Cy3)	FACS 1:100	# 715-175-151/ # 715-165-151
Goat anti-rabbit IgG	HRP	WB, 1:10000	# 111-035-144
Donkey anti-rabbit IgG	FITC	IF, FACS, 1:100	# 711-095-152
Goat anti-rabbit IgG	Cy3	IF, FACS, 1:100	# 111-165-144
Donkey anti-rabbit IgG	Cy5	IF, FACS, 1:100	# 711-175-152
Goat anti-rat IgG	HRP	WB, 1:10000	# 112-035-167
Goat anti-rat IgG	FITC	IF, 1.100	# 112-095-143
Donkey anti-sheep IgG	HRP	WB, 1:10000	# 713-035-147
Donkey anti-sheep IgG	FITC	IF, 1:100	# 713-095-147

Antibody	Conjugated with	Application, dilution	Order number
Donkey anti-sheep IgG	Cy3, Cy5	IF, FACS, 1:100	# 713-165-147/ # 713-175-147
Goat anti-human IgG, Fc fragment	HRP Cy5	WB, 1:10000 IF, 1:100	# 109-035-098/ # 109-175-008

All secondary antibodies were purchased from Dianova.

2.1.6 Vectors

2.1.6.1 Vectors used for cloning

The vectors described are used for expression in mammalian cell lines with the exception of the pJET1.2 vector. This vector was used as shuttles for cloning of PCR products.

Table 6: Provided vectors

Vector	Resistance	Application	Source
pEGFP-C1	Kanamycin	EGFP-tag C-terminal	Clontech Laboratories
pEF Bos	Ampicillin	Flag-tag C-terminal	provided by B. Schraven
pCMS4	Ampicillin	expression of shRNA-like transcripts	Gomez et al., 2005
pRK5	Ampicillin	IgG Fc-tag C-terminal	provided by S. Kliche
pJET1.2	Ampicillin	blunt-end cloning	Fermentas

2.1.6.2 Vectors for transfection of mammalian cells

Table 7: Generated or provided vectors

Vector	Origin vector	Insert	Source
Evl-I			
pRK5-Evl-I	pRK5	WT Evl-I full length	generated by J. Degen
VASP			
pEGFP-VASP	pEGFP	WT VASP full length	provided by T. Stradal
pRK5-Ig-VASP	pRK5	WT VASP full length	generated by J. Degen
ADAP			
pEF Bos-Flag-ADAP	pEF Bos	WT ADAP full length	(Marie-Cardine et al., 1998a)
RIAM			
pCMV-Flag-RIAM	pCMV	WT RIAM full length	Ménasché et al., 2007

Table 8: Generated or provided vectors

shRNA-containing vector	Origin vector	Knockdown of	Source
pCMS4-shEvl-I 3	pCMS4	Evl-I	generated by J. Degen
pCMS4-shVASP 4	pCMS4	VASP	generated by J. Degen
pCMS4-ADAP	pCMS4	ADAP	Horn et al., 2009
pCMS4-SKAP55	pCMS4	SKAP55	Kliche et al., 2006
pCMS4-RIAM	pCMS4	RIAM	Horn et al., 2009

All constructs were transfected into HEK293T cells, and the expression of the recombinant proteins and tags were analyzed by Western Blot.

2.1.7 Oligonucleotides

Oligonucleotides were purchased from Thermo Scientific or biomers.net.

2.1.7.1 Oligonucleotides for the generation of various vectors

Table 9: Oligonucleotides for the generation of vectors

Name (species)	5' -> 3' sequence	Direction	Restriction site
WT Evl-I full length (human)	CCC AGA TCT ATG GCC ACA AGT GAA CAG AGT ATC	forward	BglII
WT Evl-I full length (human)	CCC GTC GAC CTA CGT GGT GCT GAT CCC ACT CAG	reverse	SalI
WT Evl-I full length (human)	GCG CGC ACG CGT GCC ACC ATG GCC ACA AGT GAA CAG	forward	MluI
WT Evl-I full length (human)	GCG CGC GCG GCC GCT TCA CGT GGT GCT GAT CCC	reverse	NotI
WT VASP full length (human)	GCG CGC GGA TCC ACG CGT ATG AGC GAG ACG GTC ATC TGT	forward	BamHI, MluI
WT VASP full length (human)	GCG CGC GCG GCC GCT TCT AGA TCA GGG AGA ACC CCG CTT	reverse	NotI, XbaI

Underlined nucleotides represent restriction sites.

2.1.7.2 Oligonucleotides for sequencing

Table 10: Oligonucleotides for sequencing of vectors

Name	5’ -> 3’ sequence	Direction	Binding to
Evl-I Seq2	GAC GAG AGC TCC ATG TCA GG	for	Evl-I
pEF Bos	TCG CTT CAT GTG ACT CCA CG	for	EF promotor

2.1.7.3 Oligonucleotides for the generation of shRNA vectors

Table 11: Oligonucleotides for the generation of shRNA vectors

Name	5’ -> 3’ sequence	Knockdown of	Source
Evl-I for	GAT CCC CCG GCT TAA ACT TTG CAA GTA ATT CAA GAG ATT ACT TGC AAA GTT TAA GCC GTT TTT A	human Evl-I	Sigma
Evl-I rev	AGC TTA AAA ACG GCT TAA ACT TTG CAA GTA ATC TCT TGA ATT ACT TGC AAA GTT TAA GCC GGG G	human Evl-I	Sigma
VASP for	GAT CCC CCC AAG GAT GAA GTC GTC TTC TTT CAA GAG AAG AAG ACG ACT TCA TCC TTG GTT TTT A	human VASP	Sigma
VASP rev	AGC TTA AAA ACC AAG GAT GAA GTC GTC TTC TTC TCT TGA AAG AAG ACG ACT TCA TCC TTG GGG G	human VASP	Sigma

2.1.7.4 Oligonucleotides for the genotyping of ADAP knockout mice

Table 12: Oligonucleotides for the genotyping ADAP knockout mice

Name	5’ -> 3’ sequence
ADAP 3’	CCC ACC CCA AGG TCC TTT CTT AC
ADAP 5’	CCG TGG GGC CAA AGT CAG GAG AA
Neo sense	GAT GCC GCC GTG TTC C
Neo antisense	GCC CCT GAT GCT CTT CGT C

2.1.8 Cell lines and bacteria

Table 13: Cell lines and bacteria used

Cell line	Culture conditions	Source
Jurkat T cells JE6.1	RPMI 1640 with 10%(v/v) FCS; 37°C, 5% CO_2 and 95% humidity	ATCC
Human embryonic kidney cells (HEK293T)	DMEM (Biochrom AG) with 10% (v/v) FCS and 1% (v/v) Penicillin/Streptomycin (DMEM/10%FCS/1%PS); 37°C, 5% CO_2 and 95% humidity	ATCC
Raji B cells	RPMI 1640 with 10% FCS 37°C, 5% CO_2 and 95% humidity	ATCC
Primary mouse brain microvascular endothelial cells (pMBMECs)	DMEM (Gibco) with 20% (v/v) FCS, 2% (v/v) non-essential amino acids, 2% (v/v) sodium pyruvate, 50 µg/mL Gentamycin; 37 °C, 8% CO_2 and 95% humidity	provided by R. Lyck
Bacteria		
Escherichia coli (*E. coli*) DH10B	LB medium 37°C	Promega

2.2 Methods

2.2.1 Cell culture

2.2.1.1 Cell counting

One day before the experiments, cells were split and cultured at a cell density of $0.12x10^6$ cells/mL (JE6.1) or $0.1x10^6$ cells/mL (Raji). The cell count was determined with a Neubauer counting chamber. The cell suspension was diluted 1:2 with Trypan blue (0.1% (v/v) in PBS), and cells from four large squares were counted. The cell concentration was calculated using the following equation:

$$cells/ml = value\ of\ negative\ trypan\ blue\ cells \times dilution\ factor \times 10^4$$

2.2.1.2 Thawing/freezing of cells

The freezing of cells was divided into two cooling phases to prevent the formation of ice crystals within the cells. Cells were spun down (4 min, 200xg, room temperature (RT)) and resuspended in FCS/10% (v/v) DMSO at a concentration of $2x10^6$ cells/mL. 1 mL of the cell suspension was aliquoted into a cryotube and cooled to -20°C for 2 h. The cryotubes were temporarily stored at -80°C and finally in liquid nitrogen for long-term storage.

For thawing, the cells were quickly thawed and transferred into 10 mL of the pre-warmed medium (Table 13). After centrifugation (4 min, 200xg, RT), the cell pellet was resuspended in 10-20 mL medium, and the cells were seeded in the appropriate flask or dish.

2.2.1.3 Human primary T-cell isolation

Peripheral blood mononuclear cells (PBMCs) were isolated by Ficoll gradient centrifugation from heparinized blood collected from healthy donors. Approval for these studies was obtained from the Ethics Committee of the Medical Faculty at the Otto-von-Guericke University (Application Number 79/09, GRK1167/TP11). After the initial centrifugation (30 min, 370xg, RT, without brake), the PBMCs were collected and washed three times with RPMI 1640 medium (10 min, 370xg, RT). $CD3^+$ T cells were purified by negative selection using the Pan T cell isolation kit II (Miltenyi Biotec) and the *Auto*MACS machine. PBMCs were counted (2.2.1.1) and centrifuged (10 min at 370xg). The cell pellet was resuspended in ice-cold PBS/0.5%(v/v) BSA at a concentration of $10x10^6$ cells/40 µL. The cells were stained with 5 µL Biotin-Antibody Cocktail (CD14, CD16, CD19, CD36, CD56, CD123, CD235a) per $10x10^6$ cells and incubated on ice for 10 min. Subsequently, 30 µL PBS/0.5% (v/v) BSA and 10 µL anti-Biotin MicroBeads per $10x10^6$ cells were added to the cell suspension. The suspension was incubated on ice for an additional 15 min, filled with PBS/0.5% (v/v) BSA to 10 mL and centrifuged for 10 min at 4°C at 370xg. The cells were then resuspended in 500 µL PBS/0.5% (v/v) BSA per 10^8 cells. After T-cell sorting, T cells were counted and cultured with a density of $2x10^6$/mL in RPMI/10% (v/v) FCS, supplemented with 2 µg/mL Ciprobay, for 24 hours in an incubator.

2.2.1.4 Transfection of HEK293T cells

One day prior to transfection of HEK293T, cells with a 90% confluence were diluted 1:5 in DMEM/10% (v/v) FCS/1% (v/v) PS and seeded in either a 6-well plate or a 100-mm culture dish. On the day of transfection, the cell density was 40-50%. Transfection was performed using the following mixture.

	6-well plate	100 mm dish
DNA	5 µg	10 µg
2 M $CaCl_2$ (sterile)	37 µL	62 µL
dd H_2O	300 µL	500 µL

The DNA mix was supplemented with 2x HEPES-buffered saline (280 mM NaCl, 10 mM KCl, 1.5 mM $Na_2HPO_4x2H_2O$, 12 mM glucose, 50 mM HEPES, pH 7.05) and incubated for 20 min

at RT. Afterward, DMEM/10%FCS/1%PS (3 mL for 6-well or 6 mL for 100 mm dish) was added to the mixture, and the whole solution was transferred onto the plates.

2.2.1.5 Transfection of Jurkat T cells

Jurkat T cells ($20x10^6$ at a density of $0.2\text{-}0.3x10^6$ cells/mL) were centrifuged (4 min, 200xg, RT) and washed once in PBS with Ca^{2+}, Mg^{2+}. After washing, cells were resuspended in 350 µL PBS with Ca^{2+}, Mg^{2+}, and 30 µg vector DNA was added. The cell-DNA suspension was electroporated (230 V, 950 µF). The formed DNA/dead cell aggregates were removed from the cuvette using a Pasteur pipette, and cells were transferred into 50 mL medium (25 mL fresh medium + 25 mL old medium). The cells were cultured up to 72 h at 37°C in an incubator.

2.2.2 Cell biology

2.2.2.1 Adhesion assay

96-well plates were coated with either 100 µL recombinant ICAM-1 (10 µg/mL) or fibronectin (5 µg/mL) in PBS overnight. The wells were washed once with PBS and blocked overnight with 0.1% (v/v) BSA/PBS at 4°C or for 2 h at 37°C. $1x10^6$ Jurkat T cells were washed in HBSS, resuspended in 500 µL HBSS, and stimulated with 5 µg/mL OKT3, 1 mM $MnCl_2$, or 100 ng/mL PMA at 37°C for 30 min. The wells were washed twice with 200 µL HBSS, and 100 µL cell suspension (in triplicates) was added into the wells and incubated at 37°C for an additional 30 min. Non-adherent cells were removed by washing three times with HBSS. The number of adherent cells was counted and calculated as the percentage of input cells.

2.2.2.2 Conjugation assay

For the analysis of T-B-cell conjugates by flow cytometry or confocal microscopy, $2x10^6$ Raji B cells in 1 mL RPMI/10%FCS were incubated with 20 µL *Staphylococcus* enterotoxin (Jurkat T cells: E; hTC: a mix of B, C, and E; 200 µg/mL) for 2 h at 37°C. After centrifugation, Raji B cells were stained with 1 µM DDAO-SE (for FACS) or 5 µM blueCMAC (for confocal microscopy) for 30 min at 37°C. Equal numbers (each $0.2x10^6$) of T cells and superantigen (SA)-loaded Raji B cells were mixed and incubated for 15 and 30 min at 37 °C to allow conjugate formation.

For flow cytometry analysis, non-specific aggregates were disrupted by pipetting (three times), and cells were fixated with 1% PFA (device: FACSCalibur, software: CellQuest™ Pro). The percentage of GFP and DDAO-SE double-positive cells was calculated from unloaded and SA-loaded Raji B cells conjugated with shRNA-transfected Jurkat T cells.

For immunofluorescence staining, T-B-cell-conjugates were incubated on a 12-spot slide (pre-coated with poly-L-lysine). Washing the slide with ice-cold PBS for 1 min terminated the T-B-cell-conjugation. Fixation, permeabilization, and staining of the cells were performed as described in 2.2.4.2.

2.2.2.3 Spreading assay

The spreading assay was used to analyze in detail the co-localization of proteins with F-actin. Moreover, the IS with lamellipodia can be illustrated using this method (Bunnell et al., 2001). On cleaned glass slides, squares were drawn with a Pap pen. 50 µL poly-L-lysine (0.5 µg/µL) were added to each square and incubated for one hour at 37°C. Afterward, 30 µL antibody solution was added to each square and incubated for 3 h at 37°C. After washing in PBS, the cells were resuspended in RPMI1640/25 mM HEPES/0.1% (v/v) BSA and dropped onto the squares (Jurkat T cells: 125.000/square). The incubation at 37°C was performed for the indicated times. The reaction was stopped by washing the slide with ice-cold PBS. Fixation, permeabilization, and staining of cells were performed as described in 2.2.4.2. The quantification of the cell area was performed with Adobe Photoshop CS3 Extended software.

2.2.2.4 F-actin polymerization/depolymerization assay

The F-actin content was determined by flow cytometry. In short, a suspension of $0.1x10^6$ T cells in 100 µL PBS was introduced into a FACS tube. Cells were left untreated or were stimulated with 10 µg OKT3 or 100 ng CXCL12/CCL21 for the indicated times. The reaction was stopped by adding 100 µL FAT buffer (4% (v/v) formaldehyde, 1% (v/v) Triton-X containing FITC- or Alexa633-phalloidin in PBS) and incubating for 15 min at RT. As a negative control, cells were incubated with 100 µL FAT buffer in the absence of phalloidin. The cells were washed with 1 mL PBS (5 min, 200xg), resuspended in 500 µL PBS/1% (v/v) PFA, and analyzed by flow cytometry (device: FACSCalibur, software: CellQuest™ Pro).

2.2.2.5 Transwell migration assay

The migration of T cells was determined using a Transwell migration assay. The Transwell filters were coated with 6.5 µg/mL fibronectin for 90 min at 37°C. 100 ng CXCL12 resuspended in 500 µL assay medium were placed in the lower part of the chamber. Before being placed on the Transwell, the T cells were washed three times with RPMI 1640 (200xg, 4 min, RT) and resuspended in the assay medium (RPMI 1640, 10 mM HEPES pH 7.4, 0.1% (w/v) BSA) at a density of $2x10^6$ cells/mL. 200 µL of this cell suspension were placed in the upper part of the Transwell. The addition of 10 mM EDTA pH 7.4 after 2.5 h terminated

the migration by releasing T cells from the Transwells. The total cell count of the migrated cells was determined by manual counting (2.2.1.1).

2.2.3 Molecular methods

2.2.3.1 Polymerase chain reaction (PCR)

For the generation of various vectors listed in Table 7, the following protocol was used to amplify the different DNA fragments. The primers used are summarized in Table 8.

Reaction:	200 ng template	Program:	95°C	2 min	
	1x Pfu buffer with $MgSO_4$		95°C	30 sec	⎫
	100 ng primer for		1°C/sec	to 70°C	⎬ 30x
	100 ng primer rev		72°C	1:30 min	⎭
	2 mM dNTP-Mix		72°C	10 min	
	2.5 U Pfu-Polymerase		4°C	∞	
	ad 50 µL ddH_2O				

Amplified fragments were analyzed by agarose gel electrophoresis (2.2.3.9).

2.2.3.2 Isolation of vector DNA

2.2.3.2.1 Mini-DNA preparation

Vector isolation was performed from overnight bacterial culture. For this purpose, single-cell colonies were picked and incubated in 3 mL LB medium, supplemented by Ampicillin (200 µg/mL) or Kanamycin (30 µg/mL) overnight at 200 rpm/min at 37°C.

Vector DNA was prepared using buffers S1, S2, and S3 from the NucleoBond Xtra Maxi Kit (Macherey-Nagel). 1 mL of the overnight culture was spun down, the supernatant removed, and the pellet resuspended in 100 µL S1 buffer. The solution was incubated in a shaker for 10 min at 37°C at 600 rpm. Then, 100 µL S2 buffer was added to lyse the bacteria for 5 min at RT. Proteins and chromosomal DNA were precipitated on ice by adding 100 µL S3 buffer for an additional 5 min. The lysate was centrifuged for 10 min at 4°C at 16100xg. The supernatant was transferred into a fresh tube and supplemented with the same amount of phenol/chloroform solution (300 µL). The tube was vortexed for 10 sec and centrifuged at 9300xg at RT for 1 min. This resulted in an upper aqueous and a lower organic phase. The upper aqueous phase (250 µL) was transferred into a fresh tube, and the same amount of isopropanol was added and mixed. After centrifugation (15 min, 4°C, 16100xg), the supernatant was removed by aspiration, and the DNA was washed twice with 500 µL 70%

ethanol for 5 min at 16100xg at 4°C. The vector DNA was dried at RT for 15 min and dissolved in 50 µL ddH_2O for 10 min at 37°C at 300 rpm. 5 µL of the isolated vector DNA were analyzed for quality by agarose gel electrophoresis (2.2.3.9).

2.2.3.2.2 Maxi-DNA preparation

For the transfection of vector DNA into different cell lines or for the subcloning of DNA fragments into other vectors, the vector DNA was isolated from 200 mL overnight culture using the NucleoBond Xtra Maxi Kit (Macherey-Nagel). The isolation was performed according to the manufacturer's protocol. The quality of DNA was analyzed by agarose gel electrophoresis (2.2.3.9), and the concentration was determined by UV-spectroscopy (2.2.3.10).

2.2.3.3 Digestion of DNA with endonucleases

The following endonucleases were used to restrict the DNA: *Bam*HI, *Nhe*I, *Bgl*II, *Hind*III, *Sal*I, *Xba*I, *Mlu*I, and *Not*I, together with enzyme-specific buffers. The analytical digestion was used to clarify whether the cloning of the insert into the vector was successful, and it contained the following components:

5 µL vector DNA (from Mini-DNA preparation)
1x endonuclease-specific buffer
1 U endonuclease of each enzyme
ad 20 µL ddH_2O

The reaction was incubated overnight at 37°C.

If the vector DNA was used for ligation, it was necessary to extract and isolate the digested DNA fragments from an agarose gel. The following mixture was prepared for this purpose:

5 µg vector DNA (from Maxi-DNA preparation)
1x endonuclease-specific buffer
10-15 U endonuclease of each enzyme
ad 50 µL ddH_2O

After overnight incubation, 20 U alkaline phosphatase was added, and the mix was incubated for two hours at 37°C in a thermomixer to remove the 5'-phosphate group of the vector. The DNA fragments were separated by agarose gel electrophoresis (2.2.3.9).

2.2.3.4 Extraction of fragments

The fragments were extracted from agarose gel using the NucleoSpin Gel and the PCR Clean-up Kit (Macherey-Nagel) according to the manufacturer's protocol. The quality of the fragments were analyzed by agarose gel electrophoresis (2.2.3.9), and the concentration was determined by UV-spectroscopy (2.2.3.10).

2.2.3.5 Ligation

For cDNA ligation, the following equation was used to determine the amount of insert needed:

$$x\ ng\ (Insert) = \frac{bp\ (Insert) \times\ 50\ ng\ (Vector)}{bp\ (Vector)}$$

Digested vectors and cDNA fragments were ligated in the indicated reaction:

50 ng vector
x ng inserts
400 U T4 DNA ligase
1x T4 DNA ligase buffer
ad 10 µL ddH_2O

To increase the efficiency, the ligation was performed in a ratio of 1:2 and 1:3 (vector:insert). The ligation mix was incubated for 16-18 h at RT. Subsequently, the reaction mixture was used to transform *E. coli* DH10B as described in 2.2.3.12.

2.2.3.6 Cloning of oligonucleotides in pCMS4

The oligonucleotides (Table 11) were dissolved in ddH_2O at a concentration of 3 mg/mL (37°C, 600 rpm, 10 min). To anneal the oligonucleotides, 1 µL of each oligo (forward + reverse) was mixed with 48 µL annealing buffer (100 mM NaCl, 50 mM HEPES pH 7.4) and annealed with the PCR machine using the following protocol:

90°C	5 min	30°C	5 min
80°C	5 min	20°C	5 min
70°C	5 min	15°C	5 min
60°C	5 min	10°C	5 min
50°C	5 min	4°C	∞
40°C	5 min		

The annealed oligonucleotides were then ligated into *BglII/HindIII*-digested pCMS4 vector.

Ligation: 50 ng *BglII/HindIII*-linearized vector
2 µL annealed oligonucleotides
1x T4 DNA ligase buffer
400 U T4 DNA ligase
ad 10 µL ddH_2O

The incubation was performed for 16-18 h at RT. The reaction was then transformed into *E. coli* DH10B as described in 2.2.3.12.

2.2.3.7 Cloning using pJET1.2

The vector pJET1.2 was used as a shuttle for cloning PCR fragments into another vector system. The CloneJET PCR Cloning Kit (Fermentas) enables the cloning of sticky- or blunt-end-generated PCR fragments in a positive selection system. Ligation of Pfu-generated PCR fragments was performed according to the manufacturer's instructions.

2.2.3.8 Sequencing

The sequencing of different vector DNAs was performed by GATC (Konstanz) using Sanger's chain-termination method (Sanger et al., 1977). The sequence primers used are listed in Table 10, and standard sequence primers were provided by GATC.

2.2.3.9 Analytical agarose gel electrophoresis

Agarose gel electrophoresis was performed for the analysis of vector DNA, PCR reactions, or DNA digests. Agarose was melted in 1xTAE buffer (40 mM Tris, 1 mM EDTA, 20 mM acidic acid) for 1% or 2% gels containing 1 µg/mL ethidium bromide. The samples were mixed with 5x loading dye (50% (w/v) glycerol, 0.25% (v/v) bromophenol blue, 0.25% (v/v) xylenecyanol, 1x TAE). 5 µL DNA ladders were run together with the samples. The DNA was visualized by UV light. A photo was taken with the gel documentation system (Herolab).

2.2.3.10 Measurement of DNA concentration

To determine the DNA concentration, DNA was diluted 1:100 with ddH_2O, spectroscopically analyzed, and calculated using the following equation:

$$c_{DNA}\ (\mu g/\mu L) = \frac{dilution\ factor \times 50\ {}^{\mu g}/_{\mu L} \times A_{260}}{1000}$$

The purity of DNA was assessed by the absorption ratio at 260 nm and 280 nm, which should be between 1.8 and 2.0.

2.2.3.11 Generation of chemically competent bacteria

Cryo-conserved bacteria were streaked on an agar plate without antibiotics and cultured overnight at 37°C. A bacterial smear was cultured in 5 mL LB medium for 6-8 h at 37°C at 200 rpm. 1 mL of the bacterial suspension was added to 25 mL fresh LB medium and incubated overnight at 37°C and 200 rpm. 10 mL of this bacterial suspension was added to the 500 mL TYM medium and further cultured to an OD_{600} of 0.2-0.8 (2 h). Before pelleting of the bacteria (20 min, 3866g, 4°C), the culture was cooled to 4°C with continuous shaking. The bacteria pellet was resuspended in 100 mL ice-cold TFB1 (30 mM potassium acetate, 50 mM $MnCl_2$, 100 mM KCl, 10 mM $CaCl_2$, 15% (w/v) glycine). After centrifugation (8 min, 3866g, 4°C), the pellet was carefully resuspended into 20 mL ice-cold TFB2 (10 mM Na-MOPS pH7.0, 75 mM $CaCl_2$, 10 mM KCl, 15% (w/v) glycine), and 400 µL aliquots of the bacterial suspension was immediately frozen in liquid nitrogen. The bacteria were stored at -80°C. The competence of the bacteria was determined by transformation of different amounts of DNA.

2.2.3.12 Transformation of chemically competent *E. coli*

The ligation mixture was prepared with 50 mM $CaCl_2$ mixed with 100 µL chemically competent *E.coli* and kept on ice for 15 min to transform the competent *E. coli* with vector DNA. The mixture was then incubated for one minute at 42°C (heat shock) and kept on ice for another 5 min. After addition of 800 µL SOC medium, bacteria were grown for at least one hour at 37°C and 300 rpm. Bacteria suspension were then spread onto LB agar plates supplemented with either Ampicillin or Kanamycin (depending on the resistance provided by the vector) and grown overnight at 37°C.

2.2.4 Immunological methods

2.2.4.1 Cell surface staining

Cells (Jurkat T cells: $0.2x10^6$ cells; mTC: $1x10^6$ cells) were washed with ice-cold PBS (Jurkat T cells: 200xg, 4 min, 4°C; mTC: 370xg, 10 min, 4°C) and resuspended in 100 µL antibody solution. The cells were incubated on ice for 30 min and washed with ice-cold PBS. For indirect labeling, Jurkat T cells were additionally resuspended in 100 µL fluorescence-labeled secondary antibody solution. After an incubation period of 30 min on ice and in the dark, cells were washed, fixed with 1% PFA, and analyzed by flow cytometry (device: FACSCalibur,

software: CellQuest™ Pro). Unstained cells or cells stained only with fluorescence-labeled secondary antibody or specific isotype controls were used as controls.

2.2.4.2 Immunofluorescence

The following immunofluorescence techniques were used to analyze the localization of proteins in the cell. In general, for all immunofluorescence applications, cells were fixed with 3.5% PFA for 20 min and permeabilized with 0.1% (v/v) Triton-X-100 in PBS for 10 min. After washing once with PBS, the cells were blocked with 5% (v/v) horse serum in PBS. Afterward, cells were stained with primary antibody for one hour at RT. The cells were then washed three times with PBS and incubated for one hour at RT in the dark with fluorescence-labeled secondary antibodies. In the next step, F-actin was stained with FITC- or TRITC-phalloidin for one hour at RT in the dark. The slide was washed three times in PBS and embedded in mounting medium (2.4 g Mowiol 4-88, 6 g glycerol, 6 mL water, 12 mL 0.2 M Tris pH8.5). Afterward, the coverslip was encircled and fixed with nail varnish for long-term storage. T cells were imaged on a LEICA TCS SP2 laser-scanning confocal system using 63x/1.32 oil objective. Multi-color overlays were produced with Adobe Photoshop CS3 Extended.

2.2.5 Biochemical methods

2.2.5.1 Stimulation with soluble anti-CD3 antibodies and chemokines

2-5x10^6 T cells were resuspended in 150/300 µL RPMI 1640 and incubated at 37°C for one minute. Stimulation was performed by adding 150/300 µL RPMI 1640 containing OKT3 (10 µg/mL), CXCL12 (1 µg/mL), or CCL21 (1 µg/mL) to the cells at different times. The reaction was stopped with 1 mL ice-cold PBS. The cells were then centrifuged briefly (200xg, 2 min, 4°C).

2.2.5.2 Cell lysis

After stimulation or for immunoprecipitation, the cells were lysed in a defined amount lysis buffer (1% NP-40, 1% LM, 150 mM NaCl, 50 mM Tris pH7.4, 10 mM EDTA, 1 mM Na_3VO_4, 10 mM NaF, 1 mM PMSF, PEFA). The cell pellet was resuspended in lysis buffer (40 µL or 60 µL for 2x10^6 primary T cells or Jurkat T cells, respectively, and 100 µL for 5x10^6 primary T cells). HEK293T cells grown in a 100 mm plate were lysed in 200 µL buffer. Lysates were incubated on ice for 20 min and centrifuged (16100xg, 10 min, 4°C). Supernatants were transferred into new tubes.

2.2.5.3 Bradford assay

To ensure equal protein loading on the SDS-polyacrylamide gels, the protein concentration of cell lysate was determined using the Bradford protein assay. RotiNanoquant was prepared according to the manufacturer's instructions. The samples were pre-diluted with ddH_2O. 50 µL dilution were transferred onto a 96-well plate and supplemented with 200 µL 1x RotiNanoquant. After five minutes incubation at RT, the absorption at 570 nm was measured with an ELISA plate reader. The protein concentration was calculated using a BSA calibration curve (0-100 µg/mL).

2.2.5.4 SDS-PAGE

SDS polyacrylamide gel electrophoresis (SDS) was used to separate the proteins. 50 µg cell lysate was mixed with 5x reducing loading buffer (50% (w/v) glycerol, 100 mM Tris pH6.8, 5% (w/v) SDS, 0.01% (w/v) bromophenol blue, 10% (v/v) 2-mercaptoethanol) and boiled at 99°C for 5 min. Samples were loaded onto 8% or 10% SDS gels. 2-mercaptoethanol and SDS disrupt the secondary and tertiary protein structure and apply a negative charge to the proteins. Therefore, the migration of proteins in SDS-PAGE is related to their mass. Polyacrylamide gel electrophoresis was performed with the Bio-Rad Protein system. The gels were run at 120 V for 90 min.

Running buffer: 25 mM Tris, 250 mM glycine, 0.1% (w/v) SDS
Separating gel buffer: 1.5 M Tris, 0.4% (v/v) SDS pH8.8
Stacking gel buffer: 0.5 M Tris, 0.4% (v/v) SDS pH6.8

	8% gel	10% gel	Stacking gel (2 gels)
dd H_2O	4.35 mL	3.75 mL	5.15 mL
0.5 M Tris	-	-	2.1 mL
1.5 M Tris	2.25 mL	2.25 mL	-
30% acrylamide	3 mL	3 mL	1.13 mL
10% APS	60 µL	60 µL	60 µL
TEMED	12.5 µL	12.5 µL	17.5 µL

5 µL PageRuler pre-stained protein ladder was used to monitor protein migration during SDS-PAGE and to calculate protein size.

2.2.5.5 Western blot and immunodetection

The Western blot was performed with the semi-dry system, in which separated proteins from

the SDS polyacrylamide gel are transferred to a nitrocellulose membrane. The membrane and filter papers were saturated with a blotting buffer (25 mM Tris, 86.3 mM glycine, 0.2% (w/v) SDS, 20% (v/v) methanol) and used for protein transfer at 140 mA for one hour. To monitor the equal protein transfer, the membrane was stained with Ponceau S solution (0.1% (w/v) Ponceau S, 5% (v/v) acidic acid). Washing with PBS removed the Ponceau S staining. The membrane was then incubated with a blocking buffer (5% (w/v) milk powder in PBS/0.1% (v/v) Tween) to prevent unspecific binding of antibodies. After washing with PBS/0.1% (v/v) Tween, the membrane was incubated with the primary antibody for one hour at RT with gentle shaking. The membrane was washed three times with PBS/0.1% (v/v) Tween before being incubated with secondary antibodies (HRP-labeled) for one hour. The membrane was further washed four times with PBS/0.1% (v/v) Tween, and the bound antibodies were visualized by chemiluminescence using Roti Lumin. If necessary, and after inactivation of the peroxidase from the secondary antibodies with 1% (w/v) NaN_3 in TBS (150 mM NaCl, 100 mM Tris-HCl, pH 7.5) for 45 min at RT, the membranes were reprobed with other primary antibodies of different species.

2.2.5.6 Immunoprecipitation

Immunoprecipitation was performed to identify protein-protein interactions. 500 or 1000 µg protein lysate were supplemented with 15 or 30 µg BSA to reduce non-specific binding. 30 or 60 µL Protein A (or G)-agarose beads and 2-20 µL of the indicated antibody were added to the mixture. Only Protein A-agarose beads were used for immunoprecipitation of overexpressed proteins with Fc-tag. Samples were incubated for two hours at 4°C under rotation (15 rpm). 1 mL ice-cold washing buffer (10 mM Tris pH8.0, 150 mM NaCl, 0.1% (v/v) NP-40, 1 mM PMSF, 10 µg/mL PEFA) was used to wash the immunoprecipitation mix 3-5 times. The beads were subsequently incubated with 1x reducing loading buffer (10% (w/v) glycerol, 100 mM Tris pH6.8, 5% (w/v) SDS, 1% (w/v) bromophenol blue, 10% (v/v) 2-mercaptoethanol) at 99°C for 10 min.

2.2.6 Animal experiments

2.2.6.1 Mice housing and handling

The mice were kept under pathogen-free conditions in the central animal facility of the Medical Faculty of Otto-von-Guericke University.

2.2.6.2 Genomic DNA isolation from mouse tail biopsies

Isolation of genomic DNA from mouse tail biopsies was performed with the NucleoSpin Genomic DNA from the Tissue Kit (Macherey-Nagel) according to the manufacturer's

protocol. In short, a mouse-tail biopsy (approx. 0.6 cm) was pre-digested in 180 µL buffer T1 and 25 µL Proteinase K for 4-5 h at 56°C and gently shaken. After complete lysis, the residual debris was removed by centrifugation (5 min, 11000xg, RT), and the supernatant was transferred into a fresh tube. For further lysis, 200 µL buffer B3 was mixed with the supernatant. The addition of 210 µL 99% ethanol and vigorous swirling conditioned the DNA for binding to the silica membrane. The solution was applied on top of the column and centrifuged at 11000xg for 1 min. This led to the binding of the DNA to the silica membrane. The flowthrough was discarded. The silica membrane was washed with 500 µL buffer BW and 600 µL buffer B5 (1 min, 11000xg, RT). The column was centrifuged again (1 min, 11000xg, RT) to dry the silica membrane. For elution of the genomic DNA, the column was incubated 1 min at RT with 100 µL pre-warmed buffer BE (70°C) and then centrifuged for 1 min at 11000xg.

2.2.6.3 Genotyping of transgenic mice by PCR

Genotyping of ADAP knockout mice was performed by PCR. Two different PCR reactions were performed for genotyping ADAP or neomycin (recombinant alleles). The following PCR reaction was performed for ADAP genotyping.

PCR mixture		Program		
10x PCR Puffer (Invitek)	5 µL	94°C	3 min	
DMSO	2.5 µL	94°C	30 sec	⎫
$MgCl_2$ (25 mM) (Invitek)	2.5 µL	60°C	45 sec	⎬ 30x
dNTP mix (20 mM) (Fermentas)	0.5 µL	72°C	45 sec	⎭
Primer ADAP 5' (50 pmol/µL)	1 µL	72°C	10 min	
Primer ADAP 3' (50 pmol/µL)	1 µL	4°C	∞	
Taq polymerase (5 U/µL) (Invitek)	0.4 µL			
Genomic DNA	6 µL			
DEPC-water	31.1 µL			

To genotype neomycin, the PCR reaction was performed as follows:

PCR mixture		Program		
10x PCR Puffer (Invitek)	5 µL	94°C	1 min	
DMSO	2.5 µL	94°C	30 sec	⎫
$MgCl_2$ (25 mM) (Invitek)	2.5 µL	60°C	30 sec	⎬ 35x
dNTP mix (20 mM) (Fermentas)	0.5 µL	72°C	1 min	⎭
Primer Neo sense (50 pmol/µL)	1 µL	72°C	5 min	
Primer Neo antisense (50 pmol/µL)	1 µL	4°C	∞	
Taq polymerase (5 U/µL) (Invitek)	0.4 µL			

Genomic DNA	6 µL	
DEPC-water	31.1 µL	

After the PCR reactions, 5x DNA loading dye was added, and the samples were separated into 2% agarose gels with a 100 bp ladder (2.2.3.9).

2.2.6.4 T-cell purification

2.2.6.4.1 Preparation of single-cell suspensions from mouse organs

Spleen and lymph nodes were dissected from 10-14-week-old mice. The organs were mashed through a 70 µm strainer with a syringe to destroy the organs and release the cells. The cells were collected in a 50 mL tube and washed with 20 mL ice-cold PBS/0.5% (v/v) BSA. After centrifugation (370xg, 10 min, 4°C), the cell pellet was resuspended in 500 µL ACK buffer (10 mM $NaHCO_3$, 150 mM ammonium chloride, 0.1 mM EDTA pH 8) to lyse erythrocytes. Lysis was performed on ice for 3 min and stopped with 10 mL ice-cold PBS/0.5% (v/v) BSA. The cells were centrifuged and resuspended in either 25 mL (spleen) or 5 mL (lymph nodes) PBS/0.5% (v/v) BSA for counting (described in 2.2.1.1).

2.2.6.4.2 Isolation of naïve T cells from the spleen

T cells were isolated from the spleen using the Pan T cell isolation kit (Miltenyi Biotec) and negative selection. The single-cell suspension described in 2.2.6.4.1 was centrifuged at 370xg for 10 min at 4°C for this purpose. The cell pellet was resuspended in ice-cold PBS/0.5% (v/v) BSA at a concentration of $10x10^6$ cells/40 µL. The cells were stained with 5 µL/$10x10^6$ cells biotin-antibody cocktail (CD11b (Mac-1), CD45R (B220), DX5, Ter-119) and incubated on ice for 10 min. Subsequently, 30 µL PBS/0.5% (v/v) BSA and 10 µL anti-Biotin MicroBeads per $10x10^6$ cells were added to the cell suspension. The suspension was additionally incubated on ice for 15 min. The mixture was filled with PBS/0.5% (v/v) BSA to 10 mL and centrifuged at 4°C for 10 min at 370xg. The cell pellet was resuspended in 500 µL PBS/0.5% (v/v) BSA per 10^8 cells. The magnetic separation was performed with the autoMACS separator.

2.2.6.5 T-cell staining with CellTracker dyes

T cells used for shear flow or adoptive transfer into recipient mice were stained according to the following protocol. T cells were spun down (370xg, 4°C, 10 min) and resuspended in 1 mL dye solution. Cells were incubated for 20 min at 37°C in an incubator. Staining was stopped by addition of 10 mL of mouse medium (RPMI1680, 10% (v/v) FCS, 1% (v/v) Penicillin/Streptomycin, 50 µM 2-mercaptoethanol). Subsequently, the cells were centrifuged

and resuspended in the mouse medium for flow chamber experiments or in PBS for adoptive transfer.

Application \ Dye	CFSE	DDAO-SE	CMTMR	blueCMAC
Flow chamber	2.5 µM	-	5 µM	20 µM
Adoptive transfer (2-Photon)	5 µM	5 µM	5 µM	-
Adoptive transfer (homing)	0.5 µM	0.5 µM	-	-

2.2.6.6 Homing assay

Equal numbers of CFSE-labeled WT and DDAO-SE-labeled ADAP$^{-/-}$ T lymphocytes were mixed, and a total of 20x10^6 T cells (in 200 µl PBS) were injected intravenously into the tail vein of gender- and age-matched C57BL/6 recipient mice. The dyes were changed between WT and ADAP$^{-/-}$ T cells to exclude off-target effects. After 2 h and 18 h of injection, the mice were sacrificed and the organs (spleen, axillary, inguinal, and mesenteric lymph nodes) were prepared as described in 2.2.6.4.1. The total cell number was determined by manual counting (described in 2.2.1.1.2). Heart blood was taken, either analyzed with a cell counter, or erythrocytes were lysed with Ack buffer for 15 min at RT. The distribution of the transferred fluorescently labeled WT and ADAP$^{-/-}$ T cells in the different organs and blood was analyzed by flow cytometry (device: FACSCalibur, software: CellQuest™ Pro). The total number of homed WT and ADAP$^{-/-}$ T cells in the different compartments was calculated from the percentage of transferred fluorescence-labeled WT and ADAP$^{-/-}$ T cells. The homing index represents the ratio of the total number of ADAP$^{-/-}$ T cells and WT T cells present in the SLOs. Flow cytometric analysis was used to determine the ratio of CD4$^+$ and CD8$^+$ T lymphocytes within fluorescence-labeled WT and ADAP$^{-/-}$ T cells prior to adoptive transfer as well as after 2 and 18 hours of transfer within the homed, labeled lymphocytes to the spleen and lymph nodes. The CD4/CD8 ratio was calculated by analysis of CD4 and CD8 expression within gated CFSE- or DDAO-SE-positive cells.

2.2.6.7 Live cell imaging with 2-photon intravital microscopy

Live cell imaging with 2-photon intravital microscopy was performed in collaboration with Dr. P. Reichardt (Institute for Molecular and Clinical Immunology, Magdeburg). Isolated splenic WT and ADAP$^{-/-}$ T cells were fluorescently labeled with either CFSE or DDAO-SE (described in 2.2.6.5), and a total of 5x10^6 cells were intravenously injected into the tail vein of C57BL/6

recipient mice (provided by Dr. P. Reichardt). The dyes were swapped between the experiments to exclude any dye-related effects. 2 h after adoptive transfer, T cells were imaged in the inguinal lymph node. The blood vessels were highlighted by additional injection of Rhodamine-Dextran/FITC-Dextran (1:1 v/v). Intravital imaging was performed by Dr. P. Reichardt as previously reported (Reichardt et al., 2013). In short, the anesthesia of mice was initiated with i.p. application of 30 mg/kg ketamine plus 3 mg/kg xylazine followed by intratracheal intubation and ventilation with oxygen isoflurane. The inguinal LN was exposed by careful surgical removal of surrounding tissue, sparing the blood and lymph vessels. The quality of regional perfusion and oxygenation under anesthesia was oxymetrically monitored, and the temperature was maintained at 37°C. The 2-photon microscopy was performed using a ZeissLSM710 microscope equipped with a MaiTai DeepSee Femtosecond Laser typically tuned to 800 nm on an AxioExaminer upright stage with a 20x, NA 1.0 water dipping lens. Image detection was performed with three non-descanned detectors (NDD), typically equipped with emission detection filters of 565–610 nm (red), 500–500 nm (green), and ShortPass 485 nm (blue). Individual RGB scans in fields of view, typically 303x303 µm, were recorded in time-lapse sequences typically every four seconds and lasting up to 30 min. Image rendering was performed using Velocity 4.3 (Improvisation, Waltham, MA, USA). Fluorescence-labeled T cells in contact with the vessel wall (visible by the rhodamine-dextran i.v. tracer) were indicated, and the contact time was estimated based on occurrence in the individual image planes of the time lapse. The time was measured before cells that appeared in the vessel lumen for at least two consecutive frames, i.e., at least four seconds, floated away with the bloodstream. In total, more than 100 T cells of each type were quantified in three independent experiments. For data analysis, contacts were considered ‘stable’ when exceeding a time span of ten seconds according to an earlier classification (Ebisuno et al., 2010).

2.2.6.8 Live cell imaging under shear flow

For live cell imaging under shear flow, µ-dishes were incubated with TNF-α-stimulated primary mouse brain microvascular endothelial cells (pMBMECs) (25 ng/mL TNF-α) for 16-18 h. Before the experiments, 100 µM CCL21 were added to the cells and incubated for 30 min at 37°C in an incubator. Subsequently, µ-dishes coated with endothelial cells were fixed in a heating stage (37°C, 5% CO_2) of an inverted microscope. The parallel flow chamber was connected to an automated syringe pump and coupled to the top of the µ-dish. T cells in a concentration of $20x10^6$ cells/mL were transferred into a migration medium (DMEM (Gibco), 5% FCS, 25 mM HEPES, 2% L-glutamine, without phenol red). The shear stress (dyn/cm^2) was calculated according to the following equation (Lawrence et al., 1990; Steiner et al., 2011):

$$\tau = \frac{3\,\mu Q}{2a^2 b}$$

τ…wall shear stress

μ…coefficient of viscosity

Q…volumetric flow rate

a…half channel height

b…channel width

T cells were allowed to accumulate on endothelial cells for three or four minutes at low shear stress (0.25 dyn/cm^2). The dynamic T-cell interaction was recorded under physiologic shear stress (1.5 dyn/cm^2) with a monochrome CCD camera (AxioCam MRm Rev, Carl Zeiss). The examination of T cells on endothelial cells was performed using a 20x objective (LD Plan Neofluar). Time-lapse videos were created from one frame every 20 sec over a recording time of 30 min.

T cells were counted as arrested T cells if they attached on the endothelium during the accumulation phase (0.25 dyn/cm^2) in the field of view (FOV) and resisted immediate detachment after one minute of increased shear flow rate at 1.5 dyn/cm^2. These arrested T cells were tracked manually using the ImageJ software (National Institute of Health, Bethesda, MD, USA) with manual tracking (Institute Curie, Orsay, France), chemotaxis, and a migration plugin (Ibidi GmbH, Martinsried, Germany). T cells that detached upon the increase of shear flow, entered, or left the FOV during the recording time were excluded from the analysis.

3 Results

3.1 Impaired Short-Term Homing of ADAP$^{-/-}$ T Cells into SLOs

Naïve T-cell homing into SLOs depends on the chemokines CCL19 and CCL21 presented on HEVs. Both CCL19 and CCL21 are ligands of the chemokine receptor CCR7 (Marelli-Berg et al., 2008). This chemokine receptor is crucial for LFA-1 activation, which facilitates firm attachment of naïve T cells to HEVs, a prerequisite for the transmigration of T lymphocytes through the endothelium. Recently, Kliche *et al.* showed that the ADAP/SKAP55-module is required for CCL21-mediated T-cell chemotaxis *ex vivo* (Kliche et al., 2012). To address the role of the ADAP/SKAP55-module for T-cell migration *in vivo*, I analyzed the homing of naïve ADAP$^{-/-}$ T cells into the SLOs of mice. Note that loss of the ADAP/SKAP55-module did not alter the percentage of naïve CD4^{+} and CD8^{+} T cells (CD44^{low} and CD62L^{high}) within the spleen or lymph node (data not shown).

For T-cell homing, equal numbers of isolated WT and ADAP$^{-/-}$ T cells were adoptively transferred into sex- and age-matched WT recipient mice. To distinguish between WT and ADAP$^{-/-}$ lymphocytes, cells were either labeled with CFSE or DDAO-SE. In order to exclude off-target effects of dyes during the experiments, dyes were exchanged between T cells. The percentage of labeled WT and ADAP$^{-/-}$ transferred T cells was analyzed in blood, spleen, and lymph nodes (axillary (ALN), inguinal (ILN), and mesenteric (MLN)) by flow cytometry. Two hours after transfer, only 20 – 50% of the adoptively transferred ADAP$^{-/-}$ T cells reached the different lymphoid organs in comparison to the WT T cells (**Fig. 9A**). Reduced numbers of ADAP$^{-/-}$ T cells were detected in the spleen and lymph nodes, whereas increased ADAP$^{-/-}$ T cell numbers were found in the blood (**Fig. 9A**). In contrast to this short-term homing, approx. 80% of transferred ADAP$^{-/-}$ T cells were found in the spleen and lymph nodes after 18 h (**Fig. 9A**). In addition, similar numbers of WT and ADAP$^{-/-}$ T cells were detected in the blood (**Fig. 9A**). To exclude a particular migration defect of either CD4^{+} or CD8^{+} T cells, the CD4/CD8 ratio was analyzed in the SLOs. Similar ratios of migrated CD4^{+} and CD8^{+} T cells were detected, indicating that the delayed homing capacity was not due to a migration defect of a specific T cell subset (**Fig. 9B**). Moreover, analysis of the surface markers CCR7 as well as the α-subunit (CD11a) and the β-subunit (CD18) of LFA-1 revealed that ADAP-deficiency did not alter the surface expression of these receptors. Also, CD62L, which is required for T-cell homing into lymph nodes (Arbonés et al., 1994), did not show an altered expression. This excludes the possibility that differential expression of these receptors causes the delayed homing of ADAP$^{-/-}$ T cells (**Fig. 9C**). In summary, these data indicate that the ADAP/SKAP55-module is required for short-term T-cell homing into the SLOs *in vivo*.

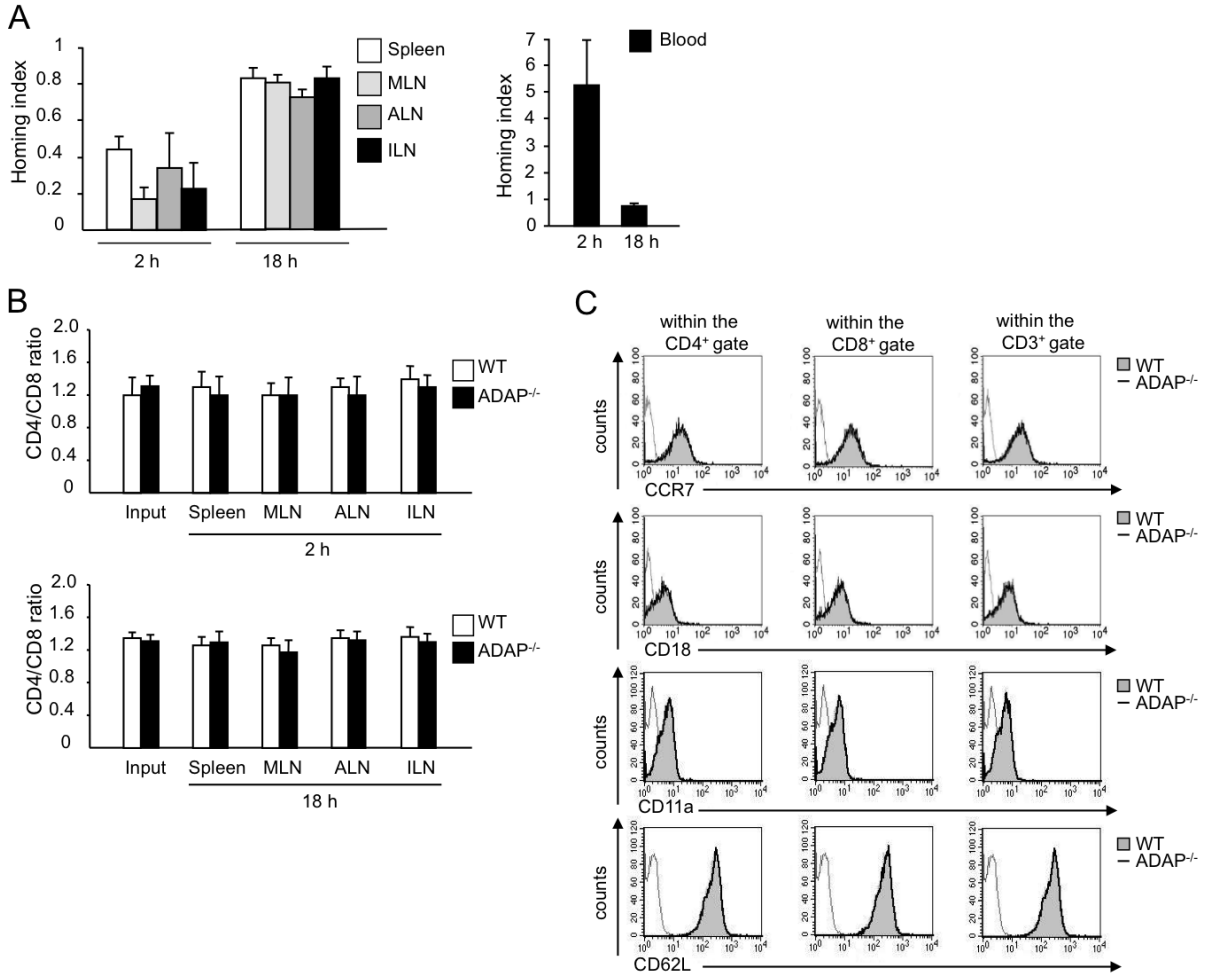

Figure 9: ADAP deficiency in T cells affects short-term homing into secondary lymphoid organs (SLOs). **(A)** Equal numbers of CFSE-labeled WT or DDAO-SE-labeled ADAP$^{-/-}$ T cells (or *vice versa*) were adoptively transferred into WT recipient mice. After 2 h and 18 h, the distribution of WT and ADAP$^{-/-}$ T cells in the spleen, mesenteric (MLN), axillary (ALN), inguinal (ILN) lymph nodes, and blood was analyzed by flow cytometry. The homing index describes the ratio of total numbers of ADAP$^{-/-}$ T cells in relation to WT T cells migrated into the SLOs. The graph represents the data of two independent experiments (mean + SD; n = 8 recipient mice). **(B)** The percentage of CD4$^+$ and CD8$^+$ T cells was determined within the gated CFSE- and DDAO-SE positive cells prior to adoptive transfer (input) and of labeled lymphocytes after homing to the spleen and lymph nodes (MLN, ALN, and ILN) after 2 h and 18 h using flow cytometry. The graphs summarize the data of two independently performed experiments (mean + SD, n = 8 recipient mice). **(C)** Purified splenic WT or ADAP$^{-/-}$ T cells were analyzed for the expression of CCR7, CD18, CD11a, and CD62L of pre-gated CD4$^+$, CD8$^+$, or CD3$^+$-positive cells by flow cytometry. One representative experiment of two is shown.

3.2 Impaired Interaction of ADAP$^{-/-}$ T cells with the Intranodal Vessel Wall *in vivo*

The diapedesis of T cells into SLOs depends on the CCL21-mediated activation of LFA-1, which is required for the interaction of T cells with HEVs (Kinashi, 2005). We have already shown that ADAP$^{-/-}$ T cells have a defect in CCL21-mediated static adhesion to ICAM-1 (Kliche et al., 2012). Therefore, I analyzed whether the reduced short-term homing into SLOs is due to an impaired interaction of T cells with the intranodal vessel wall. Together with Dr. P. Reichardt (Institute of Molecular and Clinical Immunology), I performed 2-photon intravital microscopy of the inguinal lymph node. Prior to 2-photon intravital microscopy, rhodamine-

dextran dye was intravenously injected into the mice to label blood vessels. CFSE-labeled WT and DDAO-SE-labeled ADAP$^{-/-}$ (or *vice versa* to exclude off-target effects from the dye) T cells were adoptively transferred into the tail vein of gender- and age-matched recipient mice. The contact times between the intranodal vessels (visible due intravenously injected rhodamine-dextran) and the differentially labeled WT and ADAP$^{-/-}$ T cells were measured two hours after the adoptive transfer of the T cells. Throughout the entire recording period, it was found that the duration of interactions between the ADAP$^{-/-}$ T cells and the vessel wall was reduced compared to WT cells (WT: 689 ± 66 sec; ADAP$^{-/-}$: 382 ± 52 sec, **Fig. 10A**). To further analyze the interaction of T cells with HEVs, I determined whether the absence of the ADAP/SKAP55-module affects the transient or stable arrest of lymphocytes on HEVs. T cells detaching within 10 sec were classified as transiently arrested T cells, whereas T cells adhering longer than 10 sec are stably arrested T cells (Ebisuno et al., 2010). More ADAP$^{-/-}$ T cells were transiently arrested to HEVs than WT T cells (**Fig. 10B**). This observation is complemented by the reduced number of stably arrested ADAP$^{-/-}$ T cells compared to WT T cells (**Fig. 10B**). Our data suggest that the delayed homing of ADAP$^{-/-}$ T cells is at least partly due to their diminished capacity to perform stable interactions with the endothelium of HEVs within the inguinal lymph node.

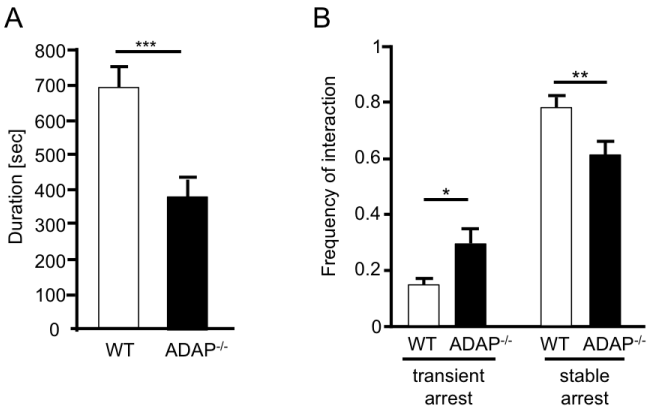

Figure 10: Interaction of WT and ADAP$^{-/-}$ T cells with the intranodal blood vessel *in vivo*. Purified CFSE-labeled WT and DDAO-SE-labeled ADAP$^{-/-}$ T cells were injected into WT recipient mice. **(A)** Analysis of the duration of the interaction of WT and ADAP$^{-/-}$ T cells with the intranodal vessel wall. The data represent mean +SEM from three independent experiments (n = 111 T cells (WT), n = 126 T cells (ADAP$^{-/-}$); Student's t-Test ***p<0.001) **(B)** Analysis of frequency of interaction within 10 sec (transient arrest) or longer than 10 sec (stable arrest). The data represent the mean +SEM from three independent experiments (n=111 T cells (WT), n = 126 T cells (ADAP$^{-/-}$); Student's t-Test *p<0.05, **p<0.01).

3.3 The ADAP/SKAP55-Module controls Attachment and Polarization of naïve T Lymphocytes on Primary Endothelial Cells *ex vivo*

To further confirm that ADAP-deficiency affects T-cell adhesion to an endothelial layer, I analyzed T-cell behavior under physiological shear stress on a primary endothelial cell layer *ex vivo* using a parallel flow chamber. Primary mouse brain microvascular endothelial cells (pMBMECs) were used for this study (Faroudi et al., 2010; Steiner et al., 2011; Soriano et al.,

2011). Prior to the experiment, pMBMECs were stimulated with TNF-α to upregulate the expression of ICAM-1 and VCAM-1 (the ligands for LFA-1 and VLA-4) on the cell surface. In addition, pMBMECs were coated with CCL21, the ligand for the chemokine receptor CCR7, to activate LFA-1 and VLA-4 (Steiner et al., 2010). For a direct comparison of T-cell behavior, purified naïve WT and ADAP$^{-/-}$ T cells were differentially labeled with CMTMR and blueCMAC, respectively, mixed 1:1, and injected into the parallel flow chamber. Again, to exclude off-target effects from dyes during the experiments, dyes were exchanged between T cells. T lymphocytes were allowed to arrest on the endothelial monolayer under low shear flow for 1 min (0.25 dyn/cm^2). Subsequently, shear flow was increased to physiological strength (1.5 dyn/cm^2) and T-cell interaction with the endothelium was recorded over 30 min under constant flow using a CCD camera. The number of arrested T cells on pMBMECs was determined after one minute of physiological shear flow (1.5 dyn/cm^2). At this time point, all T cells adhering to the endothelium in the field of view (FOV) were counted and termed as 'initially arrested' T cells. Here, equal numbers of arrested WT and ADAP$^{-/-}$ T cells were counted in the FOV, indicating that the ADAP/SKAP55-module is not involved in the initial arrest of naïve T cells at the endothelium (**Fig. 11A**). Based on the initially arrested WT T cells, the percentage of adherent lymphocytes was calculated after 5, 15, and 30 min recording under physiological flow to determine the duration of T-cell arrest at the endothelium. Within the first five minutes, equal numbers of WT and ADAP$^{-/-}$ T cells detached from the endothelium. The naïve WT T-cell adhesion began to decline after 5 min, and only 39.6 ± 7.2% of these cells were attached at the end of the recording time. In contrast to WT T cells, a reduced percentage of adhering ADAP$^{-/-}$ T cells was first detected after 15 min, and after 30 min, only 25.5 ± 5.6% of ADAP$^{-/-}$ T cells remained adherent to the endothelial monolayer compared to 39.6 ± 7.2 % of WT T cells (**Fig. 11B**). These results demonstrated that the absence of the ADAP/SKAP55-module does not alter the initial T-cell arrest but is responsible for a stable arrest on the endothelium *ex vivo*. Similar to the *ex vivo* adhesion of ADAP$^{-/-}$ T cells to pMBMECs under shear flow, ADAP$^{-/-}$ T cells did not form stable contacts to HEVs *in vivo* (**Fig. 10B**). These data confirmed my *in vivo* data that the ADAP/SKAP55-module is required for firm adhesion to the endothelium under physiological flow.

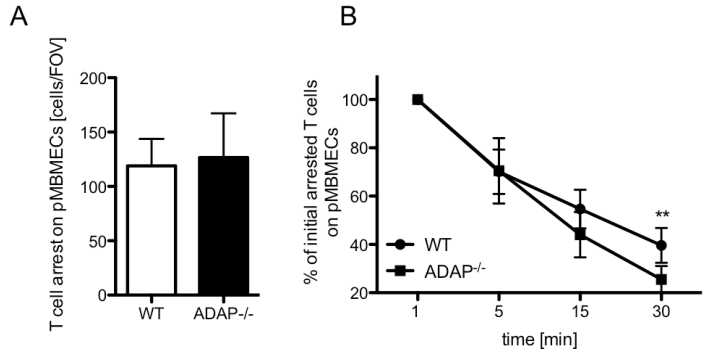

Figure 11: Impaired number of arrested ADAP$^{-/-}$ T cells on primary mouse brain microvascular endothelial cells (pMBMECs) under physiological shear stress. Equal numbers of purified fluorescence-labeled WT and ADAP$^{-/-}$ T cells were perfused in a parallel flow chamber. Low shear stress (0.25 dyn/cm^2) allowed T cells to accumulate on a monolayer of CCL21-coated TNF-α-stimulated pMBMECs. After 2 min, the shear stress was increased to physiological strength (1.5 dyn/cm^2), and T-cell interactions with pMBMECs were recorded under constant flow for 30 min. **(A)** Shear-resistant arrested WT and ADAP$^{-/-}$ T cells were counted after 1 min of increased to physiological shear per field of view (FOV). **(B)** The remaining WT and ADAP$^{-/-}$ T cells were represented as a percentage of initially arrested WT T cells or ADAP$^{-/-}$ T cells on pMBMECs after 5, 15, and 30 min of physiological shear stress. The data represent the mean (SD) of five films from two independent experiments (Student's t-Test **p<0.01)

The above experiment does not provide information as to why, at the 30 min point, ADAP$^{-/-}$ T cells were less well-attached to pMBMECs than WT T cells. One possibility could be that the cells migrate through the endothelium monolayer to enter the underlying environment. To address this question, I also investigated the behavior of shear-arrested WT and ADAP$^{-/-}$ T cells on the endothelium with respect to their different phenotypes as shown in **Figure 12**: '*Crawling with diapedesis,*' '*crawling,*' and '*detachment.*' '*Crawling with diapedesis*' describes a T cell that crawls over the endothelium and transmigrates through the endothelium. A T cell that only crawls over the endothelium without diapedesis was categorized as '*crawling*' T cell. The last category, '*detachment*' describes T cells that detach from the endothelial layer under physiological shear stress. The total number of arrested WT and ADAP$^{-/-}$ T cells was set as 100%, and each T cell was analyzed with respect to its phenotype on the endothelium layer as shown in **Figure 12** (Steiner et al., 2010). If a T cell was not related to any of the categories, it was not counted.

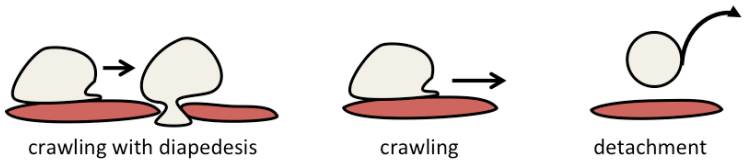

Figure 12: Characterization of individual T-cell behavior on the endothelium layer. *Crawling with diapedesis*: T cells start to polarize and crawl over the endothelium and transmigrate through the endothelium. *Crawling:* T cells that crawl but do not transmigrate across the endothelium. *Detachment:* T cell detaches under physiological shear flow.

Figure 13A shows that under physiological shear stress, slight but not significant differences were observed between WT and ADAP$^{-/-}$ T cells with respect to their capability to crawl with

diapedesis. In contrast, I observed a significantly reduced number of ADAP$^{-/-}$ T cells continuously crawling on pMBMECs (WT: 20.1 ± 4.5% vs. ADAP$^{-/-}$: 7.47 ± 2.31%). Similar to the interaction of ADAP$^{-/-}$ T cells with HEVs *in vivo*, a significantly increased number of ADAP$^{-/-}$ T cells also detached during the recording period (59.07 ± 5.68% vs. 79.2 ± 6.3%) *ex vivo* (**Fig. 13A**). This result indicates that the reduced cell count of ADAP$^{-/-}$ T cells that adhered to pMBMECs after 30 min under physiological shear stress (**Fig. 11B**) is caused by an enhanced 'detachment' from the endothelium. Cell polarization is required for T-cell crawling (Iden and Collard, 2008). As depicted in **Figure 13C**, WT T cells (red) showed a polarized phenotype with a leading edge and a uropod, whereas ADAP$^{-/-}$ T cells (blue) displayed a round, non-polarized phenotype. To investigate whether loss of ADAP affects T-cell polarization, I measured the cell length of the individual cells. ADAP$^{-/-}$ T cells showed a significantly reduced cell length (7.32 ± 2.18 µm) compared to WT T cells (8.18 ± 2.29 µm) (**Fig. 13B**). In summary, ADAP deficiency impairs the polarization of T cells on primary endothelial cells.

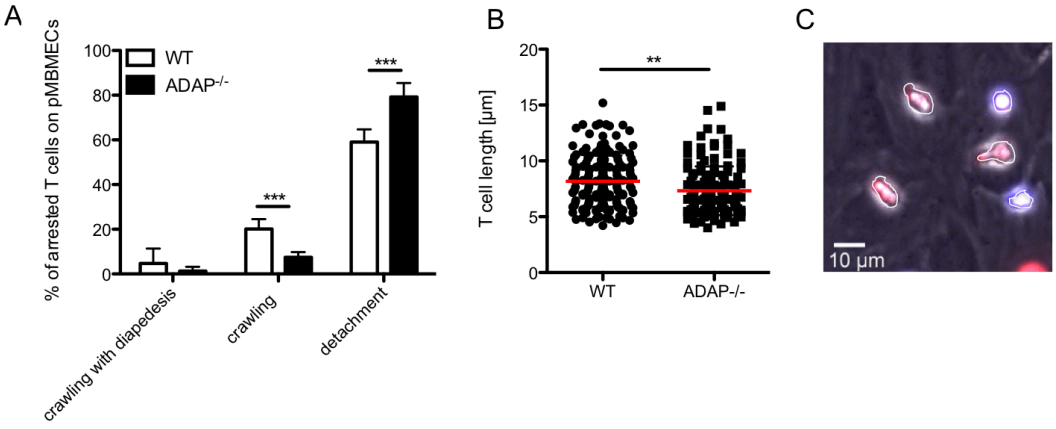

Figure 13: Individual behavior of WT and ADAP$^{-/-}$ T cells on pMBMECs. (A) CMTMR-labeled WT and blueCMAC-labeled ADAP$^{-/-}$ T cells were analyzed on CCL21-coated TNF-α-stimulated pMBMECs under physiological shear flow (1.5 dyn/cm^2) for 30 min. The T-cell dynamics were presented as the percentage of initially arrested WT and ADAP$^{-/-}$ T cells. '*Crawling with diapedesis'* represents T cells that polarized, crawled, and crossed the endothelial cell monolayer (identified by changing brightness). '*Crawling'* means that T cells migrated to the endothelium but did not perform diapedesis. '*Detachment'* indicates T cells that have detached themselves from the endothelium. The data represent the mean value (SD) of five films from two independent experiments (Student's t-Test ***p<0.001. **(B)** The mean T-cell length from the leading edge to the uropod (polarized cell) or diameter (non-polarized cell) was determined for each attached T cell after 10 min of physiological shear. Each dot represents the length of one T cell of three films from two independent experiments (Student's t-Test **p<0.01). **(C)** Representative image of polarized WT (red) and non-polarized ADAP$^{-/-}$ (blue) T cells on CCL21-coated TNF-α-stimulated pMBMECs during shear flow.

3.4. Chemokine-Mediated F-Actin Depolymerization is Increased in the Absence of the ADAP/SKAP55-Module

The analysis of ADAP$^{-/-}$ T cells on the endothelial monolayer revealed a defect in T-cell polarization (**Fig. 13B/C**). In addition to integrin-mediated adhesion, reorganization of the

actin cytoskeleton causes morphological changes of T cells that are crucial for crawling and extravasation into the tissue (Burkhardt et al., 2008). Therefore, I hypothesized that the ADAP/SKAP55-module also regulates actin cytoskeleton remodeling. To investigate a possible link between ADAP and actin dynamics, I determined F-actin levels induced by CCL21 at different times using flow cytometry analysis of purified T lymphocytes from WT and ADAP$^{-/-}$ mice. The mean fluorescence intensity of the F-actin content in untreated WT T cells was set as 100%. The stimulation of purified naïve WT T cells with CCL21 led to an increased F-actin content, which reached its peak 1 min after CCL21 stimulation (**Fig. 14A**). This was followed by F-actin depolymerization, which was reflected by a net decrease of the F-actin content over time. After 20 min of CCL21 stimulation, the F-actin content reached background levels. As depicted in **Figure 14A**, absence of the ADAP/SKAP55-module had no effect on the basal F-actin content in resting T cells. However, stimulation with CCL21 resulted in a reduced F-actin polymerization within 1 min as compared to WT T cells. Already 10 min after CCL21 stimulation, the F-actin content of ADAP$^{-/-}$ T cells had decreased to nearly basal F-actin levels (**Fig. 14A**).

Like CCL21, CXCL12, the ligand for the chemokine receptor CXCR4, is also responsible for T-cell extravasation into tissues (Ward and Marelli-Berg, 2009). Similar to impaired CCL21-mediated T-cell migration in ADAP-deficient T cells (Kliche et al., 2012), stimulation with CXCL12 led to reduced T-cell migration *ex vivo* in the absence of the ADAP/SKAP55-module in human primary T cells (Horn et al., 2009). Therefore, I investigated whether CXCL12 treatment leads to similar changes in F-actin polymerization or depolymerization in ADAP/SKAP55$^{-/-}$ T cells. Comparable to CCL21, CXCL12 stimulation led to F-actin polymerization of WT T cells within one minute. Subsequently, the F-actin content declined and reached a background level after 20 minutes (**Fig. 14B**). Again, ADAP deficiency did not influence the basal F-actin level upon CXCL12 stimulation, as shown by the CCL21 treatment (**Fig. 14A**). However, CXCL12-mediated F-actin polymerization in ADAP$^{-/-}$ T cells was more reduced after 1 min of stimulation compared to WT T lymphocytes. Similar to CCR7 triggering, CXCL12-induced F-actin depolymerization increased much more rapidly in the absence of the ADAP/SKAP55-module.

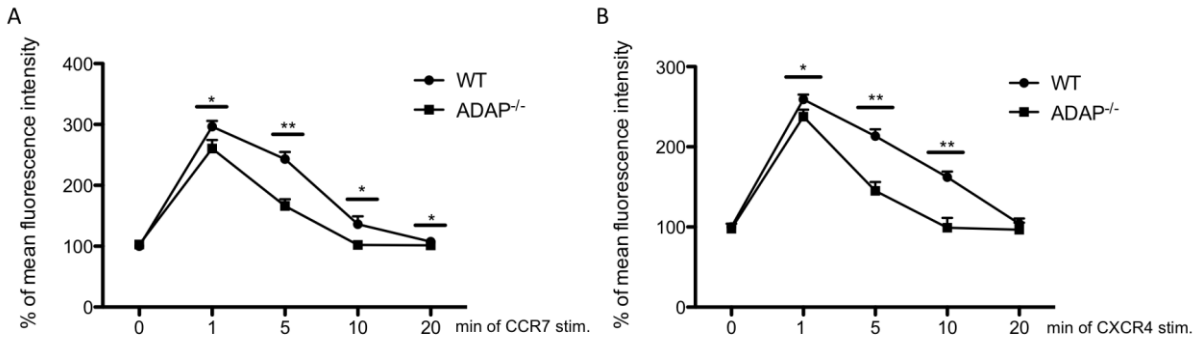

Figure 14: The ADAP/SKAP55-module is required for chemokine-mediated F-actin polymerization and depolymerization in T cells. Isolated naïve WT and ADAP$^{-/-}$ T cells were either stimulated with **(A)** CCL21 (500 ng/mL) or **(B)** CXCL12 (100 ng/mL) for the indicated times. T cells were permeabilized, fixed, and stained with Phalloidin-FITC to mark the F-actin. The F-actin content was measured by flow cytometry. The mean fluorescence intensity of untreated WT T cells was set as 100%. The data represent the mean from four independent experiments (Student's t-Test *p>0.05, **p<0.01).

Collectively, the results from this experimental section show that the ADAP/SKAP55-module modulates short-term T-cell homing but does not influence long-term homing *in vivo.* Moreover, attenuated interaction with HEVs *in vivo* and increased detachment *ex vivo* suggest that the ADAP/SKAP55-module is required for stable adhesion to the endothelium, which can be in part responsible for the delayed homing of ADAP$^{-/-}$ T cells. Further analysis showed an impaired T-cell crawling and polarization upon CCL21 treatment *ex vivo*. This altered T-cell polarization was accompanied by a reduced chemokine-mediated F-actin polymerization and enhanced depolymerization in the absence of the ADAP/SKAP55-module. Thus, the ADAP/SKAP55-module is crucial for T-cell adhesion *in vivo* and *ex vivo* and regulates chemokine-mediated F-actin dynamics. The mechanisms of how the ADAP/SKAP55-module regulates F-actin dynamics need further investigations.

3.5 Analysis of Ena/VASP Proteins

Ena/VASP proteins regulate F-actin dynamics in various cellular systems (Bear et al., 2000, 2002; Coppolino et al., 2001; Krause et al., 2003). To my knowledge, the functional role of Ena/VASP proteins regarding TCR- and chemokine-mediated T-cell adhesion and migration and F-actin dynamics had also not yet been addressed. Therefore, I speculated that Ena/VASP proteins have the capacity for actin rearrangement of T cells. Furthermore, I considered that Ena/VASP proteins could be involved in the altered actin reorganization in the absence of ADAP/SKAP55-module (**Fig. 14**). A potential link of Ena/VASP proteins to the ADAP/SKAP55-module has been shown in three publications (Krause et al., 2000; Lafuente et al., 2004; Lehmann et al., 2009). VASP and/or Evl can be associated with the ADAP/SKAP55-module by either directly binding to ADAP (Krause et al., 2000) and/or via RIAM (Lafuente et al., 2004), an interaction partner of SKAP55 (Ménasché et al., 2007). It was found that ADAP, SKAP55, and RIAM form the ADAP/SKAP55/RIAM-module, but it is

not clearly resolved whether ADAP and/or RIAM interact with Evl and/or VASP. Therefore, in the second part of my thesis, I addressed whether Ena/VASP proteins are associated with the ADAP/SKAP55-module and RIAM. Moreover, I investigated their localization within the immunological synapse of T-B cell pairs and within the lamellipodia of T cells.

3.5.1 Expression of Ena/VASP proteins in lymphocytes

The expression of Evl, VASP and Mena was incompletely analyzed in mouse and human tissues/organs (Reinhard et al., 1992; Aszódi et al., 1999; Hauser et al., 1999; Lanier et al., 1999; Lambrechts et al., 2000). For Evl, two isoforms have been described, Evl and Evl-I (Lambrechts et al., 2000). Therefore, I first analyzed lysates prepared from primary human/mouse T and B cells, Jurkat T cells, and Raji B cells by Western blotting for the expression of Evl/Evl-I, VASP, and Mena. HEK293T cells were included in the analysis because I intended to use them to investigate the interaction of ADAP and RIAM with Ena/VASP proteins in overexpression studies (**Fig. 19**). As shown in **Figure 15**, Evl-I is expressed in primary human/mouse T cells, Jurkat T cells, and mouse B cells. In contrast to Evl-I, the smaller isoform Evl was only detected in mouse T and B cells (**Fig. 15**). In comparison, VASP was expressed in primary human and mouse T cells as well as mouse B cells. Lower expression levels of VASP were found in Jurkat T cells and Raji B cells (**Fig. 15**). Interestingly, anti-VASP immunostaining revealed a double band in primary T and B cells, which might represent a VASP isoform, similar to Evl/Evl-I. However, to my knowledge, no second isoform for VASP has been identified, but several authors have described that phosphorylation of VASP at serine 157 induces a mobility shift (Aszódi et al., 1999; Butt et al., 1994). Further investigations are needed to clarify this issue. In contrast to primary mouse lymphocytes, VASP, but neither Evl nor Evl-I, was detectable in Raji B cells. It is important to note that neither VASP nor Evl/Evl-I were detectable in HEK293T cells. In contrast to VASP and Evl/Evl-I, Mena was not detected in T lymphocytes, but it was expressed in HEK293T cells and primary mouse B cells as reported by Krause and colleagues (Krause et al., 2003) (**Fig. 15**).

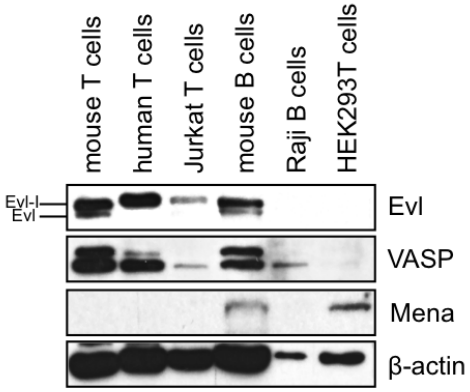

Figure 15: Expression of Ena/VASP proteins in different cells. Cell lysates of primary human and mouse T cells, Jurkat T cells, primary mouse B cells, Raji B cells, and HEK293T cells were analyzed by Western blotting for the expression of Evl/Evl-I, VASP, and Mena. β-actin served as the loading control.

3.5.2 Localization of Evl-I and VASP in T cells

3.5.2.1 Evl-I and VASP localize in the immunological Synapse

Krause et al. demonstrated the localization of Evl in the contact zone of T cells stimulated with anti-CD3 Abs-coated beads (Krause et al., 2000). To address whether Ena/VASP proteins localize at the immunological synapse (IS), purified primary human T cells were allowed to form conjugates with unloaded or superantigen (SA)-loaded Raji B cells for 15 min. The IS is characterized by an accumulation of F-actin at the interface between T and B cells (Chhabra and Higgs, 2007; Gomez and Billadeau, 2008; Yokosuka and Saito, 2010), which can be visualized by F-actin staining using Phalloidin-TRITC (red) (**Fig. 16A lower panel**). F-actin is equally distributed below the plasma membrane in unstimulated cells with no distinct accumulation of F-actin in the contact zone of T and B cells (ring shape). F-actin was evenly spread as a clear ring within the entire cell (**Fig. 16A upper panel**). The same holds true for the localization of Evl-I and VASP in unstimulated T cells (**Fig. 16A/B upper panel**).

The interaction of SA-loaded Raji B cells and T cells induced the formation of an IS as indicated by an accumulation of F-actin in the contact zone. Immunofluorescence analysis of both Evl-I (**Fig. 16A**) and VASP (**Fig. 16B**) showed that both Ena/VASP proteins were recruited to the IS and within the IS they co-localized with F-actin.

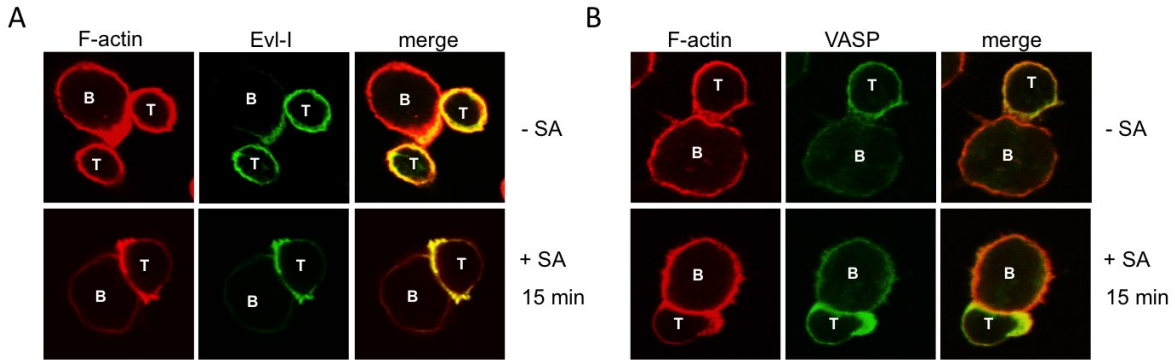

Figure 16: Localization of Evl-I and VASP in the immunological synapse. Purified human primary T cells were incubated for 15 min without superantigen (- SA)- or with SA-loaded (+SA) Raji B cells. T/B cell conjugates were fixed, permeabilized, and stained with an anti-Evl-I mAbs **(A)** or with an anti-VASP mAbs **(B)** in combination with anti-mouse IgG-FITC (green). F-actin was visualized by Phalloidin-TRITC (red). The conjugates were imaged by confocal microscopy. Representative conjugates are shown. Each study was repeated two times and more than 25 conjugates were examined per conditions and experiments.

3.5.2.2 Evl-I and VASP co-localize with F-actin within lamellipodia and at the distal rim

F-actin is one of the important structures in the IS that is required for its formation and stability. Upon IS formation, F-actin accumulates in the pSMAC (Chhabra and Higgs, 2007; Gomez and Billadeau, 2008; Yokosuka and Saito, 2010). F-actin assemblies within the IS are also called lamellipodial structures. Several authors have shown in other cell systems that Ena/VASP proteins localize within and at the distal rim of the lamellipodium (Bear et al., 2000; Reinhard et al., 1992). To address whether Ena/VASP proteins are localized in this specific structure, lamellipodia formation in T cells was induced on anti-TCR Abs-coated glass slides (Bunnell et al., 2001). Lamellipodia formation during T-cell spreading was analyzed by F-actin staining with Phalloidin-TRITC and visualized by confocal microscopy. To confirm that T-cell spreading was triggered by specific activation of the TCR, I used anti-MHCII mAbs (non) as the negative control as they do not induce lamellipodia formation (**Fig. 17A, lower panel**). Confocal microscopy analysis revealed that Evl-I co-localized with F-actin within the formed lamellipodia (**Fig. 17A upper panel**). Higher magnification of the lamellipodia showed that, besides its localization in the lamellipodia, a small proportion of Evl-I was localized at the rim of this F-actin structure (**Fig. 17A middle panel**). Comparable results were obtained for the localization of VASP (**Fig. 17B**). VASP co-localized with F-actin within lamellipodia and with an additional localization at the distal rim of this structure (**Fig. 17B**). Thus, both Evl-I and VASP co-localize with F-actin within and at the distal rim of lamellipodia (**Fig. 17A/B**).

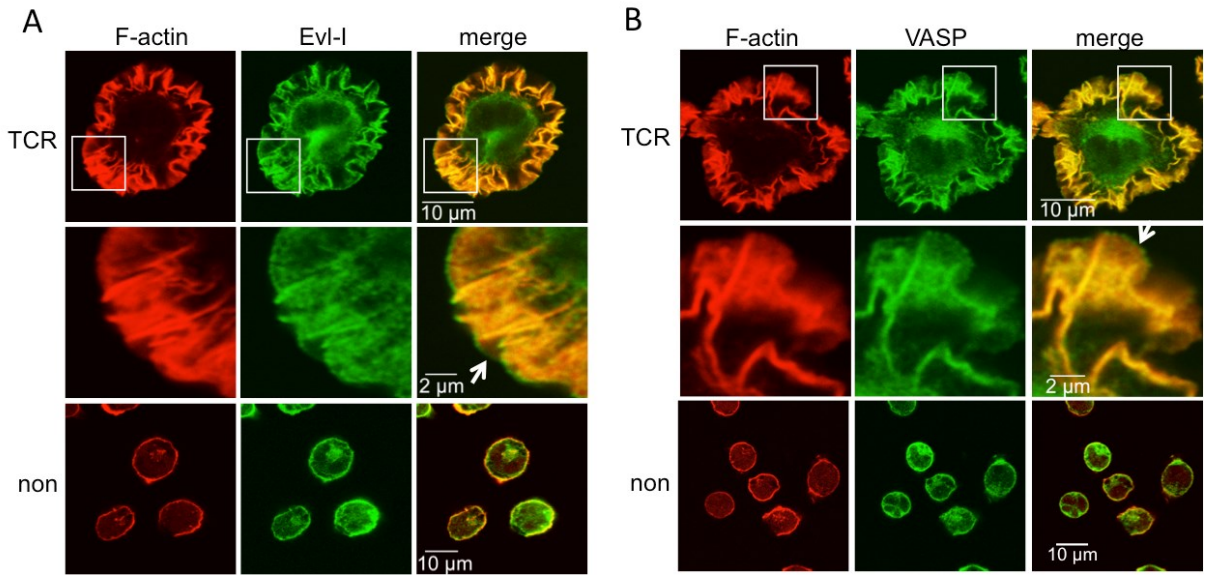

Figure 17: Localization of Evl-I and VASP at the rim and within lamellipodia of T cells. (A and B) Jurkat T cells were settled for 10 min on poly-L-lysine-coated slides pre-coated with anti-CD3 mAbs (TCR) or anti-MHCII mAbs (non). The cells were fixed, permeabilized, and stained with anti-Evl-I mAbs **(A)** or anti-VASP mAbs **(B)** in combination with anti-mouse IgG-FITC (green). The F-actin was visualized with TRITC-Phalloidin (red), and cells were imaged by confocal microscopy. The squares indicate the areas that were captured at higher magnifications. The arrows indicate the thin rim of the lamellipodia. Representative images are shown. Each study was repeated two times and more than 25 cells were examined per condition.

In addition, I analyzed the localization of ADAP and RIAM (interaction partners of Ena/VASP proteins) to determine if they have the same distribution as the Ena/VASP proteins within and at the distal rim of lamellipodia upon T-cell stimulation. Since SKAP55 is constitutively associated with ADAP and part of the ADAP/SKAP55/RIAM-module, the localization of this protein was also included in this study (Kliche et al., 2006, 2012; Marie-Cardine et al., 1998a; Ménasché et al., 2007). Here, too, lamellipodia formation was induced by immobilized anti-TCR Abs on a glass slide. In fact, ADAP, SKAP55, and RIAM co-localized with F-actin within lamellipodia after TCR stimulation and in addition were found at the rim of the lamellipodia (**Fig. 18A-C**). In conclusion, both Ena/VASP proteins and the ADAP/SKAP55/RIAM-module are recruited to TCR-induced lamellipodia and co-localized with F-actin and independently of F-actin they are also localized at the distal rim of this structure.

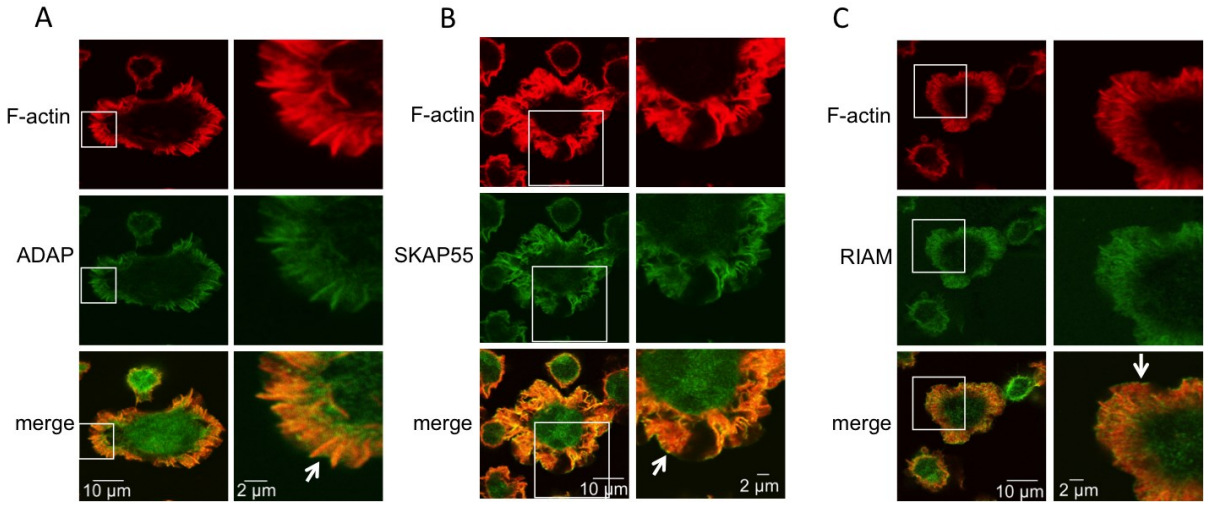

Figure 18: Localization of ADAP, SKAP55, and RIAM at the rim and within lamellipodia of T cells. Jurkat T cells were settled for 10 min on poly-L-lysine slides pre-coated with anti-CD3 mAbs (TCR) or anti-MHCII mAbs (non). The cells were fixed, permeabilized, and stained with anti-ADAP mAbs (**A**), anti-SKAP55 mAbs **(B)**, or anti-RIAM mAbs **(C)** in combination with anti-rat IgG-FITC (green). F-actin was visualized with TRITC-Phalloidin (red), and cells were imaged by confocal microscopy. The squares indicate the areas that were imaged with higher magnifications. The arrows indicate the thin rim of the lamellipodia. Each study was repeated two times and more than 25 cells were examined per conditions and experiments.

3.5.3 Evl-I and VASP interact with ADAP and RIAM

3.5.3.1 Evl-I and VASP interact with ADAP and RIAM in HEK293T cells

Three studies have shown that Ena/VASP proteins interact with ADAP and RIAM (Krause et al., 2000; Lafuente et al., 2004; Lehmann et al., 2009). Furthermore, both ADAP and RIAM contain F/Y/L/WPPPP motifs that mediate the interaction with the EVH-1 domain of Evl and VASP (Krause et al., 2000; Lafuente et al., 2004). To confirm whether Evl-I (the isoform of Evl) and/or VASP associate with ADAP and/or RIAM, I used a heterologous transfection system with HEK293T cells. In HEK293T cells, these proteins are not expressed, which allows studying their interaction (**see Fig. 15**). For these interaction studies, two constructs were generated in which full-length Evl-I or VASP were fused to a C-terminal Immunoglobulin (Ig)-Fc tag. The Ig-tag consists of the Fc-part of human IgG, which binds to Protein A, thus allowing precipitation studies using only Protein-A-agarose.

HEK293T cells were transfected with pRK5-Ig-Evl-I (Ig-Evl-I) together with either Flag-tagged ADAP (FADAP) or Flag-tagged RIAM (FRIAM) to address this question whether ADAP or RIAM interact directly with Evl-I. The cells were lysed, and a Protein A-agarose pulldown was performed. Western blot analysis showed an interaction of Evl-I with both ADAP and RIAM (**Fig. 19A**). To exclude unspecific binding of ADAP and RIAM to Protein A-agarose, only FADAP and FRIAM were transfected into HEK293T cells (**Fig. 19A**). The pulldowns corroborated that these proteins do not bind unspecifically to the beads (**Fig. 19A, lanes 3 and 4**). Similar to Evl-I binding, Ig-tagged VASP also interacted with ADAP and RIAM

(**Fig. 19B**). These results show that i) ADAP and RIAM have the capacity to interact with Evl-I and confirm ii) the previous interaction studies of ADAP and RIAM with VASP (Krause et al., 2000; Lafuente et al., 2004).

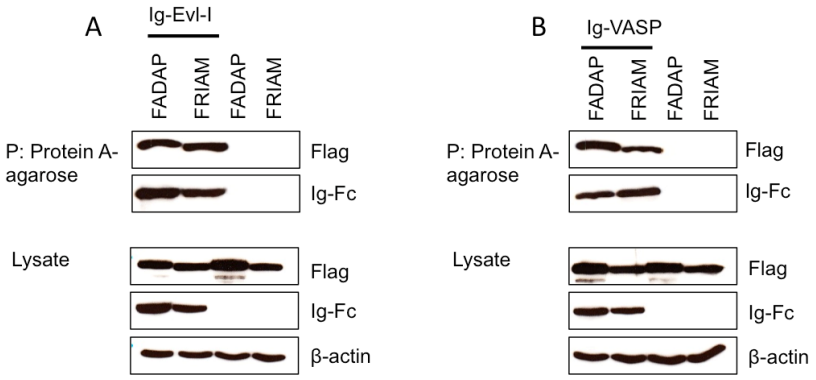

Figure 19: Interaction of Ena/VASP proteins with ADAP and RIAM in HEK293T cells. (A) HEK293T cells were transfected with either Flag-tagged (F)-ADAP or Flag-tagged (F)-RIAM with or without Ig-tagged Evl-I. The cells were lysed and subsequently subjected to precipitation using Protein A-agarose. Western blot analyses of lysates and precipitates were performed using anti-human Fc, anti-Flag, and anti-β-actin mAbs, respectively. **(B)** HEK293T cells were transfected with either Flag-tagged (F)-ADAP or Flag-tagged (F)-RIAM with or without Ig-tagged VASP. The cells were lysed, and the precipitation was performed using Protein A-agarose. Western blot analysis of lysates and precipitates were performed as described in **(A)**. One representative experiment of two is shown.

3.5.4 Evl-I and VASP are associated with the ADAP/SKAP55/RIAM-module in T cells

We have shown that two independent pools of the ADAP/SKAP55-module exist in T cells. They are linked either to RIAM or to RAPL (Kliche et al., 2012). Based on this observation, Evl-I and VASP could interact with both complexes through the interaction with ADAP (**Fig. 19**), or they could bind exclusively to the ADAP/SKAP55/RIAM-module via the association with RIAM (**Fig. 19**). To address this question, primary human T cells were isolated and left unstimulated or treated with anti-CD3 mAbs, CXCL12, or CCL21. Lysates were used for immunoprecipitations using either RIAM or RAPL Abs to distinguish between the ADAP/SKAP55/RIAM-module and the ADAP/SKAP55/RAPL-module, respectively. Western blot analysis of anti-RIAM precipitates revealed that besides the previously described interaction partners ADAP, SKAP55, Mst1, and Kindlin-3, Evl-I and VASP also interacted with RIAM in untreated or TCR- and chemokine-stimulated T cells (**Fig. 20A**). RAPL, as part of the second ADAP/SKAP55-module, was not present in RIAM-immunoprecipitates (as previously reported in Kliche et al., 2012) (**Fig. 20A**). In contrast to RIAM-immunoprecipitates, in RAPL-immunoprecipitates only ADAP, SKAP55, and Mst1 but not RIAM, Evl-I, or VASP were detected (**Fig. 20B**). The stimulation of T cells induced the interaction of Rap1 with the two Rap1 effector molecules, RIAM, and RAPL and thus showed that the activation of cells was successful (**Fig. 20A/B**). In conclusion, Ena/VASP proteins are exclusively associated with the ADAP/SKAP55/RIAM-module and not with the

ADAP/SKAP55/RAPL-module in T cells. Furthermore, this association is constitutive since no alterations in binding upon the various stimuli were observed.

To further substantiate the association of Ena/VASP proteins with the ADAP/SKAP55/RIAM-module, RAPL was depleted from unstimulated primary human T-cell lysates by sequential immunoprecipitations. The RAPL-depleted lysate was used for immunoprecipitation with anti-RIAM Abs and was analyzed for co-precipitation of ADAP, SKAP55, Mst1, Kindlin-3, Evl-I, and VASP by Western blotting. As demonstrated in **Figure 20C**, ADAP, SKAP55, Mst1, and Kindlin-3 were co-precipitated with RIAM even after complete depletion of RAPL. Furthermore, Evl-I and VASP were precipitated with RIAM in RAPL-depleted lysates (**Fig. 20C**). In addition, the precipitation of RAPL in RIAM-depleted lysates corroborated the presence of ADAP, SKAP55, and Mst1 (**Fig. 20D**). However, neither Evl-I nor VASP nor Kindlin-3 could be detected in RIAM-depleted RAPL-precipitates. Thus, Ena/VASP proteins are exclusively part of the ADAP/SKAP55/RIAM/Mst1/Kindlin-3-complex in resting primary human T cells.

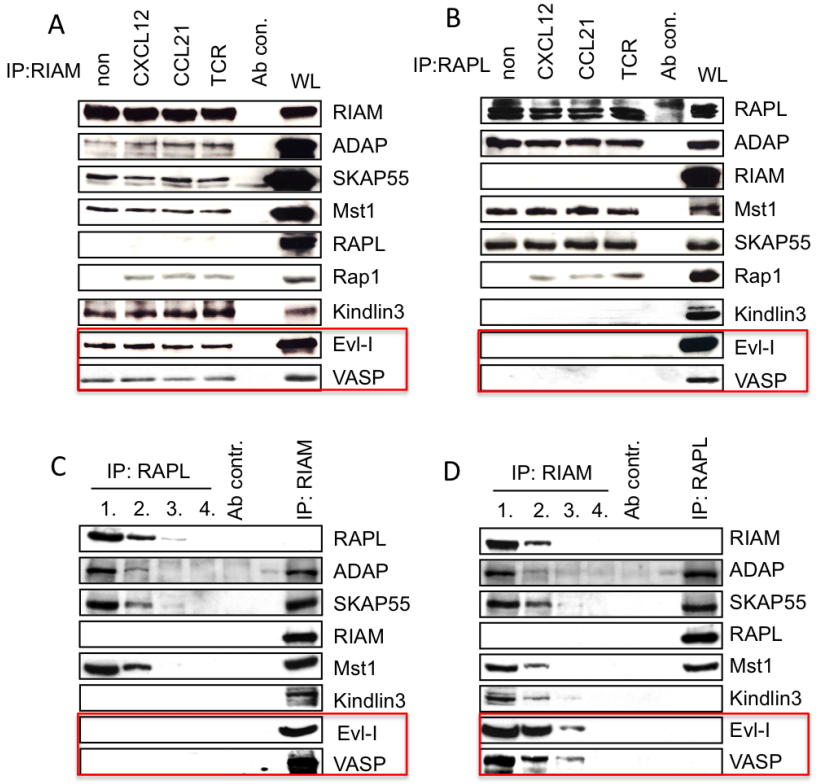

Figure 20: Evl-I and VASP are linked to the ADAP/SKAP55/RIAM-complex in primary human T cells. Primary human T cells were left untreated or were stimulated with CXCL12 or CCL21 for 1 min or with anti-CD3 for 5 min. Immunoprecipitations were performed using (**A**) anti-RIAM or (**B**) anti-RAPL antibodies. Precipitates were analyzed by Western blotting using the indicated antibodies. The successful stimulation was confirmed by recruitment of Rap1 to the ADAP/SKAP55/RIAM-module and the ADAP/KSAP55/RAPL-module. One representative experiment of three is shown. (**C** and **D**) Resting primary human T cells underwent four sequential immunoprecipitations, either anti-RAPL (**C**) or anti-RIAM (**D**) Abs. After these sequential immunoprecipitations with the indicated Abs, the final immunoprecipitations with the respective antibodies were performed using either anti-RIAM (**C**) or anti-RAPL (**D**) Abs. The precipitates were analyzed by Western blotting with the indicated antibodies. One representative experiment of two is shown.

In summary, Evl-I and VASP are expressed in T lymphocytes and are interaction partners of ADAP and RIAM. The co-localization with F-actin was observed using immunofluorescence analysis. Here, Ena/VASP proteins were found to localize in the IS of T/B cell pairs and co-localize with F-actin within lamellipodia and additionally at the distal rim of lamellipodia. ADAP, SKAP55, and RIAM were found to localize in the same compartments as Evl-I and VASP. Whether Ena/VASP proteins are required for F-actin reorganization and therefore could affect adhesion and migration of T cells is elusive. This issue is addressed in the following part of my thesis.

3.6 Function of Ena/VASP Proteins in T-cell Adhesion and Migration

3.6.1 Establishment of knockdowns for Evl-I and VASP in Jurkat T cells

To evaluate the functional relevance of Evl-I and VASP for adhesion, migration, and F-actin dynamics in Jurkat T cells, I established a knockdown of Ena/VASP proteins using a vector-based shRNA approach. I used the pCMS4 vector, which contains an H1 promoter for shRNA expression, an SV40 promoter mediating the expression of GFP, and a CMV promoter that can be used for the re-expression of an shRNA-resistant Flag-tagged protein of interest (Gomez et al., 2005). These suppression constructs were tested first in HEK293T cells that do not express Evl-I or VASP for the knockdown specificity against Evl-I or VASP, respectively (**Fig. 15**). Hence, exogenous Flag-tagged Evl-I or Flag-tagged VASP were co-transfected together with the control vector (shC), shEvl-I, or shVASP. **Figure 21A** demonstrates that shEvl-I suppresses the expression of Evl-I but not of VASP. Similar to the suppression of Evl-I, co-expression of shVASP with Flag-tagged Evl-I or Flag-tagged VASP reduced the expression of VASP but not of Evl-I (**Fig. 21B**). To analyze the reduction of endogenous Evl-I and VASP expression in T cells, I determined the knockdown capacity of shEvl-I and shVASP in Jurkat T cells. The analysis showed that Evl-I or VASP expression is almost completely suppressed 48 h after transfection (**Fig. 21C**). The suppression efficiency was approx. 70% for endogenous Evl-I and 85% for endogenous VASP. The downregulation of either Evl-I or VASP specifically suppressed the expression of Evl-I or VASP, respectively.

To rule out the possibility that downregulation of Evl-I and/or VASP may affect the expression of the ADAP/SKAP55-module and its interaction partners (RIAM, RAPL, Mst1, and Kindlin-3) were analyzed by Western blotting. The expression of none of these molecules was affected by suppression of Evl-I and/or VASP (**Fig. 21D**).

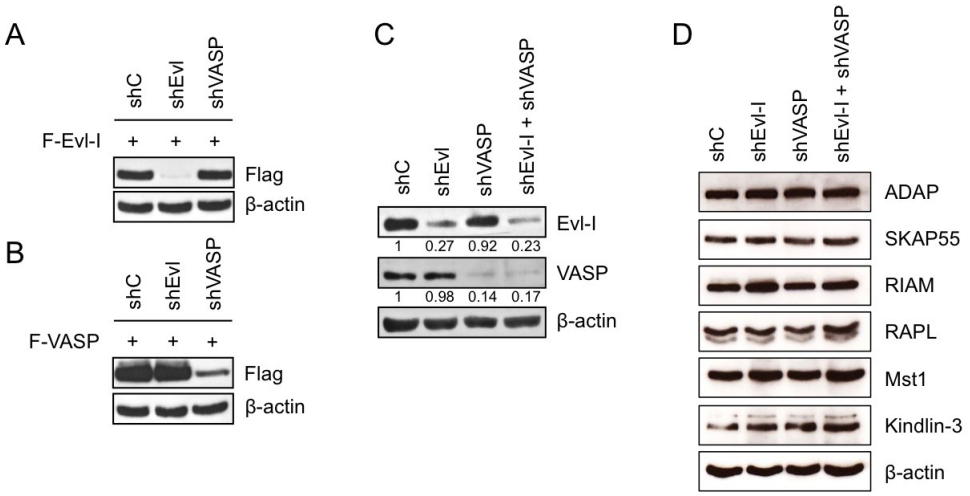

Figure 21: Vector-based shRNA-mediated suppression of Evl-I or VASP in T cells. (**A**) HEK293T cells were co-transfected with Flag-tagged Evl-I together with the control vector (shC), the Evl-I suppression vector (shEvl-I), and the VASP suppression vector (shVASP). The lysates were analyzed by Western blotting using the indicated Abs. (**B**) HEK293T cells were co-transfected with Flag-tagged VASP together with shC, shEvl-I, and shVASP. Lysates were analyzed as described in (A). One representative experiment of two is shown. (**C**) Jurkat T cells were transfected with shC, shEvl-I, shVASP, or shEvl-I/shVASP. 48 h after transfection, cells were lysed, and lysates were analyzed for the expression of endogenous Evl-I and VASP using anti-Evl-I and anti-VASP Abs. β-actin was used as a loading control. (**D**) The same lysates were analyzed by Western blotting for the expression of ADAP, SKAP55, RIAM, RAPL, Mst1, and Kindlin-3 to exclude off-run targets effects of shEvl-I and/or shVASP. One representative experiment of two is shown.

To ensure that my generated suppression vectors did not affect the surface expression of receptors important for the subsequent studies, I determined the surface expression of the TCR, the β-subunits of LFA-1 (CD18) and VLA-4 (CD29), and the chemokine receptor CXCR4. The pCMS4 vector contains an SV40 promoter mediating the expression of GFP. This allows the analysis of GFP-expressing cells, which are transfected with these suppression vectors. The surface expression was analyzed by flow cytometry after gating on GFP-expressing cells. **Figure 22** shows histograms with an overlay of control-transfected cells (shC) (filled curve in gray) and cells with Evl-I (shEvl-I) and/or VASP (shVASP) suppression (black line). The gray line indicated the control staining with secondary Abs. The results show that neither the individual knockdown of Evl-I and VASP nor the simultaneous suppression of both molecules had any effect on the surface expression of the analyzed receptors (**Fig. 22**).

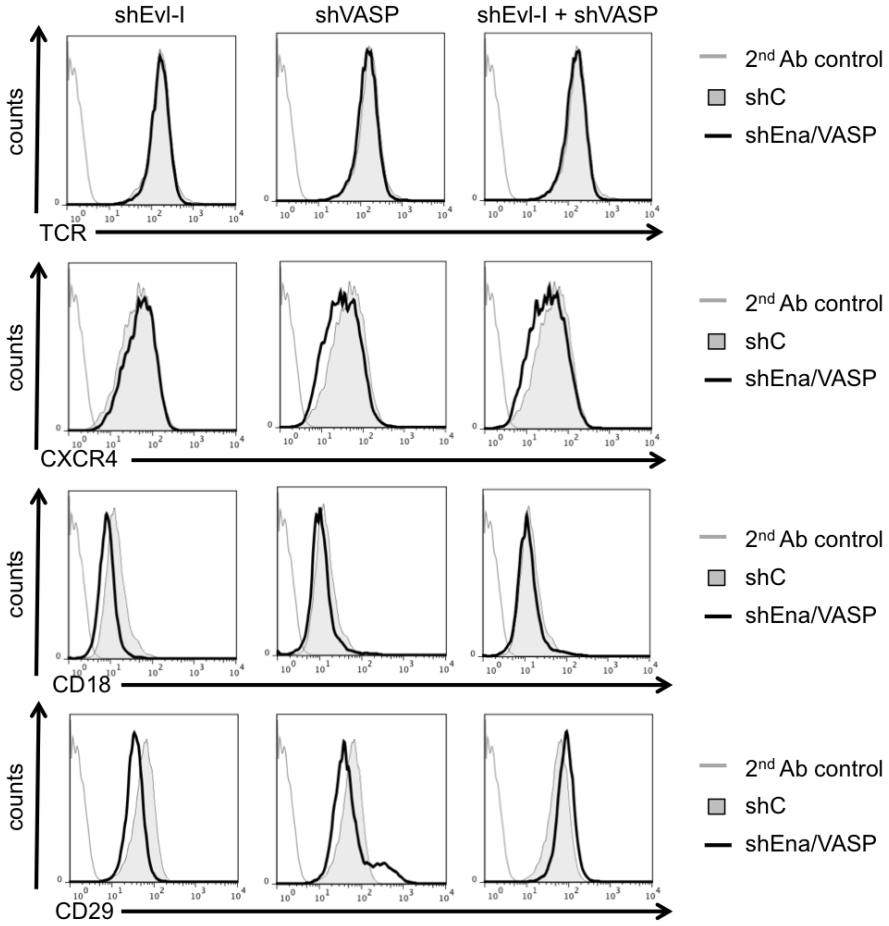

Figure 22: Suppression of Evl-I and/or VASP does not affect the surface expression of TCR, LFA-1, VLA-4, and CXCR4. Jurkat T cells were transfected with the control vector (shC), the Evl-I suppression vector (shEvl-I), the VASP suppression vector (shVASP), or the combination of shEvl-I and shVASP (shEvl-I/shVASP). After 48 h of transfection, the surface expression of the TCR, the chemokine receptor CXCR4, the β2-subunit of LFA-1 (CD18), and the β1-subunit of VLA-4 (CD29) was determined by flow cytometry by gating on GFP-positive cells. The gray lines indicate only control staining with secondary Abs. The filled curves show control transfected Jurkat T cells (shC), and the black line shEna/VASP transfectants. One representative experiment of three is shown.

In summary, I established a vector-based shRNA-approach to knockdown specifically Evl-I or VASP. The downregulation of Evl-I and/or VASP did not influence the expression of other members of the ADAP/SKAP55-module including its interaction partners or the surface expression of the TCR, the chemokine receptor CXCR4, or LFA-1 and VLA-4. These specific knockdowns for Evl-I and VASP allowed me to further analyze the relevance of Ena/VASP proteins for T-cell adhesion and migration.

3.6.2 Functional role of Ena/VASP proteins upon TCR stimulation

3.6.2.1 Ena/VASP proteins are crucial for LFA-1- and VLA-4-mediated T-cell adhesion

Previous studies showed that the ADAP/SKAP55-module and RIAM regulate TCR-mediated adhesion to ICAM-1 and fibronectin (Kliche et al., 2006; Lafuente et al., 2004; Ménasché et al., 2007; Wang et al., 2007). Considering that Evl-I and VASP are part of the ADAP/SKAP55/RIAM-module (**Fig. 20**), I asked whether Ena/VASP proteins contribute to TCR-mediated T-cell adhesion. To address this question, I performed a static adhesion assay to analyze TCR-mediated adhesion to ICAM-1. Transfected cells were stimulated with anti-CD3 mAbs (TCR), phorbol ester (PMA), or manganese chloride ($MnCl_2$). PMA activates Protein kinase C, induces T-cell adhesion, and was therefore used as an alternative agonist. The binding of Mn^{2+} to the cation-binding site of integrins leads to a structural change within the integrin and thus induces its active conformation (Campbell and Humphries, 2011) independent of TCR-mediated signaling pathways.

Neither downregulation of Evl-I nor VASP affected TCR-mediated adhesion to ICAM-1 compared to control-transfected cells (shC) (**Fig. 23A**). In contrast to the individual knockdowns of Evl-I or VASP, the absence of both Ena/VASP proteins surprisingly induced an increased TCR-mediated adhesion to ICAM-1, while basal, PMA, or $MnCl_2$ mediated adhesion were comparable to shC-transfected cells (**Fig. 23A**). To address whether the increased adhesion is only limited to LFA-1, I analyzed the adhesive capacity of VLA-4 to fibronectin upon knockdown of Evl-I or/and VASP. Similar to the increased LFA-1 binding to ICAM-1, in the absence of Ena/VASP proteins, VLA-4-mediated adhesion upon TCR triggering was also enhanced in the absence of Evl-I and VASP (**Fig. 23B**). In contrast to TCR stimulation, treatment of shEvl-I/shVASP-transfected cells with PMA or $MnCl_2$ did not reinforced T-cell adhesion to fibronectin. Again, the individual knockdown of Evl-I or VASP had no effect on adhesion to fibronectin (**Fig. 23B**). These data suggest a redundant function of Evl-I and VASP for T-cell adhesion. In addition, the knockdown of both Ena/VASP proteins increased TCR-mediated ICAM-1- and fibronectin-dependent adhesion, respectively. Thus, the data shown in **Figure 23** indicate that Ena/VASP proteins might act as negative regulators of TCR-induced LFA-1- and VLA-4-mediated T-cell adhesion.

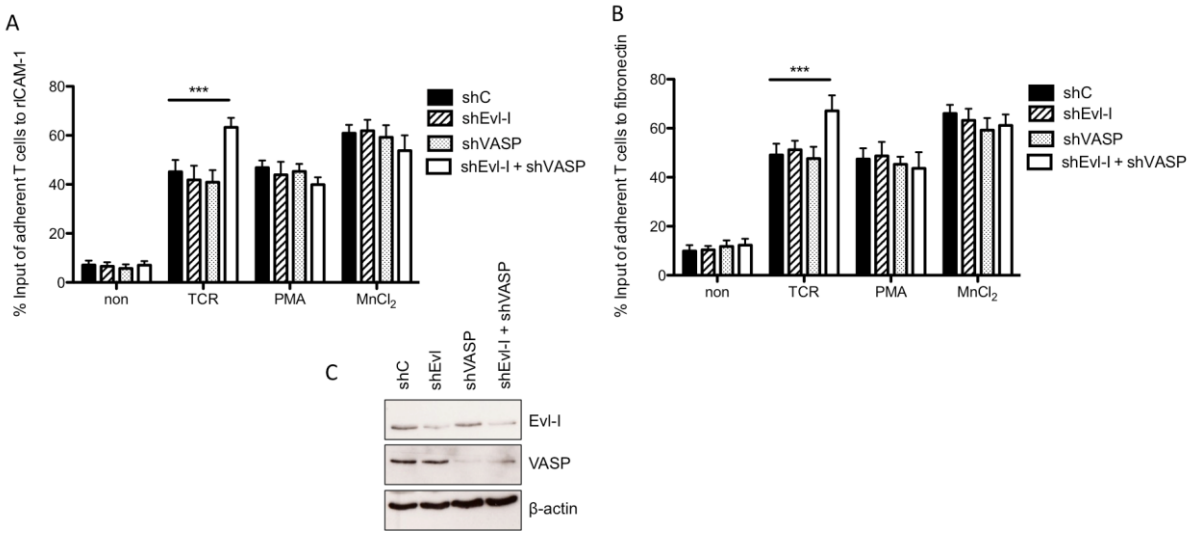

Figure 23: Increased TCR-mediated adhesion in the absence of Evl-I and VASP. Jurkat T cells were transfected with the control vector (shC) the Evl-I suppression vector (shEvl-I), the VASP suppression vector (shVASP), or the combination of shEvl-I and shVASP (shEvl-I + shVASP). After 48 h, transfectants were analyzed for their capacity to bind to **(A)** ICAM-1 or **(B)** fibronectin. Transfected Jurkat T cells were either left unstimulated (non) or stimulated with anti-CD3 mAbs (TCR), phorbol ester (PMA), or $MnCl_2$ for 30 min. The number of bound T cells was determined by counting and was calculated as the percentage of input cells. The graph summarizes the mean (SD) of three independently performed experiments (Student's t-Test ***p<0.001). **(C)** 48 h after transfection, the cells were lysed, and the lysates were analyzed for the expression of Evl-I and VASP using anti-Evl-I and anti-VASP Abs. β-actin was used as a loading control.

3.6.2.2 Relevance of Ena/VASP proteins for TCR-mediated F-actin polymerization and remodeling

It has been reported that VASP is required for F-actin polymerization *in vitro* and *in vivo* (Benz et al., 2009; Breitsprecher et al., 2011). Thus, I assessed whether changes in the F-actin polymerization and/or depolymerization account for the enhanced TCR-mediated T-cell adhesion in the absence of Ena/VASP proteins. The F-actin content was determined by flow cytometry. The mean fluorescence intensity of fluorescence labeled F-actin of untreated shC-transfected Jurkat T cells was set at 100%. The F-actin content of untreated T cells in the absence of Evl-I and/or VASP was not affected, indicating that Ena/VASP do no influence the basal F-actin content in Jurkat T cells. TCR activation led to F-actin polymerization of control-transfected Jurkat T cells within 15 min, which then decreased after 30 min of stimulation. The individual knockdown of Evl-I or VASP induced a slightly, but not significant reduced F-actin polymerization within 15 min upon TCR stimulation compared to shC-transfected Jurkat T cells (**Fig. 24**). After 30 min of TCR triggering, the F-actin content achieved near-initial amounts in the absence of the individual Ena/VASP proteins. Interestingly, the simultaneous knockdown of Evl-I and VASP significantly attenuated the amount of F-actin at 15 and 30 min after TCR triggering compared to control cells (**Fig. 24**). These data suggest a redundant function of Evl-I and VASP to control TCR-mediated F-actin polymerization and depolymerization. However, these results do not explain the enhanced

TCR-mediated adhesion to ICAM-1 and fibronectin in the absence of these proteins.

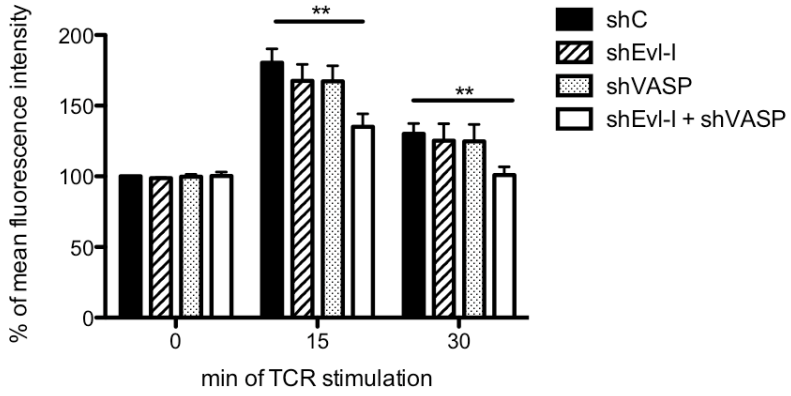

Figure 24: Attenuated TCR-mediated F-actin polymerization in the absence of Ena/VASP proteins. Jurkat T cells were transfected with control vector (shC), Evl-I suppression vector (shEvl-I), the VASP suppression vector (shVASP), or the combination of shEvl-I and shVASP (shEvl-I/shVASP). 48 h after transfection, shRNA-transfected T cells were stimulated with anti-CD3 mAbs (TCR) for the indicated times, permeabilized, fixed, and stained with Phalloidin-Alexa633 for F-actin. The amount of F-actin was determined by flow cytometry by gating on GFP-positive cells. The graph summarizes data from three independent experiments. The F-actin content was calculated as a percentage of mean fluorescence intensity relative to shC-transfected untreated T cells, which were set as 100% (n = 3, Student's t-Test **p<0.01). The represented Western blot for downregulation of Ena/VASP proteins is depicted in **Fig. 23C** since the same transfected cells were used in these experiments.

Since I observed that Ena/VASP proteins localize in the lamellipodia of T cells (**Fig. 17B/C**) and modulate F-actin polymerization and depolymerization (**Fig. 24**), I next analyzed whether the absence of Ena/VASP proteins has an influence on TCR-mediated lamellipodia formation. Lamellipodia were induced by anti-TCR Abs-coated glass slides (Bunnell et al., 2001). T-cell spreading and lamellipodia formation were determined by F-actin staining with Phalloidin-TRITC and analyzed by confocal microscopy. The pCMS4 vector system, which I used to downregulate the expression of Ena/VASP proteins, allowed me to distinguish transfected cells by the expression of the reporter protein GFP. To confirm that T-cell spreading was triggered by the specific activation of the TCR, I used anti-MHCII Abs (non) as a negative control, since these Abs do not induce T-cell spreading (**Fig. 17A**, lower panel). As shown in **Figure 25A**, middle panel, 10 min after TCR stimulation, T-cell spreading and lamellipodia formation of control-vector-transfected Jurkat T cells occurred, evidently by an enlarged cell area and a wide F-actin ring (colored in red) around the cell. This was not found in non-stimulated control-vector-transfected T cells (**Fig. 25A**, left panel). The mean cell area of 30 random T cells was quantified. TCR-stimulated control vector-transfected cells achieved a mean T-cell area of 420.8 μm^2 whereas non-stimulated T cells exhibited a mean T-cell area of only 99.3 μm^2. Individual suppression of Evl-I and VASP neither affected lamellipodia formation nor the cell areas of TCR stimulated Jurkat T cells (data not shown). In addition, areas of non stimulated T cells either transfected with suppression vector of Evl-I, or VASP were similar to non-stimulated shC-transfected T cells (data not shown). Interestingly, the knockdown of both Ena/VASP proteins led to a strong decrease in

lamellipodia formation, which then resulted in a reduced T-cell area of 293.8 µm^2 compared to control-vector transfected T cells (420.8 µm^2) (**Fig. 25B**). Note, areas of non-stimulated T cells transfected with shEvl-I/shVASP were similar to non-stimulated shC-transfected T cells (data not shown).

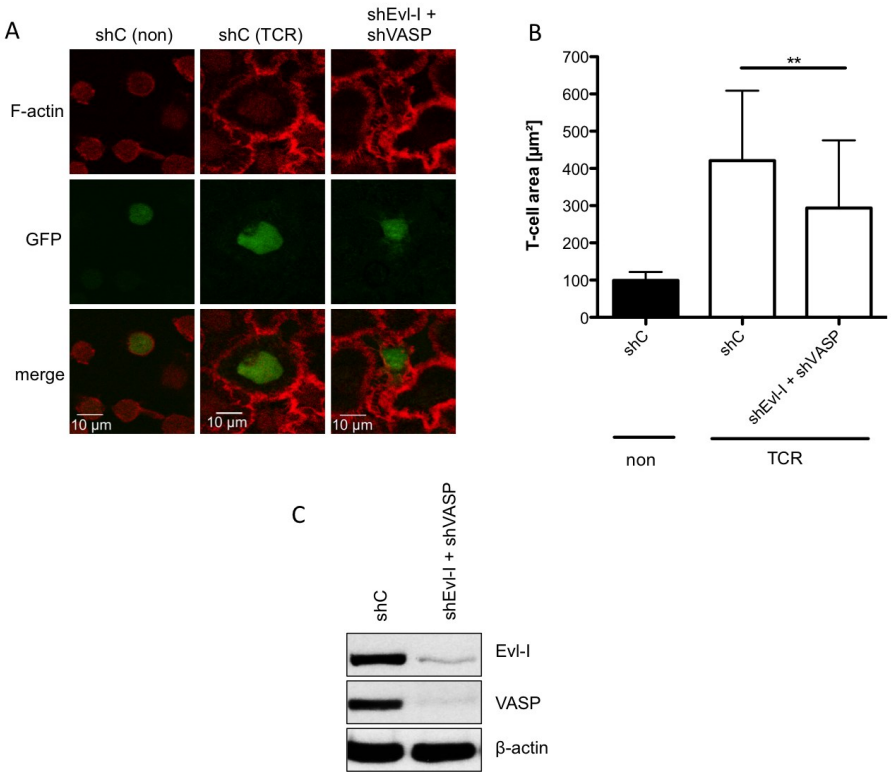

Figure 25: Loss of both Evl-I and VASP impairs lamellipodia formation of T cells. (A) Jurkat T cells were transfected with the control vector (shC) or the combination of the Evl-I and shVASP suppression vector (shEvl-I + shVASP). After 48 h of transfection, a spreading assay was performed for 10 min on anti-MHCII (non) or anti-CD3 (TCR) mAb coated poly-L-lysine slides. T cells were fixed, permeabilized, and stained with TRITC-Phalloidin (red) to visualize the F-actin. The GFP-expressing T cells were imaged by confocal microscopy. The images show a representative T cell. All images were taken with the same magnification. **(B)** Quantification of T cell area from 30 T cells for each transfection and conditions. The data represent the mean (±SD) of two independent experiments (Student's t-Test **p<0.01). **(C)** 48 h after transfection, the cells were lysed, and lysates were analyzed for the expression of Evl-I and VASP using anti-Evl-I and anti-VASP Abs. β-actin was used as a loading control.

This result clearly demonstrates the Ena/VASP proteins possess TCR-mediated F-actin modulating function in T cells. These proteins control F-actin polymerization and depolymerization. Thereby, Ena/VASP proteins might modulate lamellipodia formation, which is probably crucial for the establishment of the IS (Chhabra and Higgs, 2007).

3.6.2.3 Defective T cell-APC interaction in the absence of Ena/VASP proteins

The polymerization of F-actin, the formation of lamellipodia, and the interaction of LFA-1 with ICAM-1 are crucial for the establishment and stabilization of T cell-APC interactions (Sims and Dustin, 2002; Burkhardt et al., 2008). Due to the discrepancy that the absence of Ena/VASP proteins increased LFA-1-mediated T-cell adhesion but attenuated T-cell

spreading and the F-actin content upon TCR stimulation, I investigated whether the absence of Ena/VASP alters conjugate formation. Superantigen (SA)-non loaded and loaded fluorescence-labeled Raji B cells (APC) were incubated with shRNA-transfected GFP-expressing Jurkat T cells for 30 or 60 min. The formation of T cell-APC conjugates was determined using flow cytometry. In the absence of SA, about 10% of conjugates of shC- or shEvl-I + shVASP-transfected cells with Raji B cells were detected (**Fig. 26**). However, shC-transfected Jurkat T cells formed stable conjugates (approx. 50-60%) with SA-loaded Raji B cells after 30 and 60 min of incubation. In contrast to the enhanced TCR-mediated adhesion in the absence of Evl-I and VASP, the suppression of Ena/VASP proteins led to a two-fold decrease of conjugate formation (**Fig. 26**). The individual knockdown of Evl-I or VASP had no effect on the interaction with SA-loaded B cells (data not shown). The simultaneous knockdown of Evl-I and VASP in T cells decreased T cell-APC interactions, which suggests that the defective F-actin reorganization (**Fig. 26**) might be more important than the enhanced LFA-1-mediated T-cell adhesion (**Fig. 26**) for stable conjugate formation. Therefore, it seems that F-actin dynamics are crucial for IS formation and stabilization, independent of LFA-1-mediated adhesion.

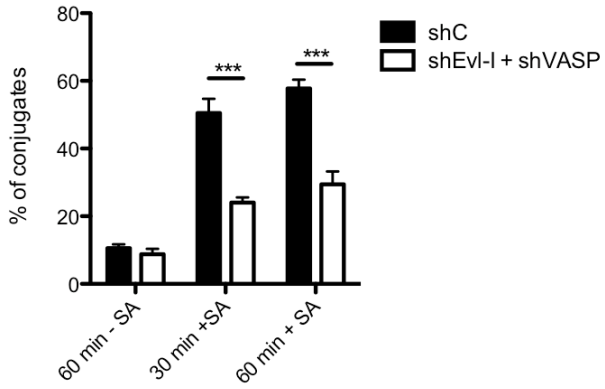

Figure 26: Diminished conjugate formation in the absence of Ena/VASP proteins. Jurkat T cells were transfected with the control vector (shC) or the combination of shEvl-I and shVASP (shEvl-I/shVASP). 48 h after transfection, equal numbers of transfected Jurkat T cells were incubated for 30 and 60 min without superantigen (-SA) or with SA-loaded (+SA) DDAO-SE-labeled Raji B cells. The percentage of double-positive conjugates was determined by flow cytometry. The graph summarizes the mean (SD) of three independently performed experiments (Student's t-Test ***p<0.001). The represented Western blot, which shows the knockdown of Evl-I/VASP, is presented in **Fig. 25C** because the same transfected cells were used in this study.

3.6.3 Requirement of Ena/VASP proteins for CXCR4-mediated F-actin dynamics, adhesion, and migration

F-actin remodeling is a key factor in cell migration processes (Rottner and Stradal, 2011). As shown in **Figure 24 and 25**, Ena/VASP proteins control TCR-mediated F-actin dynamics. Therefore, I addressed whether Evl-I and VASP are involved in chemokine-mediated F-actin polymerization and depolymerization. As described in Section 3.6.2.2, the suppression of

Evl-I and VASP had no effect on basal F-actin content in resting T cells. Compared to control-vector-transfected cells (shC), the level of F-actin content in cells deficient for both Evl-I and VASP was significantly reduced after 5 min of CXCR4 stimulation. After 15 min of CXCR4 triggering, the F-actin content in the absence of Ena/VASP proteins reached nearly basal levels and was significantly reduced compared to control cells (**Fig. 27B**). Individual suppression of Evl-I or VASP did not affect the basal F-actin content or upon CXCR4 stimulation (data not shown). As observed in response to TCR stimulation, Evl-I and VASP play a redundant role in the regulation of F-actin polymerization and depolymerization in the response to CXCR4 triggering. In conclusion, Ena/VASP proteins control CXCR4-mediated as well as TCR-induced F-actin polymerization and depolymerization (**Fig. 24**).

Next, I investigated whether the reduced CXCR4-mediated F-actin content has an effect on CXCR4-mediated T-cell adhesion. Jurkat T cells were transfected with the control vector (shC) and were left untreated or stimulated with CXCL12 or $MnCl_2$. CXCL12 and $MnCl_2$ stimulation of shC-transfected cells led to enhanced adhesion to ICAM-1 and fibronectin. In contrast to TCR triggering, suppression of Evl-I and VASP did not affect CXCL12-mediated adhesion to ICAM-1 and fibronectin (**Fig. 27C/D**). In conclusion, Ena/VASP proteins increases TCR-mediated but not CXCR4-mediated adhesion, under the assumption that Ena/VASP proteins may regulate TCR-driven LFA-1 and VLA-4 but not chemokine-mediated integrin activation.

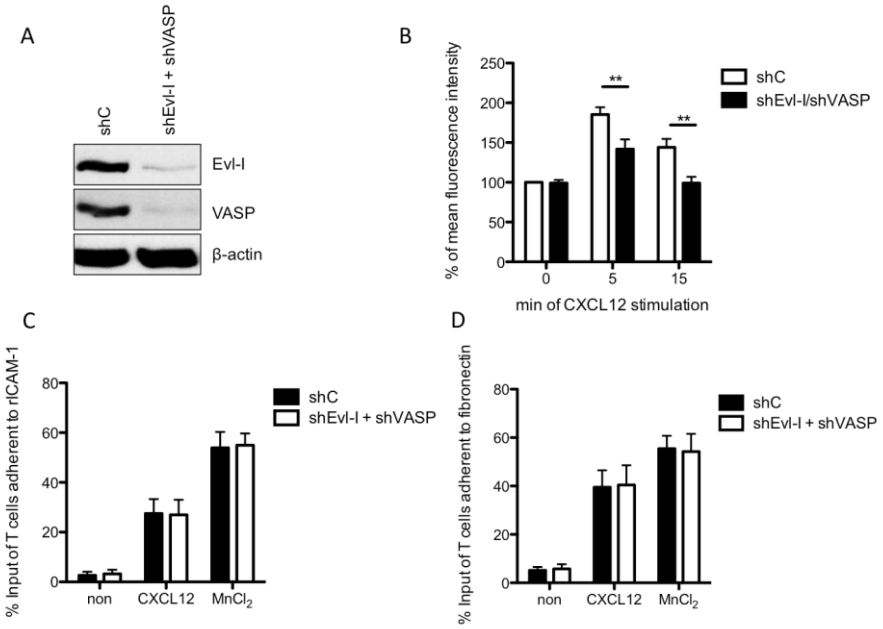

Figure 27: Impaired F-actin polymerization, but unaltered T-cell adhesion in the absence of Ena/VASP proteins upon CXCR4 stimulation. Jurkat T cells were transfected with the control vector (shC) or the combination of shEvl-I and shVASP (shEvl-I/shVASP). **(A)** 48 h after transfection, the cells were lysed, and the lysates were analyzed for the expression of Evl-I and VASP using anti-Evl-I and anti-VASP Abs. β-actin was used as a loading control. **(B)** After 48 h of transfection, shRNA-transfected T cells were stimulated with CXCL12 for the indicated times, permeabilized, fixed, and stained with Alexa633-Phalloidin to visualize F-actin. The amount of F-actin in GFP-expressing cells was determined by flow cytometry. The graph summarizes the data from three independent experiments. The F-actin content is shown as the percentage of F-actin in shC-transfected untreated T cells, which was set at 100 % (Student's t-Test **p<0.01). **(C and D)** 48 h after transfection, an adhesion assay was used to analyze whether Ena/VASP-suppressed Jurkat T cells are able to adhere to **(C)** ICAM-1 or **(D)** fibronectin. Transfected Jurkat T cells were either left unstimulated (non) or were stimulated with CXCL12 or $MnCl_2$ for 30 min and analyzed for their adhesive capacity. The number of bound T cells was determined by counting the adherent cells and is expressed as the percentage of the input cells. The data represent the mean (±SD) of three independent experiments.

It has been shown that Ena/VASP proteins regulate cell migration of various cell types such as fibroblasts, endothelial cells, and neutrophils (Bear et al., 2000; Eckert and Jones, 2007; García Arguinzonis et al., 2002; Schlegel and Waschke, 2009). Hence I investigated whether Ena/VASP proteins control T-cell migration in response to CXCL12 in a Transwell system. To this end, the migration capacity of Ena/VASP-suppressed Jurkat T cells was analyzed on ICAM-1 and fibronectin-coated Transwells. The basal migration of untreated shC- and shEvl-I/shVASP-co-transfected T cells was comparable on ICAM-1- and fibronectin-coated Transwells (**Fig. 28A/B**). Supplementation of CXCL12 in the lower chamber induced CXCL12-dependent T-cell migration of shC-transfected T cells. Similar to shC-transfected cells, suppression of Evl-I and VASP did not reduced the CXCL12-mediated migratory capacity of Jurkat T cells either on ICAM-1- or fibronectin-coated Transwells (**Fig. 28A/B**). These data indicate that Ena/VASP proteins are not required for the CXCR4-mediated Transwell migration of Jurkat T cells.

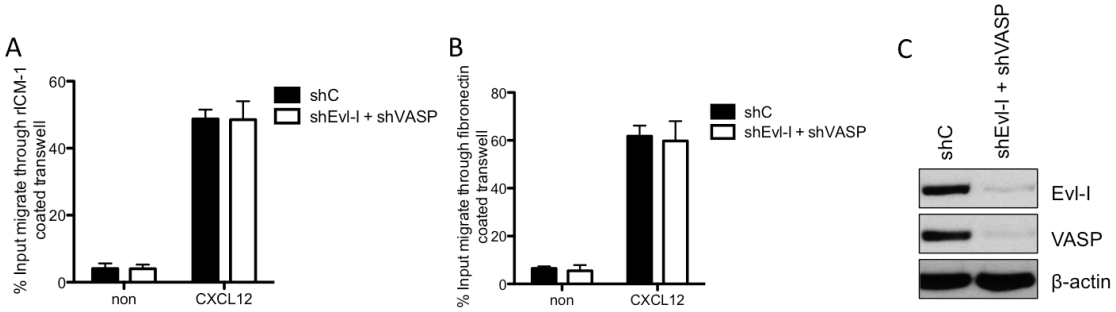

Figure 28: Ena/VASP proteins do not facilitate CXCR4-mediated Transwell migration. Jurkat T cells were transfected with the control vector (shC) or the combination of shEvl-I and shVASP (shEvl-I + shVASP). After 48 h of transfection, transfected Jurkat T cells were placed into the upper part of Transwell chambers coated with either recombinant ICAM-1 **(A)** or fibronectin **(B)**. The cells were incubated either in the absence or the presence of CXCL12 in the lower chamber for 2.5 h. The number of migrated T cells in the lower chamber was counted and calculated as the percentage of input cells. The data represent the mean (±SD) of three independent experiments. **(C)** 48 h after transfection, the cells were lysed, and the lysates were analyzed for the expression of Evl-I and VASP using anti-Evl-I and anti-VASP Abs. β-actin was used as a loading control.

In summary, the functional analyses of Ena/VASP proteins for TCR- or CXCR4-mediated signaling pathways required for adhesion, migration, and F-actin dynamics suggest that Evl-I and VASP have redundant roles in T-cells. I have shown that Evl-I and VASP act as negative regulators of TCR-mediated adhesion. In contrast to T-cell adhesion, Ena/VASP proteins were identified as positive regulators for TCR-mediated F-actin dynamics. Since both activated integrins and F-actin dynamics are involved in IS formation and stabilization, it was surprising to find that the absence of Ena/VASP proteins decreased the number of cells forming stable conjugates with B cells as APCs. These findings suggest an unexpected possibility that F-actin dynamics play a key role in IS formation, independently of enhanced LFA-1-mediated adhesion. In addition, I showed that Ena/VASP proteins control chemokine-mediated F-actin polymerization and depolymerization. Surprisingly, the reduced F-actin content in response to CXCR4 triggering did not affect LFA-1- and VLA-4-mediated adhesion or T-cell migration using a Transwell assay. Whether this is due to a differentially regulated signaling pathway upon TCR or chemokine stimulation is unclear and should be investigated in future studies.

4 Discussion

The extravasation of naïve T cells into SLOs such as lymph nodes or the spleen is essential for the induction of an adaptive immune response against foreign antigens (Chaplin, 2006; Ward and Marelli-Berg, 2009). T cells enter the lymph node via the specialized HEVs. It has generally been accepted that lymphocyte migration through HEVs involves the subsequent steps of rolling, adhesion, migration on and transmigration through the endothelium, and navigation within the T-cell zone. These processes are mediated by several families of molecules, including selectins, chemokines, and integrins like LFA-1 (Hogg et al., 2011; Schmidt et al., 2012). Chemokine-mediated T-cell adhesion and migration involve an interplay between signaling pathways leading to LFA-1 activation and/or actin remodeling (**Fig. 1**) (Burkhardt et al., 2008; Hogg et al., 2011). Before naïve T cells enter the lymph nodes they circulate in the bloodstream and roll along the vessel wall, a process that is mediated by selectins (Lawrence et al., 1997). Endothelium-bound CCL21, which binds to the chemokine receptor CCR7, leads to the activation of LFA-1 on naïve T cells (Hogg et al., 2011; Ward and Marelli-Berg, 2009). This enables T cells to adhere to the endothelium, polarize, and crawl along the endothelium. The T lymphocytes then squeeze between the endothelial cells to enter the underlying tissue and migrate within the T-cell zone in search of APCs (Burkhardt et al., 2008; Schmidt et al., 2012). The T cell-APC interaction, which is based on the interaction of the TCR with peptide-MHC-complexes, induces a corresponding signal that activates T cells. The individual interactions between T cells and APCs strongly depend on the activation of LFA-1. The conformational change of LFA-1 after TCR (or CCR7) triggering increases its affinity for ICAM-1 and facilitates clustering of LFA-1. Due to the interaction between ICAM-1 and LFA-1, a co-stimulatory signal is transmitted into the T cells, thereby driving activation, differentiation, and proliferation (Hogg et al., 2011).

The ADAP/SKAP55-module is known to regulate chemokine-mediated LFA-1 adhesion, migration, and activation of LFA-1 by affinity and avidity modulation *ex vivo* (Horn et al., 2009; Kliche et al., 2012; Parzmair et al. 2017). Therefore, in the first part of my thesis, I addressed whether the ADAP/SKAP55-module is required for T-cell homing *in vivo* and, moreover, which step(s) of T-cell extravasation is/are controlled by this module under shear flow *ex vivo*. In the course of this work, it became apparent that the ADAP/SKAP55-module is involved in the stable adhesion of T cells to the endothelium, polarization, and crawling. The polarization of cells depends on the rearrangement of the F-actin cytoskeleton (Chhabra and Higgs, 2007), and I showed that the chemokine-mediated F-actin content is reduced in the absence of the ADAP/SKAP55-module. Members of the Ena/VASP family such as Evl and VASP have been identified to interact with ADAP and RIAM (Krause et al., 2000; Lafuente et al., 2004; Lehmann et al., 2009). Since I observed that human primary T cells

and Jurkat T cells express the isoform Evl-I, I confirmed that Evl-I like Evl and VASP interacts with the ADAP/SKAP55/RIAM-module. Ena/VASP proteins are involved in F-actin reorganization in different cellular systems (Bear et al., 2000, 2002; Lambrechts et al., 2000; Lanier et al., 1999; Reinhard et al., 1992; Rottner et al., 2001). To my knowledge, not much is known whether the Ena/VASP proteins regulate the TCR or chemokine signaling events for adhesion and migration of T cells. I addressed this question in the second part of my thesis.

4.1 Function of the ADAP/SKAP55-Module in T-Cell Extravasation into SLOs

4.1.1 The ADAP/SKAP55-module is required for stable adhesion to the endothelium *in vivo* and *ex vivo*

Since T cells without ADAP expression exhibit a defective adhesion upon chemokine stimulation *ex vivo* (Horn et al., 2009; Kliche et al., 2012; Parzmair et al., 2017), I first asked whether the reduced adhesive capacity could affect the homing of ADAP$^{-/-}$ T cells into the lymph node (LN). *In vivo* analysis revealed a defective homing capacity of both ADAP-deficient CD4^{+} and CD8^{+} T cells to this organ after two hours of adoptive transfer (**Fig. 9A**). Intravital microscopy was used to study the interaction of T cells with the intranodal vessel wall *in vivo*. By using this technique, I observed reduced number of stably arrested ADAP$^{-/-}$ T cells compared to WT T cells (**Fig. 10**).

This defective adhesion with the vessel walls could explain why ADAP$^{-/-}$ T cells show a delayed entry into LNs. While my data showed a clear impairment in LN-homing after two hours of adoptive transfer, it was somehow unexpected that after 18 hours, most of the cells had found their way into these organs (**Fig. 9A**). My data are in line with previously published data of Mitchell and colleagues, who have also observed a delayed homing of ADAP$^{-/-}$ CD4^{+} T cells to LNs (Mitchell et al., 2013). In their experimental setup, four to eight hours after injection of WT and ADAP$^{-/-}$ CD4^{+} T cells, reduced numbers of ADAP$^{-/-}$ T cells were found in LNs (Mitchell et al., 2013). In contrast, twelve hours after injection, similar numbers of WT and ADAP$^{-/-}$ T cells were detected in LNs as observed in my experiments (**Fig. 9A**). This suggests that ADAP$^{-/-}$ T cells have the capability to home to the lymph nodes but probably require more time. ADAP$^{-/-}$ T cells need 24 h to refill these organs because they adhere less strongly to HEVs of the LNs compared to WT T cells (**Fig. 10 and 11**; Kliche et al., 2012) and therefore might have first to overcome a critical point of stable arrest prior to transmigrate to LN at later time.

By using shear flow experiments on primary endothelial cell monolayers, pMBMEC, surfaces, *ex vivo*, I confirmed that ADAP deficiency diminishes the adhesion of T cells to the endothelium (**Fig. 11**). Furthermore, I observed that ADAP$^{-/-}$ T cells did not polarize, crawled less on the endothelium, and showed reduced (although not significant) transmigration through the endothelial layer (**Fig. 13A**). Similar to my data, Lek and colleagues also observed that the diapedesis of T cells through the endothelium is slightly reduced in the absence of the ADAP/SKAP55-module under shear flow. In contrast to my work, ADAP-deficient T cells in their experimental set up adhered equally in comparison to WT T cells under shear flow (San Lek et al., 2013). The reason for this discrepancy could be that I have used naïve T cells, but Lek and colleagues performed their shear flow experiments with preactivated T cells (San Lek et al., 2013). What is striking, however, is how Lek and colleagues generated these preactivated ADAP$^{-/-}$ T cells. These cells were stimulated with anti-CD3 antibodies, and the preactivated cells were maintained in the presence of exogenous of IL-2. Previous studies showed that ADAP deficiency in T cells strongly attenuates proliferation, upregulation of CD25 and CD69, and IL-2 release upon CD3 or CD3/CD28 stimulation (Griffiths et al., 2001; Mueller et al., 2007; Peterson et al., 2001). Furthermore, the addition of exogenous IL-2 did not rescue the ADAP-dependent proliferation defect (Peterson et al., 2001), suggesting that it is probably difficult to generate preactivated ADAP-deficient T cells under these stimulation conditions. However, it is not clear what type of preactivated ADAP$^{-/-}$ T cells described by Lek et al. was used in their study leading to their adherent phenotype (San Lek et al., 2013). One possible experimental approach to answer the question whether preactivated ADAP$^{-/-}$ T cells have a similar phenotype for adhesion and migration as preactivated WT T cells would be to stimulate naïve ADAP-deficient T cells with PMA plus ionomycin. Under these stimulation conditions, ADAP-deficient T cells similar to WT T cells showed a proliferative behavior (Peterson et al., 2001).

As depicted in **Figure 20**, ADAP is constitutively associated in a multi-protein complex consisting of SKAP55, RIAM, RAPL, Mst1, Kindlin-3, Talin, and Rap1 to regulate integrin function (**Fig. 20**). The functional relevance of these proteins for T-cell homing to LNs and adhesion to the HEVs *in vivo* is summarized in **Table 14.** Similar to ADAP$^{-/-}$ T cells, attenuated short-term homing (1-2 hours) of T cells lacking RIAM, RAPL, Mst1, Talin, or Rap1 was detected (**Table 14**). In contrast to ADAP$^{-/-}$ T cells, Kindlin-3-deficient T cells had a long-term homing defect to LNs. The reason for this discrepancy is unknown. Only Rap1- and RAPL-deficient T cells were used for intravital microscopy studies to assess their capability to adhere to the HEVs *in vivo* (Ebisuno et al., 2010). Here, the studies from the group of T. Kinashi observed a phenotype similar to the one I have found for ADAP$^{-/-}$ T cells.

Obviously, it would be interesting to investigate RAPL$^{-/-}$, Rap1$^{-/-}$, RIAM$^{-/-}$, Mst1$^{-/-}$, or Talin$^{-/-}$ T cells in a similar experimental setup as used in my studies for naïve ADAP$^{-/-}$ T cells to see if they would enter LNs with a similar delay as I have found for T cells deficient in the ADAP/SKAP55-module.

Table 14: Summary of main findings on the migration and adhesive properties of RAPL$^{-/-}$, RIAM$^{-/-}$, Mst1$^{-/-}$, Rap1$^{-/-}$, Kindlin-3$^{-/-}$, Talin and ADAP$^{-/-}$ T cells

	Homing (< 2h)	Homing (> 2h)	Adhesion to HEVs *in vivo*	Shear resistance adhesion on endothelial monolayer *in vitro*
RAPL	decreased numbers of cells (Katagiri et al., 2004)	n.i.*	decreased numbers of stably arrested cells (Ebisuno et al., 2010)	decreased numbers of stably arrested cells (Katagiri et al., 2004)
RIAM	decreased numbers of cells (Su et al., 2015)	n.i.*	n.i.*	n.i.*
Mst1	decreased numbers of cells (Katagiri et al., 2009)	n.i.*	n.i.*	decreased numbers of stably arrested cells (Katagiri et al., 2009)
Rap1	decreased numbers of cells (Su et al., 2015)	n.i.*	decreased numbers of stably arrested cells (Ishihara et al., 2015)	decreased numbers of stably arrested cells (Ishihara et al., 2015)
Kindlin-3	n.i.*	decreased numbers of cells (Morrison et al., 2013)[1]	n.i.*	decreased numbers of stably arrested cells (Moretti et al., 2013)[1]
Talin	decreased numbers of cells (Wernimont et al., 2011)	n.i.*	n.i.*	n.i.*
ADAP	decreased numbers of cells (in this study (Mitchell et al., 2013)	not affected (Kliche et al., 2012, Mitchell et al., 2013)	decreased numbers of stably arrested cells (in this study)	decreased numbers of stably arrested cells (in this study)

* n.i. (not investigated); [1]preactivated T cells

In **Table 14,** I have also summarized the function of these molecules for shear resistance adhesion to endothelial cells *ex vivo*. With the exception of RIAM and Talin (not

investigated), all interaction partners of the ADAP/SKAP55-module showed a defect for adhesion on endothelial cells under shear flow. Here it is important to note that in addition to the activation status of T cells (preactivated Kindlin-3$^{-/-}$ T cells), various endothelial cell types were used to study shear resistance adhesion but also diapedesis under shear flow *ex vivo*. Kinashi's lab (study of Rap1, RAPL, and Mst 1) used a mouse brain capillary endothelial cell line (MBEC4) because these cells efficiently support transmigration (Shimonaka et al., 2003), whereas Moretti *et al.* (study of Kindlin-3 (Moretti et al., 2013) and I performed the experiments with primary mouse brain microvascular endothelial cells (pMBMECs) that were freshly isolated from the blood-brain barrier and that less sufficiently support transmigration (Steiner et al., 2011). Therefore, it cannot be excluded that these two cell types have different characteristics with respect to the tightness of the cell layer and expression of tight junction molecules, which both influence T-cell crawling and transmigration (Watanabe et al., 2013). For example, Steiner et al. demonstrated the differences between pMBMECs and a mouse brain endothelioma cell line (bEND5). The diapedesis of T cells across the pMBMECs was dramatically reduced compared to bEND5, which was due to differences in the F-actin architecture and the tight junction organization of these cells. BEND5 cells failed to establish a restrictive permeability barrier similar to the pMBMECs layer *ex vivo* (Steiner et al., 2011). To gain comparable insights into the function of ADAP, RIAM, Kindlin-3, Talin, RAPL, Mst1, and Rap1 for crawling and diapedesis *ex vivo*, it would be necessary to study T cells (either naïve or preactivated) that lack the expression of these molecules on the same endothelial cell monolayer, preferably on HEVs isolated from LNs.

Besides the homing of T cells to LNs, I also analyzed the homing capacity of ADAP$^{-/-}$ T cells for navigation to the spleen. In contrast to my data, which shows an altered homing of ADAP$^{-/-}$ T cells to the spleen (**Fig. 9**), Mitchell *et al.* did not observe an attenuated homing of ADAP$^{-/-}$ T cells to the spleen (Mitchell et al., 2013). The reason for this conflicting data is unclear. However, Mitchell and colleagues used ADAP$^{-/-}$ mice on a BALB/c background for their studies (Mitchell et al., 2013), whereas I used ADAP$^{-/-}$ mice on a C57/BL6 background for my experiments. Therefore, it is possible that differences in the genetic background of the mice used for the adoptive transfer of T cells could account for the attenuated migratory behavior of T lymphocytes to the spleen.

In contrast to the well-studied events of T-cell interactions with HEVs, very little is known about the molecules and processes involved in lymphocyte migration to the spleen. The spleen does not contain any HEV-like vessels, but it is described that T and B cells can enter the white pulp from the marginal sinus (Kraal, 1992; Girard and Springer, 1995). Similar to T-cell homing to LNs, the migration of lymphocytes into the white pulp of the spleen requires

the chemokine receptor CCR7 and G-proteins coupled to this receptor (Cyster and Goodnow, 1995; Förster et al., 1999; Potsch et al., 1999). In contrast to the integrin-dependent navigation of T cells to LNs or the Peyers patches, the inhibition of integrins or their substrates by the addition of blocking antibodies or by using knockout mice lacking integrin expression for members of the β2-, α4-, or α4β7 had no effect on lymphocyte entry to the spleen (Berlin-Rufenach et al., 1999; Kraal et al., 1995; Nolte et al., 2002). These data suggest that probably another unknown receptor(s) is (are) required to mediate the entry of T cells into the spleen.

Similar to ADAP, the two interaction partners of the ADAP/SKAP55-module RAPL and Mst1 are required for T-cell extravasation to the spleen (Katagiri et al., 2004, 2009). Both RAPL and Mst1 are involved in the regulation of actin dynamics/structures (Katagiri et al., 2006, 2009) since the polarization of T cells is attenuated in the absence of Mst1 or RAPL upon chemokine stimulation (Katagiri et al., 2006, 2009). These data are consistent with ADAP-deficiency in T cells since I observed defects in chemokine-induced actin remodeling (such as polarization and F-actin polymerization/depolymerization, see **Fig. 13 and 14**). In addition, loss of known regulators of actin dynamics like the GTPases Rac, WASP, and WIP in T cells showed reduced capability to home into this organ (Faroudi et al., 2010; Gallego et al., 2006). Therefore, it may be possible that integrin- and actin-dependent processes are required for T-cell homing to the LN, whereas chemokine-induced actin-regulating pathways regulate the entry into the spleen independently of integrin activation/binding modulated by ADAP, Mst1, and RAPL.

4.1.2 The ADAP/SKAP55-module regulates actin cytoskeleton reorganization

Figure 29 summarizes my findings and suggests that ADAP deficiency (i) leads to reduced stable arrest of T cells at the endothelium, including defective T-cell polarization and crawling and (ii) leads to altered F-actin polymerization/depolymerization. These integrins and/or actin-dependent phenotypes are probably the main causes of the reduced T-cell homing to lymph nodes and the spleen.

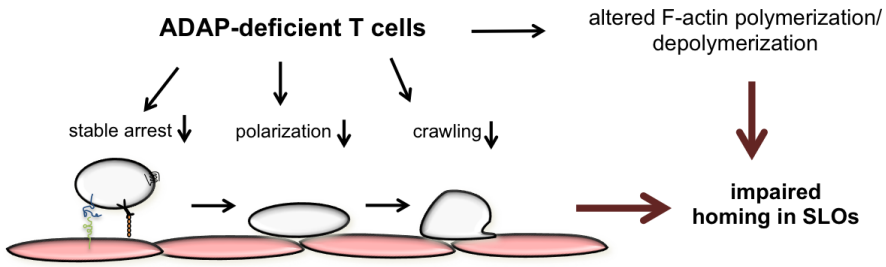

Figure 29: ADAP$^{-/-}$ T cells show attenuated short-term-homing in SLOs and F-actin reorganization. Analysis of ADAP$^{-/-}$ T cells has shown that the absence of the ADAP/SKAP55-module impairs CCL21-mediated stable arrest on HEVs, cell polarization, and crawling. Moreover, the absence of ADAP alters the F-actin dynamics in CCL21 stimulation. These data suggest that the impaired LFA-1-dependent stable arrest, polarization, crawling, and altered F-actin reorganization are major causes of the observed impaired homing of ADAP$^{-/-}$ T cells to SLOs *in vivo*.

Previously, it was shown that knockdown of ADAP in peripheral human blood T lymphocytes diminishes the activation of the GTPase Rac upon CXCR4 triggering (Dios-Esponera et al., 2015). The Rac GTPase is a well-known regulator of cytoskeleton remodeling (Iden and Collard, 2008; Mun and Jeon, 2012). The family of Rac GTPases includes Rac1, Rac2, and Rac3, whereby the former two isoforms are expressed in T cells (Faroudi et al., 2010). Faroudi and colleagues showed that Rac1 and Rac2 are crucial for chemokine-mediated F-actin polymerization, T-cell adhesion, and migration (Faroudi et al., 2010). Similar to ADAP$^{-/-}$ T cells, lymphocytes without Rac1 and Rac2 showed impaired adhesion to ICAM-1 and F-actin polymerization. Moreover, the migration of those knockout cells is diminished by the CCL21 and CXCL12 stimulation *ex vivo*. T-cell homing studies revealed that Rac1 and Rac2 are involved in homing of lymphocytes to LNs and the spleen one hour after adoptive transfer. After 20 hours, however, similar amounts of WT and Rac$^{-/-}$ T cells were found in the spleen and the peripheral LN (Faroudi et al., 2010). These data indicated that the ADAP/SKAP55 signaling module might regulate F-actin polymerization upon CCL21 and CCXL12 stimulation via Rac activation in T cells. Further experiments are necessary to prove and to confirm whether the loss of the ADAP/SKAP55-module diminishes CCL21/CXCL12-mediated Rac activation.

In addition to Rac, ADAP is connected to Ena/VASP proteins (Coppolino et al., 2001; Krause et al., 2000; Lehmann et al., 2009), which have been described to regulate F-actin polymerization (Krause et al., 2003; Kwiatkowski et al., 2003). Therefore, it is also possible that these proteins contribute to attenuated F-actin polymerization/depolymerization as found for ADAP$^{-/-}$ T cells in response to chemokine stimulation. The relevance of these Ena/VASP proteins for these processes is discussed in the following section.

4.2 The Role of Ena/VASP Proteins for T-Cell Adhesion and Migration

4.2.1 Ena/VASP proteins are associated with the ADAP/SKAP55/RIAM-complex and localize at the rim and within lamellipodia

ADAP and RIAM are associated with the Ena/VASP proteins Evl and VASP (Krause et al., 2000; Lafuente et al., 2004; Lehmann et al., 2009). Moreover, Ena/VASP proteins are involved in F-actin dynamics, probably in the process of F-actin polymerization (Bear et al., 2002; Breitsprecher et al., 2011). In this part of my thesis, I have shown that the isoform of Evl, namely Evl-I, is predominantly expressed in human T cells, whereas Evl and Evl-I are co-expressed in mouse T and B cells (**Fig. 15**). Whether these two isoforms of Evl have redundant function in murine lymphocytes requires further investigations. Since only Evl-I is found in human T cells, I speculated that Evl-I might be a binding partner for ADAP and RIAM, as it was previously reported for Evl (Lafuente et al., 2004; Lehmann et al., 2009). Indeed, as depicted in **Figures 19 and 20** Evl-I as well as VASP are constitutively associated with ADAP and RIAM in the ADAP/SKAP55/RIAM-module in human T cells.

The core sequence of the EVH1-binding site within ADAP and RIAM is the F/Y/L/WPPPP motif (Niebuhr et al., 1997). Within the ADAP protein, four of these binding motives are proposed (Krause et al., 2000). Krause et al. found that the interaction of ADAP with VASP is mediated by the F_{616}PPPP-motif (Krause et al., 2000). In contrast to ADAP, RIAM contains two putative EVH1-binding sites within the N-terminal PRR, whereas the C-terminal PRR contains five EVH1-binding sites (Coló et al., 2012; Lee et al., 2009). The high number of these EVH1-binding motifs within RIAM could explain this, while I found exclusively that these Ena/VASP proteins are bound to the ADAP/SKAP55/RIAM-module (11 EVH1-binding sites) and not to the ADAP/SKAP55/RAPL-module (4 EVH1-binding site). Obviously, further interaction studies are required to answer the question of which of these motifs within RIAM is/are involved in the interaction with Ena/VASP proteins.

Localization of Ena/VASP proteins

My analysis of the localization of Ena/VASP proteins revealed that Evl-I and VASP are localized to the IS of T/B cell conjugates. The IS is characterized by an accumulation of F-actin (lamellipodia formation) at the contact zone between T and B cells (Yokosuka and Saito, 2010) and here both Ena/VASP proteins co-localized with F-actin (**Fig. 16**). Using a TCR-mediated spreading assay, which mimics the lamellipodia formation within the IS (Bunnell et al., 2001), revealed that both Evl-I and VASP localize at the rim of the lamellipodia and co-localize with F-actin within lamellipodial structures (**Fig. 17B/C**). These two localizations of Ena/VASP proteins are consistent with several reports in other cellular

systems, demonstrating that these proteins can be visualized within the lamellipodia and/or at the rim of F-actin structure below the plasma membrane (Gomez et al., 2007; Kwiatkowski et al., 2003; Lambrechts et al., 2000; Reinhard et al., 1992).

Similar to Ena/VASP proteins, their interaction partners ADAP, SKAP55, and RIAM are localized below the plasma membrane at the rim of the lamellipodium and within the lamellipodial structures (**Fig 18**). To explain the localization at the plasma membrane, our group has previously shown that the presence of the ADAP/SKAP55-module is mandatory for the recruitment of RIAM to the plasma membrane (Ménasché et al., 2007). The following model for the TCR-mediated recruitment of the ADAP/SKAP55/RIAM-module to the plasma membrane has been proposed: TCR triggering activates the Src kinases Lck and Fyn. In turn, Lck activates ZAP-70, which subsequently phosphorylates the adapter proteins LAT and SLP76 (Horejsí et al., 2004). Together with the small cytosolic adapter, Gads SLP76 and LAT will provide a signaling platform for the recruitment of ADAP. In this scenario, the two tyrosine YDDV motifs of ADAP (Y595 and Y651) become phosphorylated by the Src kinase Fyn (Raab et al., 1999; Veale et al., 1999) and mediate an inducible interaction with the SH2 domain of SLP76 (**see Fig. 30**). When these two tyrosine residues have mutated, the capability of ADAP to facilitate TCR-mediated activation of LFA-1 is reduced (Wang et al., 2003, 2004). Moreover, the loss of SLP76 by RNAi attenuates the recruitment of the ADAP/SKAP55/RIAM-module to the plasma membrane (Horn et al., 2009). Therefore, I assume that RIAM serves as an F/Y/L/WPPPP-ligand-binding protein within the ADAP/SKAP55-module to target these Ena/VASP proteins to the plasma membrane via the inducible interaction with SLP76/Gads/LAT.

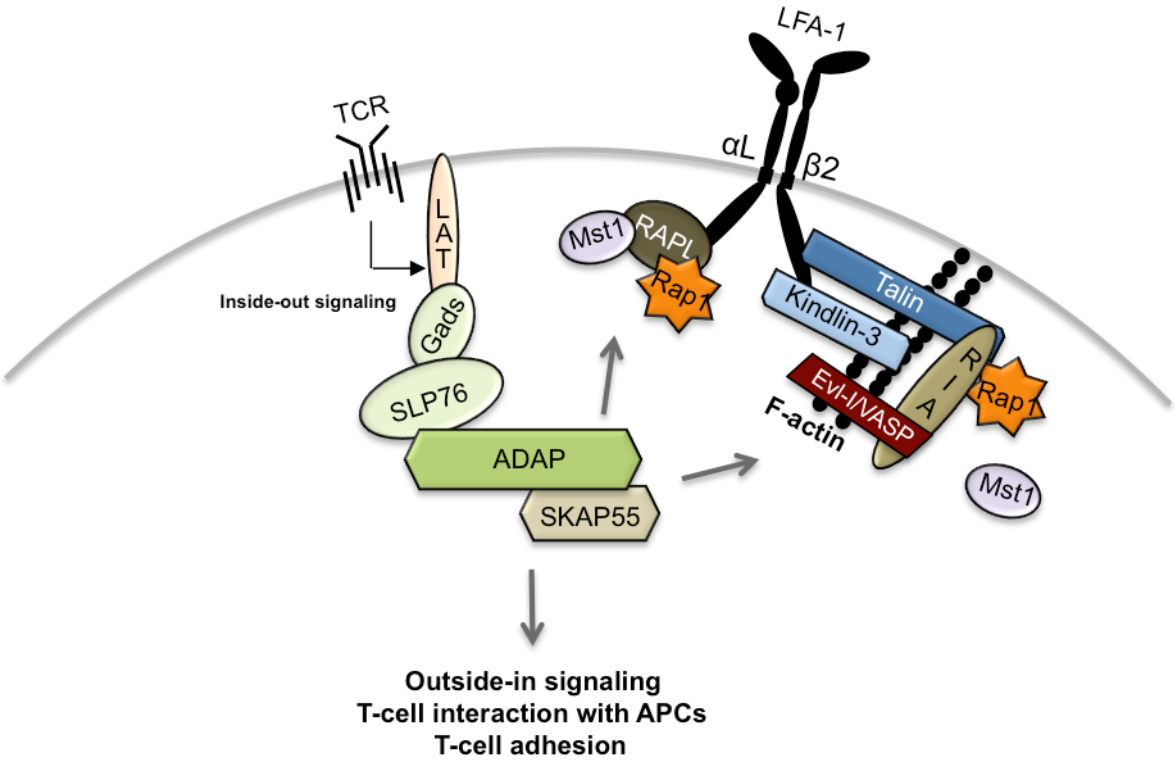

Figure 30: Model how Evl-I and VASP are recruited to the plasma membrane upon TCR-stimulation. Stimulation of the TCR induces inside-out signaling, leading to LFA-1 activation. The ADAP/SKAP55-module plays a pivotal role in providing a platform for several signaling molecules at the plasma membrane by an inducible association with SLP76/Gads/LAT. Inside-out signaling is characterized by the association of the ADAP/SKAP55-module with either RAPL/Mst1/Rap1 linked to the α-chain of LFA-1 or RIAM/Rap1/Mst1/Kindlin-3/Talin/Evl-I/VASP linked to the β-chain of LFA-1 (Kliche et al., 2012). The TCR-mediated activation of LFA-1 then leads to outside-in signaling, which promotes adhesion and T-cell interactions with APCs. The presence of Ena/VASP proteins within the RIAM/Rap1/Mst1/Kindlin-3/Talin-module initiates F-Actin polymerization at the plasma membrane. Adapted and modified from Witte and colleagues (Witte et al., 2012).

The co-localization of Ena/VASP proteins with F-actin within the lamellipodia can be explained by direct interaction of these proteins via their EVH2 domain, which contains an F-actin-binding site. *In vitro* studies on the EVH2 domain of VASP showed that this domain is involved in direct F-actin binding (Bachmann et al., 1999). To my knowledge, neither ADAP, SKAP55, nor RIAM directly interacts with F-actin. Therefore, I speculate that the direct interaction of Ena/VASP proteins with F-actin allows recruitment together with its interaction partners ADAP, SKAP55, and RIAM to the lamellipodia as depicted in **Figures 17 and 18**. However, the signaling pathways or molecules that promote or help the ADAP/SKAP55/RIAM-module, together with the Ena/VASP proteins for positioning within the lamellipodial structures of T cells, clearly require further investigations.

4.2.2 The relevance of Ena/VASP proteins for TCR- and CXCR4-mediated adhesion and migration of T cells

To further investigate the role of Evl-I and VASP for T-cell adhesion and migration, I have established a shRNA-mediated suppression system to knockdown the expression of either

Evl-I or VASP in Jurkat T cells. Individual suppression of Evl-I or VASP did not alter TCR- and chemokine-mediated integrin activation or F-actin dynamics. Only the simultaneous knockdown of Evl-I and VASP revealed a role of these proteins for integrin activation and the actin cytoskeleton in Jurkat T cells. Therefore, the functional studies I have done for my thesis are based on the double knockdown of Evl-I and VASP in T cells, and I now use the term: Ena/VASP proteins.

4.2.2.1 Altered TCR-mediated function of T cells in the absence of Ena/VASP proteins

In this section, I focused on the role of Ena/VASP proteins for TCR-mediated signaling events leading to actin cytoskeleton rearrangements, interaction with APCs, and adhesion. The contribution of these proteins for these functional processes will be discussed below. The data from this paragraph are summarized in **Figure 31**.

The role of Ena/VASP proteins for TCR-regulated F-actin dynamics and T-cell interaction with APCs

As depicted in **Figure 24,** I observed that suppression of Ena/VASP proteins reduces the TCR-mediated F-actin polymerization. In addition, the loss of these proteins attenuated the formation of lamellipodia as shown by microscopic studies using a TCR-mediated spreading assay (**Fig. 25**).

Several *in vivo* and *in vitro* studies have identified different mechanisms by which Ena/VASP proteins regulate F-actin dynamics. These mechanisms include F-actin polymerization, actin-filament branching, F-actin filament bundling, and actin filament nucleation for lamellipodia and filopodia formation (Bear and Gertler, 2009). Depending on their localization (see **Fig. 17**), Ena/VASP proteins can have two different functions to regulate F-actin dynamics in T cells, such as F-actin polymerization and the frequency of F-actin branching. F-actin polymerization is initiated at the rim of lamellipodia below the plasma membrane (Pollard and Borisy, 2003). *In vitro* studies have shown that Ena/VASP proteins promote F-actin elongation, suggesting that they may participate in the F-actin polymerization at the rim (Barzik et al., 2005). *In vivo*, the mechanism by which Ena/VASP proteins regulate F-actin polymerization is based on the findings of Breitsprecher and colleagues (Breitsprecher et al., 2008, 2011). Here, VASP localizes at the plasma membrane, through the interaction of its EVH1 domain, with its binding partners and facilitates actin filament elongation. The tetramerization of VASP produces a protein complex in which one VASP molecule of four molecules binds to the elongated actin filament via its EVH2 domain. The other three VASP molecules contain a free EVH2 domain that recruits actin monomers for the actin filament, increasing the amount of F-actin (Breitsprecher et al., 2008, 2011).

Obviously, additional experiments are necessary to image the impact of Ena/VASP proteins on TCR-mediated F-actin dynamics. Total internal reflection fluorescence (TIRF) microscopy enables selective visualization of surface regions such as the plasma membrane and individual molecules within living cells (Fish, 2009). GFP-tagged LifeAct can be used to visualize F-actin dynamics in living cells using TIRF microscopy. This 17-amino acid peptide, which is linked to GFP, stains F-actin structures in eukaryotic cells and does not interfere with actin dynamics *ex vivo* (Riedl et al., 2008). With this tool, I can examine whether the presence of Ena/VASP proteins is necessary for the initiation of F-actin polymerization at the rim. Besides F-actin polymerization, the addition of actin monomers to the barbed ends of branched actin filaments at the rim generates a pushing force that drives the F-actin network inward (termed as F-actin flow) which could be affected in the absence of Ena/VASP proteins in TCR-mediated spreading of T cells.

In contrast to the rim, lamellipodia represent branched actin networks. In fibroblasts, Bear and colleagues observed that the absence of Ena/VASP proteins at the plasma membrane leads to shorter but highly branched actin filaments, whereas the presence of Ena/VASP proteins at the plasma membrane induces long and more sparsely branched actin filaments (Bear et al., 2002). These data suggest that Ena/VASP proteins regulate the length and branching of actin filaments, indicating that these proteins are involved in the assembly and/or turnover of actin filaments within the lamellipodia. It would be of interest to perform electron microscopy studies to analyze the architecture of the actin network, in particular, the structure of the branched actin filaments in a TCR-mediated spreading assay in the presence and absence of Ena/VASP proteins.

Due to the defective TCR-mediated F-actin dynamics in the absence of Ena/VASP proteins, it was not surprising to find that the loss of these proteins attenuated the T-cell interaction with APCs (**Fig. 26**). The interaction of an APC with a T cell initiates F-actin polymerization in the periphery of the contact zone followed by a centripetal retrograde F-actin flow to the cSMAC (Babich et al., 2012; Yi et al., 2012). TCR-mediated signaling in the contact zone is initiated by microclusters containing surface receptors such as the TCR and downstream signaling molecules like SLP76 (Nguyen et al., 2008). Newly generated microclusters arise in the periphery of the IS and translocate via the F-actin flow to the cSMAC (Bunnell et al., 2002; Lee et al., 2002; Yokosuka et al., 2005). Therefore, it is possible that Ena/VASP proteins, similar to WAVE2 and the Arp2/3 complex, direct the polymerization of newly synthesized (or branched) F-actin filaments to push the F-actin network to flow inward to the cSMAC (Nolz et al., 2006, 2007, 2008)

The role of Ena/VASP proteins for TCR-mediated static adhesion to ICAM-1 and fibronectin

In contrast to the attenuated T-cell interaction with APCs, it was very surprising that the loss of Ena/VASP in Jurkat T cells had enhanced TCR-mediated adhesion for both integrins VLA-4 and LFA-1 (**Fig. 23**). These data suggest that Ena/VASP proteins act as negative regulators for integrin activation. Similar to my data, a previous study has shown that VASP acts as a negative regulator of platelet adhesion, leading to enhanced β3-mediated adhesion of platelets in VASP$^{-/-}$ mice *in vitro* (Aszódi et al., 1999). In contrast to this study, Massberg and colleagues showed that increased platelet adhesion *in vivo* to the vascular endothelium in VASP$^{-/-}$ mice is not caused by the loss of VASP in platelets (Massberg et al., 2004). The authors hypothesized that the presence of VASP in the vascular cells is necessary to control the platelet-endothelial cell interaction (Massberg et al., 2004). In addition to platelets, LFA-1-mediated neutrophil adhesion is diminished in the absence of VASP *ex vivo* (Deevi et al., 2010). In contrast to neutrophils, Estin and colleagues observed no defect in shear-resistant adhesion of preactivated Evl/VASP double knockout (dko) CD4+ T cells (Estin et al., 2017). These controversial data indicate that the functional relevance of Ena/VASP proteins for adhesion processes may vary in different immune cell types in response to the different stimuli and assay systems used to study adhesion.

The reduction of Ena/VASP proteins led to strongly enhanced static TCR-mediated adhesion to ICAM-1 and fibronectin in Jurkat T cells (**Fig. 23**). Currently, I cannot explain how the loss of Ena/VASP proteins led to an increase in TCR-mediated adhesion. How Ena/VASP proteins enhance TCR-mediated adhesion in T cells clearly requires further investigation. T-cell adhesion is regulated by affinity modulation and/or clustering of LFA-1 and VLA-4 in response to TCR stimulation. The conformational changes (affinity regulation) of these two integrins could be analyzed by KIM127 and mAb24 for LFA-1 and by HUTS4 mAb for VLA-4 binding using flow cytometry. These antibodies recognize epitopes in the headpiece that are accessible when these integrins are in the intermediate or high-affinity conformation (Hogg et al., 2011; Mould et al., 2003).

It might also be possible that the lack of Ena/VASP proteins releases LFA-1 and VLA-4 from the cytoskeleton. This, in turn, could increase the mobility of these integrins to facilitate clustering (avidity modulation) and promote adhesion. In support of this hypothesis, a low dose of Cytochalasin D, an inhibitor that interferes with F-actin polymerization, increases LFA-1-mediated leukocyte adhesion to its ligand (van Kooyk et al., 1999; Lub et al., 1997; Stewart et al., 1998; Yu et al., 2010). This increased adhesion is due to enhanced LFA-1 clustering on the plasma membrane without affecting the affinity regulation of LFA-1 (van Kooyk et al., 1999). The authors proposed that LFA-1 clusters are formed in response to

their release from cytoskeletal constraints (probably due to Talin and/or Kindlin-3, both proteins interact with LFA-1 and F-actin) to enhance adhesion. Immunoprecipitation studies could confirm whether Talin and/or Kindlin-3 are not bound to LFA-1 and VLA-4 upon reduction of Ena/VASP protein expression in TCR-stimulated Jurkat T cells.

Whether the loss of these Ena/VASP proteins led to enhanced integrin affinity modulation with or without integrin clustering in response to TCR stimulation could also be analyzed by confocal microscopy (Horn et al., 2009; Kliche et al., 2012). This latter technique could also be used to address whether these integrin clusters contain activated integrins. With these experiments, it might be possible to address whether the reduction of Ena/VASP proteins expression in Jurkat T cells causes integrin clustering independent or dependently of affinity regulation of integrins.

4.2.2.2 Altered chemokine-mediated functions of T cells in the absence of Ena/VASP proteins

Similar to TCR-mediated actin polymerization, the CXCL12-mediated F-actin content was impaired by reducing the Ena/VASP protein expression in T cells (**Fig. 27**). Using a Transwell migration assay, this diminished F-actin polymerization neither affects the CXCL12-mediated static adhesion (**Fig. 27**) nor the migration of T cells (**Fig. 28**). These findings are in line with a previously published report by Estin and colleagues. Preactivated T cells from Evl/VASP dko mice lead to reduced chemokine-mediated F-actin polymerization, and these T cells show no defective chemotaxis in a Transwell assay (Estin et al., 2017).

Estin and colleagues also showed that preactivated Evl/VASP dko $CD4^+$ T cells are competent in shear-resistant adhesion and migration on endothelial cells but show impaired T-cell diapedesis *ex vivo* (Estin et al., 2017). This observation was unexpected as they noticed that the deletion of Evl and VASP decreases the expression of the α4-subunit (CD49d) of β1-integrins and increases the αL-subunit (CD11a) of β2-integrins on the T-cell surface. This reduced α4β1 expression leads to an attenuated affinity modulation of this integrin. However, this defective affinity modulation did not account for adhesion but rather for the diapedesis of T-cells. These findings are very unique for known actin cytoskeleton regulators.

In contrast to naïve ADAP-deficient T cells, unfortunately, the absence of these Ena/VASP proteins in naïve T cells did not interfere with lymphocyte homing to the spleen and LNs (Estin et al., 2017). A possible explanation for this phenotype would be that naïve Evl/VASP dko T cells exhibit normal F-actin polymerization in response to CCL21 stimulation (Estin et

al., 2017). Unfortunately, Evl/VASP dko T cells were not analyzed for their properties to adhere with HEVs *in vivo* or in an adhesion assay for ICAM-1 *ex vivo*. However, these data indicate that ADAP-dependent signaling pathways regulating F-actin dynamics are probably not dependent on Ena/VASP proteins in **naïve** T cells.

Summary

Because ADAP interacts with Ena/VASP proteins (Krause et al., 2000; Lehmann et al., 2009), which are described to modulate F-actin dynamics in various cellular systems (Bear et al., 2000, 2002; Lambrechts et al., 2000; Lanier et al., 1999; Reinhard et al., 1992; Rottner et al., 2001), and because their functional role of Ena/VASP proteins in T cells is not fully understood, I analyzed whether these proteins are involved in the F-actin reorganization in T cells. I showed that the actin-binding proteins Evl-I and VASP in response to TCR and CXCR4 stimulation also influence F-actin polymerization/depolymerization in Jurkat T cells (**Fig. 31**). My data suggest that Ena/VASP proteins are negative regulators of TCR-mediated adhesion but positive regulators with respect to actin remodeling upon TCR stimulation and interaction with APCs (**Fig. 31**). The defective F-actin polymerization/depolymerization at loss of Evl-I and VASP upon chemokine stimulation did not correlate with attenuated migration or adhesion (**Fig. 31**). With this in mind, it appears that, depending on the stimuli, differences in actin rearrangement/dynamics may account for adhesion and functional outcome in Jurkat T cells.

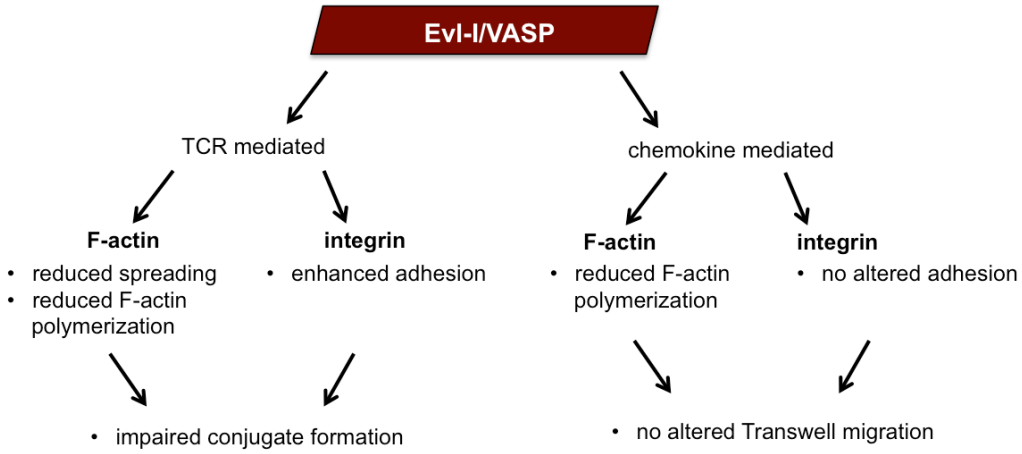

Figure 31: Various TCR- and chemokine-mediated functions of Ena/VASP proteins in T cells. The analysis of Jurkat T cells without either Evl-I or VASP revealed no functional role in terms of F-actin dynamics, adhesion, and migration of T cells. Due to this fact, the double knockdown of Evl-I and VASP indicated a redundant function of these proteins. Upon TCR-stimulation, simultaneous knockdown of Evl-I and VASP resulted in reduced spreading and F-actin polymerization, whereas the LFA-1- and VLA-4-mediated adhesion was enhanced compared to control cells. I have also shown that conjugate formation is attenuated in the absence of Ena/VASP proteins. Upon chemokine stimulation, however, only the F-actin polymerization was diminished. I did not observe any alteration in β1- and β2-integrin-mediated adhesion or Transwell migration suggesting a different function of Ena/VASP proteins within these two signaling pathways.

References

Ahern-Djamali, S.M., Comer, A.R., Bachmann, C., Kastenmeier, A.S., Reddy, S.K., Beckerle, M. ary C., Walter, U., and Hoffmann, F.M. (1998). Mutations in Drosophila enabled and rescue by human vasodilator-stimulated phosphoprotein (VASP) indicate important functional roles for Ena/VASP homology domain 1 (EVH1) and EVH2 domains. Mol. Biol. Cell *9*, 2157–2171.

Ahern-Djamali, S.M., Bachmann, C., Hua, P., Reddy, S.K., Kastenmeier, A.S., Walter, U., and Hoffmann, F.M. (1999). Identification of profilin and src homology 3 domains as binding partners for Drosophila Enabled. Proc. Natl. Acad. Sci. *96*, 4977–4982.

Alon, R., Feigelson, S.W., Manevich, E., Rose, D.M., Schmitz, J., Overby, D.R., Winter, E., Grabovsky, V., Shinder, V., Matthews, B.D., et al. (2005). Alpha4beta1-dependent adhesion strengthening under mechanical strain is regulated by paxillin association with the alpha4-cytoplasmic domain. J. Cell Biol. *171*, 1073–1084.

Arbonés, M.L., Ord, D.C., Ley, K., Ratech, H., Maynard-Curry, C., Otten, G., Capon, D.J., and Tedder, T.F. (1994). Lymphocyte Homing and Leukocyte Rolling and Migration Are Impaired in L-Selectin-Deficient Mice. Immunity *1*, 247–260.

Aszódi, A., Pfeifer, A., Ahmad, M., Glauner, M., Zhou, X.H., Ny, L., Andersson, K.E., Kehrel, B., Offermanns, S., and Fässler, R. (1999). The vasodilator-stimulated phosphoprotein (VASP) is involved in cGMP- and cAMP-mediated inhibition of agonist-induced platelet aggregation, but is dispensable for smooth muscle function. EMBO J. *18*, 37–48.

Babich, A., Li, S., O'Connor, R.S., Milone, M.C., Freedman, B.D., and Burkhardt, J.K. (2012). F-actin polymerization and retrograde flow drive sustained PLCγ1 signaling during T cell activation. J. Cell Biol. *197*, 775–787.

Bachmann, C., Fischer, L., Walter, U., and Reinhard, M. (1999). The EVH2 domain of the vasodilator-stimulated phosphoprotein mediates tetramerization, F-actin binding, and actin bundle formation. J. Biol. Chem. *274*, 23549–23557.

Barzik, M., Kotova, T.I., Higgs, H.N., Hazelwood, L., Hanein, D., Gertler, F.B., and Schafer, D.A. (2005). Ena/VASP proteins enhance actin polymerization in the presence of barbed end capping proteins. J. Biol. Chem. *280*, 28653–28662.

Bear, J.E., and Gertler, F.B. (2009). Ena/VASP: towards resolving a pointed controversy at the barbed end. J. Cell Sci. *122*, 1947–1953.

Bear, J.E., Loureiro, J.J., Libova, I., Fässler, R., Wehland, J., and Gertler, F.B. (2000). Negative regulation of fibroblast motility by Ena/VASP proteins. Cell *101*, 717–728.

Bear, J.E., Svitkina, T.M., Krause, M., Schafer, D.A., Loureiro, J.J., Strasser, G.A., Maly, I. V., Chaga, O.Y., Cooper, J.A., Borisy, G.G., et al. (2002). Antagonism between Ena/VASP proteins and actin filament capping regulates fibroblast motility. Cell *109*, 509–521.

Benz, P.M., Blume, C., Seifert, S., Wilhelm, S., Waschke, J., Schuh, K., Gertler, F.B., Münzel, T., and Renné, T. (2009). Differential VASP phosphorylation controls remodeling of the actin cytoskeleton. J. Cell Sci. *122*, 3954–3965.

Berlin-Rufenach, C., Otto, F., Mathies, M., Westermann, J., Owen, M.J., Hamann, A., and Hogg, N. (1999). Lymphocyte Migration in Lymphocyte Function-associated Antigen (LFA)-1–deficient Mice. J. Exp. Med. *189*, 1467–1478.

Bertoni, A., Tadokoro, S., Eto, K., Pampori, N., Parise, L. V., White, G.C., and Shattil, S.J. (2002). Relationships between Rap1b, affinity modulation of integrin αIIbβ3 and the actin cytoskeleton. J. Biol. Chem. *277*, 25715–25721.

Bivona, T.G., Wiener, H.H., Ahearn, I.M., Silletti, J., Chiu, V.K., and Philips, M.R. (2004). Rap1 up-regulation and activation on plasma membrane regulates T cell adhesion. J. Cell Biol. *164*, 461–470.

von Boehmer, H. (2005). Mechanisms of suppression by suppressor T cells. Nat. Immunol. *6*, 338–344.

Bos, J.L. (2005). Linking Rap to cell adhesion. Curr. Opin. Cell Biol. *17*, 123–128.

Bos, J.L., de Bruyn, K., Enserink, J., Kuiperij, B., Rangarajan, S., Rehmann, H., Riedl, J., de Rooij, J., van Mansfeld, F., and Zwartkruis, F. (2003). The role of Rap1 in integrin-mediated cell adhesion. Biochem. Soc. Trans. *31*, 83–86.

Breitsprecher, D., Kiesewetter, A.K., Linkner, J., Urbanke, C., Resch, G.P., Small, J.V., and Faix, J. (2008). Clustering of VASP actively drives processive, WH2 domain-mediated actin filament elongation. EMBO J. *27*, 2943–2954.

Breitsprecher, D., Kiesewetter, A.K., Linkner, J., Vinzenz, M., Stradal, T.E.B., Small, J.V., Curth, U., Dickinson, R.B., and Faix, J. (2011). Molecular mechanism of Ena/VASP-mediated actin-filament elongation. EMBO J. *30*, 456–467.

Bunnell, S.C., Kapoor, V., Trible, R.P., Zhang, W., and Samelson, L.E. (2001). T Cell Receptor – Induced Spreading : A Role for the Signal Transduction Adaptor LAT. Immunity *14*, 315–329.

Bunnell, S.C., Hong, D.I., Kardon, J.R., Yamazaki, T., McGlade, C.J., Barr, V.A., and Samelson, L.E. (2002). T cell receptor ligation induces the formation of dynamically regulated signaling assemblies. J. Cell Biol. *158*, 1263–1275.

Burbach, B.J., Srivastava, R., Medeiros, R.B., O'Gorman, W.E., Peterson, E.J., and Shimizu, Y. (2008). Distinct Regulation of Integrin-Dependent T Cell Conjugate Formation and NF-κB Activation by the Adapter Protein ADAP. J. Immunol. *181*, 4840–4851.

Burbach, B.J., Srivastava, R., Ingram, M.A., Mitchell, J.S., and Shimizu, Y. (2011). The Pleckstrin Homology Domain in the SKAP55 Adapter Protein Defines the Ability of the Adapter Protein ADAP To Regulate Integrin Function and NF-κB Activation. J. Immunol. *186*, 6227–6237.

Burkhardt, J.K., Carrizosa, E., and Shaffer, M.H. (2008). The actin cytoskeleton in T cell activation. Annu. Rev. Immunol. *26*, 233–259.

Butt, E., Abel, K., Krieger, M., Palm, D., Hoppe, V., Hoppe, J., and Walter, U. (1994). cAMP- and cGMP-dependent protein kinase phosphorylation sites of the focal adhesion vasodilator-stimulated phosphoprotein (VASP) in vitro and in intact human platelets. J. Biol. Chem. *269*, 14509–14517.

Calderwood, D.A., Campbell, I.D., and Critchley, D.R. (2013). Talins and kindlins: Partners in integrin-mediated adhesion. Nat. Rev. Mol. Cell Biol. *14*, 503–517.

Carl, U.D., Pollmann, M., Orr, E., Gertler, F.B., Chakraborty, T., and Wehland, J. (1999). Aromatic and basic residues within the EVH1 domain of VASP specify its interaction with proline-rich ligands. Curr. Biol. *9*, 715–718.

Chaplin, D.D. (2006). 1. Overview of the human immune response. J. Allergy Clin. Immunol. *117*, S430-5.

Chhabra, E.S., and Higgs, H.N. (2007). The many faces of actin: Matching assembly factors with cellular structures. Nat. Cell Biol. *9*, 1110–1121.

Coló, G.P., Lafuente, E.M., and Teixidó, J. (2012). The MRL proteins: Adapting cell adhesion, migration and growth. Eur. J. Cell Biol. *91*, 861–868.

Coppolino, M.G., Krause, M., Hagendorff, P., Monner, D.A., Trimble, W., Grinstein, S., Wehland, J., and Sechi, A.S. (2001). Evidence for a molecular complex consisting of Fyb/SLAP, SLP-76, Nck, VASP and WASP that links the actin cytoskeleton to Fcgamma receptor signalling during phagocytosis. J. Cell Sci. *114*, 4307–4318.

Critchley, D.R., and Gingras, A.R. (2008). Talin at a glance. J. Cell Sci. *121*, 1345–1347.

Cyster, J.G., and Goodnow, C.C. (1995). Lymphocytes into Splenic White Pulp Cords. J. Exp. Med. *182*, 581–586.

Deevi, R.K., Koney-Dash, M., Kissenpfennig, A., Johnston, J.A., Schuh, K., Walter, U., and Dib, K. (2010). Vasodilator-stimulated phosphoprotein regulates inside-out signaling of beta2 integrins in neutrophils. J. Immunol. *184*, 6575–6584.

Dios-Esponera, A., Isern de Val, S., Sevilla-Movilla, S., Garcia-Verdugi, R., Garcia-Bernal, D., Arellano-Sanchez, N., Cabanas, C., and Teixidó, J. (2015). Positive and negative regulation of SLP-76/ADAP and Pyk2 of chemokine-stimulated t lymphcyte adhesion mediated by integrin alpha4beta1. Mol. Cell. Biol. *26*, 3215–3228.

Dluzniewska, J., Zou, L., Harmon, I.R., Ellingson, M.T., and Peterson, E.J. (2007). Immature hematopoietic cells display selective requirements for adhesion- and degranulation-promoting adaptor protein in development and homeostatsis. Eur. J. Immunol. *37*, 3208–3219.

Duchniewicz, M., Zemojtel, T., Kolanczyk, M., Grossmann, S., Scheele, J.S., and Zwartkruis, F.J.T. (2006). Rap1A-deficient T and B cells show impaired integrin-mediated cell adhesion. Mol. Cell. Biol. *26*, 643–653.

Dupré, L., Houmadi, R., Tang, C., and Rey-Barroso, J. (2015). T Lymphocyte Migration : An Action Movie Starring the Actin and Associated Actors. Front. Immunol. *6*, 1–18.

Ebisuno, Y., Katagiri, K., Katakai, T., Ueda, Y., Nemoto, T., Inada, H., Nabekura, J., Okada, T., Kannagi, R., Tanaka, T., et al. (2010). Rap1 controls lymphocyte adhesion cascade and interstitial migration within lymph nodes in RAPL-dependent and -independent manners. Blood *115*, 804–814.

Eckert, R.E., and Jones, S.L. (2007). Regulation of VASP serine 157 phosphorylation in human neutrophils after stimulation by a chemoattractant. J. Leukoc. Biol. *82*, 1311–1321.

Estin, M.L., Thompson, S.B., Traxinger, B., Fisher, M.H., Friedman, R.S., and Jacobelli, J. (2017). Ena / VASP proteins regulate activated T-cell trafficking by promoting diapedesis during transendothelial migration. PNAS *114*, E2901–E2910.

Faroudi, M., Hons, M., Zachacz, A., Dumont, C., Lyck, R., Stein, J. V., and Tybulewicz, V.L.J. (2010). Critical roles for Rac GTPases in T cell migration to and within lymph nodes. Blood *116*, 5536–5547.

Fish, K.N. (2009). Total Internal Reflection Fluorescence (TIRF) Microscopy. Curr Protoc Cytom 1–21.

Förster, R., Schubel, A., Breitfeld, D., Kremmer, E., Renner-Müller, I., Wolf, E., and Lipp, M. (1999). CCR7

Coordinates the Primary Immune Response by Establishing Functional Microenvironments in Secondary Lymphoid Organs. Cell *99*, 23–33.

Gallego, M.D., de la Fuente, M.A., Anton, I.M., Snapper, S., Fuhlbrigge, R., and Geha, R.S. (2006). WIP and WASP play complementary roles in T cell homing and chemotaxis to SDF-1alpha. Int. Immunol. *18*, 221–232.

García Arguinzonis, M.I., Galler, A.B.A.B., Walter, U., Reinhard, M., Simm, A., and Garc\i a Arguinzonis, M.I. (2002). Increased Spreading , Rac / p21-activated Kinase (PAK) Activity , and Compromised Cell Motility in Cells Deficient in Vasodilator-stimulated Phosphoprotein (VASP)*. J. Biol. Chem. *277*, 45604–45610.

Geng, L., Raab, M., and Rudd, C.E. (1999). Cutting Edge: SLP-76 Cooperativity with FYB/FYN-T in the Up-Regulation of TCR-Driven IL-2 Transcription Requires SLP-76 Binding to FYB at Tyr 595 and Tyr651. J. Immunol. *163*, 5753–5757.

Germain, R.N. (2002). T-cell development and the CD4-CD8 lineage decision. Nat. Rev. Immunol. *2*, 309–322.

Gertler, F.B., Niebuhr, K., Reinhard, M., Wehland, J., and Soriano, P. (1996). Mena, a relative of VASP and Drosophila Enabled, is implicated in the control of microfilament dynamics. Cell *87*, 227–239.

Girard, J.-P., and Springer, T.A. (1995). High endothelial venules (HEVs): special enothelium for lymphocyte migration. Immunol. Today *16*, 449–457.

Gomez, T.S., and Billadeau, D.D. (2008). T cell activation and the cytoskeleton: you can't have one without the other. Adv. Immunol. *97*, 1–64.

Gomez, T.S., Hamann, M.J., McCarney, S., Savoy, D.N., Lubking, C.M., Heldebrant, M.P., Labno, C.M., McKean, D.J., McNiven, M. a, Burkhardt, J.K., et al. (2005). Dynamin 2 regulates T cell activation by controlling actin polymerization at the immunological synapse. Nat. Immunol. *6*, 261–270.

Gomez, T.S., Kumar, K., Medeiros, R.B., Shimizu, Y., Leibson, P.J., and Billadeau, D.D. (2007). Formins regulate the actin-related protein 2/3 complex-independent polarization of the centrosome to the immunological synapse. Immunity *26*, 1–10.

Griffiths, G.M. (1995). The cell biology of CTL killing. Curr. Opin. Immunol. *7*, 343–348.

Griffiths, E.K., Krawczyk, C., Kong, Y.-Y., Raab, M., Hyduk, S.J., Bouchard, D., Chan, V.S., Kozieradzki, I., Oliveira-dos-Santos, A.J., Wakeham, A., et al. (2001). Positive regulation of T cell activation and integrin adhesion by the adapter Fyb/Slap. Science (80-.). *293*, 2260–2263.

Gupton, S.L., Riquelme, D., Hughes-Alford, S.K., Tadros, J., Rudina, S.S., O.Hynes, R., Lauffenburger, D., and Gertler, F.B. (2012). Mena binds 5 integrin directly and modulates 5 1 function. J. Cell Biol. *198*, 657–676.

Halbrügge, M., Friedrich, C., Eigenthaler, M., Schanzenbächer, P., and Walter, U. (1990). Stoichiometric and reversible phosphorylation of a 46-kDa protein in human platelets in response to cGMP- and cAMP-elevating vasodilators. J. Biol. Chem. *265*, 3088–3093.

Hamamy, H., Makrythanasis, P., Al-Allawi, N., Muhsin, A.A., and Antonarakis, S.E. (2014). Recessive thrombocytopenia likely due to a homozygous pathogenic variant in the FYB gene: Case report. BMC Med. Genet. *15*, 1–5.

Hanna, S., and Etzioni, A. (2012). Leukocyte adhesion deficiencies. Ann. N. Y. Acad. Sci. *1250*, 50–55.

Harbeck, B., Hüttelmaier, S., Schlüter, K., Jockusch, B.M., and Illenberger, S. (2000). Phosphorylation of the vasodilator-stimulated phosphoprotein regulates its interaction with actin. J. Biol. Chem. *275*, 30817–30825.

Harburger, D.S., Bouaouina, M., and Calderwood, D.A. (2009). Kindlin-1 and -2 directly bind the C-terminal region of β integrin cytoplasmic tails and exert integrin-specific activation effects. J. Biol. Chem. *284*, 11485–11497.

Hart, R., Stanley, P., Chakravarty, P., and Hogg, N. (2013). The kindlin 3 pleckstrin homology domain has an essential role in lymphocyte function-associated antigen 1 (LFA-1) integrin-mediated B cell adhesion and migration. J. Biol. Chem. *288*, 14852–14862.

Hauser, W., Knobeloch, K.-P., Eigenthaler, M., Gambaryan, S., Krenn, V., Geiger, J., Glazova, M., Rohde, E., Horak, I., Walter, U., et al. (1999). Megakaryocyte hyperplasia and enhanced agonist-induced platelet activation in vasodilator-stimulated phosphoprotein knockout mice. Proc. Natl. Acad. Sci. U. S. A. *96*, 8120–8125.

Heuer, K., Kofler, M., Langdon, G., Thiemke, K., and Freund, C. (2004). Structure of a Helically Extended SH3 Domain of the T Cell Adapter Protein ADAP. Structure *12*, 603–610.

Heuer, K., Arbuzova, A., Strauss, H., Kofler, M., and Freund, C. (2005). The Helically Extended SH3 Domain of the T Cell Adaptor Protein ADAP is a Novel Lipid Interaction Domain. J. Mol. Biol. *348*, 1025–1035.

Heuer, K., Sylvester, M., Kliche, S., Pusch, R., Thiemke, K., Schraven, B., and Freund, C. (2006). Lipid-binding hSH3 Domains in Immune Cell Adapter Proteins. J. Mol. Biol. *361*, 94–104.

Hogg, N., Patzak, I., and Willenbrock, F. (2011). The insider's guide to leukocyte integrin signalling and function. Nat. Rev. Immunol. *11*, 416–426.

Horejsí, V., Zhang, W., and Schraven, B. (2004). Transmembrane adaptor proteins: organizers of immunoreceptor signalling. Nat. Rev. Immunol. *4*, 603–616.

Horn, J., Wang, X., Reichardt, P., Stradal, T.E., Warnecke, N., Simeoni, L., Gunzer, M., Yablonski, D., Schraven, B., and Kliche, S. (2009). Src homology 2-domain containing leukocyte-specific phosphoprotein of 76 kDa is mandatory for TCR-mediated inside-out signaling, but dispensable for CXCR4-mediated LFA-1 activation, adhesion, and migration of T cells. J. Immunol. *183*, 5756–5767.

Huang, Y., Norton, D.D., Precht, P., Martindale, J.L., Burkhardt, J.K., and Wange, R.L. (2005). Deficiency of ADAP / Fyb / SLAP-130 destabilizes SKAP55 in Jurkat T Cells *. J. Biol. Chem. *280*, 23576–23583.

Hynes, R.O. (2002). Integrins : Bidirectional , Allosteric Signaling Machines. Cell *110*, 673–687.

Iden, S., and Collard, J.G. (2008). Crosstalk between small GTPases and polarity proteins in cell polarization. Nat. Rev. Mol. Cell Biol. *9*, 846–859.

Ishihara, S., Nishikimi, A., Umemoto, E., Miyasaka, M., Saegusa, M., and Katagiri, K. (2015). Dual functions of Rap1 are crucial for T-cell homeostasis and prevention of spontaneous colitis. Nat. Commun. *6*, 8982.

Jobard, F., Bouadjar, B., Caux, F., Hadj-Rabia, S., Has, C., Matsuda, F., Weissenbach, J., Lathrop, M., Prud'homme, J.-F., and Fischer, J. (2003). Identification of mutations in a new gene encoding a FERM family protein with a pleckstrin homology domain in Kindler syndrome. Hum. Mol. Genet. *12*, 925–935.

Jordan, M.S., Singer, A.L., and Koretzky, G.A. (2003). Adaptors as central mediators of signal transduction in immune cells. Nat. Immunol. *4*, 110–116.

Kaizuka, Y., Douglass, A.D., Varma, R., Dustin, M.L., and Vale, R.D. (2007). Mechanisms for segregating T cell receptor and adhesion molecules during immunological synapse formation in Jurkat T cells. Proc. Natl. Acad. Sci. U. S. A. *104*, 20296–20301.

Karaköse, E., Schiller, H.B., and Fässler, R. (2010). The kindlins at a glance. J. Cell Sci. *123*, 2353–2356.

Kasirer-Friede, A., Ruggeri, Z.M., and Shattil, S.J. (2010). Role for ADAP in shear flow-induced platelet mechanotransduction. Blood *115*, 2274–2282.

Katagiri, K., and Kinashi, T. (2011). Rap1 and Integrin Inside-out Siganling. Integrin Cell Adhes. Mol. Methods Protoc. *757*.

Katagiri, K., Hattori, M., Minato, N., Irie, S., Takatsu, K., and Kinashi, T. (2000). Rap1 Is a potent activation signal for leukocyte function-associated antigen 1 distinct from Protein Kinase C and Phosphatidylinositol-3-OH. Mol. Cell. Biol. *20*, 1956–1969.

Katagiri, K., Hattori, M., Minato, N., and Kinashi, T. (2002). Rap1 functions as a key regulator of T-Cell and Antigen-Presenting Cell interactions and modulates T-Cell responses Rap1. Mol. Cell. Biol. *22*, 1001–1015.

Katagiri, K., Maeda, A., Shimonaka, M., and Kinashi, T. (2003). RAPL, a Rap1-binding molecule that mediates Rap1-induced adhesion through spatial regulation of LFA-1. Nat. Immunol. *4*, 741–748.

Katagiri, K., Ohnishi, N., Kabashima, K., Iyoda, T., Takeda, N., Shinkai, Y., Inaba, K., and Kinashi, T. (2004). Crucial functions of the Rap1 effector molecule RAPL in lymphocyte and dendritic cell trafficking. Nat. Immunol. *5*, 1045–1051.

Katagiri, K., Imamura, M., and Kinashi, T. (2006). Spatiotemporal regulation of the kinase Mst1 by binding protein RAPL is critical for lymphocyte polarity and adhesion. Nat. Immunol. *7*, 919–928.

Katagiri, K., Katakai, T., Ebisuno, Y., Ueda, Y., Okada, T., and Kinashi, T. (2009). Mst1 controls lymphocyte trafficking and interstitial motility within lymph nodes. EMBO J. *28*, 1–13.

Kinashi, T. (2005). Intracellular signalling controlling integrin activation in lymphocytes. Nat. Rev. Immunol. *5*, 546–559.

Kindler, T. (1954). Congenital poikiloderma with traumatic bulla formation and progressive cutaneous atrophy. Br. J. Dermatol. *66*, 104–111.

Kitchens, W.H., Larsen, C.P., and Ford, M.L. (2011). Integrin antagonists for transplant immunosuppression: panacea or peril? Immunotherapy *3*, 305–307.

Klapholz, B., and Brown, N.H. (2017). Talin – the master of integrin adhesions. J. Cell Sci. *130*, 2435–2446.

Klapproth, S., Sperandio, M., Pinheiro, E.M., Prünster, M., Soehnlein, O., Gertler, F.B., Fässler, R., and Moser, M. (2015). Loss of the Rap1 effector RIAM results in leukocyte adhesion deficiency due to impaired β2 integrin function in mice. Blood *126*, 2704–2712.

Kliche, S., Breitling, D., Togni, M., Pusch, R., Heuer, K., Wang, X., Freund, C., Kasirer-Friede, A., Menasche, G., Koretzky, G.A., et al. (2006). The ADAP/SKAP55 signaling module regulates T-cell receptor-mediated integrin activation through plasma membrane targeting of Rap1. Mol. Cell. Biol. *26*, 7130–7144.

Kliche, S., Worbs, T., Wang, X., Degen, J., Patzak, I., Meineke, B., Togni, M., Moser, M., Reinhold, A., Kiefer, F., et al. (2012). CCR7-mediated LFA-1 functions in T cells are regulated by 2 independent ADAP/SKAP55 modules. Blood *119*, 777–785.

Kloeker, S., Major, M.B., Calderwood, D.A., Ginsberg, M.H., Jones, D.A., and Beckerle, M.C. (2004). The Kindler Syndrome protein is regulated by transforming growth factor- ß and involved in integrin-mediated adhesion. J.

Biol. Chem. *279*, 6824–6833.

van Kooyk, Y., van Vliet, S.J., and Figdor, C.G. (1999). The actin cytoskeleton regulates LFA-1 ligand binding through avidity rather than affinity changes. J. Biol. Chem. *274*, 26869–26877.

Kraal G. (1992) Cells in the marginal zone of the spleen. Int Rev Cytol; 132:31–73

Kraal, G., Schornagel, K., Streeter, P.R., Holzmann, B., and Butcher, E.C. (1995). Expression of the mucosal vascular addressin, MAdCAM-1, on sinus-lining cells in the spleen. Am. J. Pathol. *147*, 763–771.

Krause, M., Sechi, A.S., Konradt, M., Monner, D., Gertler, F.B., and Wehland, J. (2000). Fyn-binding protein (Fyb)/SLP-76-associated protein (SLAP), ena/vasodilator-stimulated phosphoprotein (VASP) proteins and the Arp2/3 complex link T cell receptor (TCR) signaling to the actin cytoskeleton. J. Cell Biol. *149*, 181–194.

Krause, M., Dent, E.W., Bear, J.E., Loureiro, J.J., and Gertler, F.B. (2003). Ena/VASP proteins: regulators of the actin cytoskeleton and cell migration. Annu. Rev. Cell Dev. Biol. *19*, 541–564.

Kuijpers, T.W., van Bruggen, R., Kamerbeek, N., Tool, A.T.J., Hicsonmez, G., Gurgey, A., Karow, A., Verhoeven, A.J., Seeger, K., Sanal, Ö., et al. (2007). Natural history and early diagnosis of LAD-1 / variant syndrome. Blood *109*, 3529–3537.

Kuijpers, T.W., van de Vijver, E., Weterman, M.A.J., de Boer, M., Tool, A.T.J., van den Berg, T.K., Moser, M., Jakobs, M.E., Seeger, K., Sanal, Ö., et al. (2009). LAD-1 / variant syndrome is caused by mutations in FERMT3. Blood *113*, 4740–4746.

Kwiatkowski, A. V., Gertler, F.B., and Loureiro, J.J. (2003). Function and regulation of Ena/VASP proteins. Trends Cell Biol. *13*, 386–392.

Lafuente, E.M., van Puijenbroek, A.A.F.L., Krause, M., Carman, C. V., Freeman, G.J., Berezovskaya, A., Constantine, E., Springer, T.A., Gertler, F.B., and Boussiotis, V.A. (2004). RIAM, an Ena/VASP and Profilin ligand, interacts with Rap1-GTP and mediates Rap1-induced adhesion. Dev. Cell *7*, 585–595.

Lambrechts, A., Kwiatkowski, A. V., Lanier, L.M., Bear, J.E., Vandekerckhove, J., Ampe, C., and Gertler, F.B. (2000). cAMP-dependent protein kinase phosphorylation of EVL, a Mena/VASP relative, regulates its interaction with actin and SH3 domains. J. Biol. Chem. *275*, 36143.

Lanier, L.M., Gates, M.A., Witke, W., Menzies, A.S., Wehman, A.M., Macklis, J.D., Kwiatkowski, D., Soriano, P., and Gertler, F.B. (1999). Mena is required for neurulation and commissure formation. Neuron *22*, 313–325.

Lawrence, M.B., Smith, C.W., Eskin, S.G., and McIntire, L. V. (1990). Effect of venous shear stress on CD18-mediated neutrophil adhesion to cultured endothelium. Blood *75*, 227–237.

Lawrence, M.B., Kansas, G.S., Kunkel, E.J., and Ley, K. (1997). Threshold levels of fluid shear promote leukocyte adhesion through selectins (CD62L,P,E). J. Cell Biol. *136*, 717–727.

Lee, H.-S., Lim, C.J., Puzon-McLaughlin, W., Shattil, S.J., and Ginsberg, M.H. (2009). RIAM activates integrins by linking talin to ras GTPase membrane-targeting sequences. J. Biol. Chem. *284*, 5119–5127.

Lee, K.-H., Holdorf, A.D., Dustin, M.L., Chan, A.C., Allen, P.M., and Shaw, A.S. (2002). T cell receptor signaling precedes immunological synapse formation. Science (80-.). *295*, 1539–1542.

Lefort, C.T., Rossaint, J., Moser, M., Petrich, B.G., Zarbock, A., Monkley, S.J., Critchley, D.R., Ginsberg, M.H., Fässler, R., and Ley, K. (2012). Distinct roles for talin-1 and kindlin-3 in LFA-1 extension and affinity regulation. Blood *119*, 4275–4282.

Lehmann, R., Meyer, J., Schuemann, M., Krause, E., and Freund, C. (2009). A novel S3S-TAP-tag for the isolation of T-cell interaction partners of adhesion and degranulation promoting adaptor protein. Proteomics *9*, 5288–5295.

Lettau, M., Pieper, J., Gerneth, A., Lengl-Janssen, B., Voss, M., Linkermann, A., Schmidt, H., Gelhaus, C., Leippe, M., Kabelitz, D., et al. (2010). The adapter protein Nck: role of individual SH3 and SH2 binding modules for protein interactions in T lymphocytes. Protein Sci. *19*, 658–669.

Lettau, M., Kliche, S., Kabelitz, D., and Janssen, O. (2014). The adapter proteins ADAP and Nck cooperate in T cell adhesion. Mol. Immunol. *60*, 72–79.

Levin, C., Zalman, L., Tamary, H., Krasnov, T., Khayat, M., Shalev, S., Slama, I., and Koren, A. (2013). Small-platelet thrombocytopenia in a family with autosomal recessive inheritance pattern. Pediatr. Blood Cancer *60*, E128–E130.

Levin, C., Koren, a., Pretorius, E., Rosenberg, N., Shenkman, B., Hauschner, H., Zalman, L., Khayat, M., Salama, I., Elpeleg, O., et al. (2015). Deleterious mutation in the *FYB* gene is associated with congenital autosomal recessive small-platelet thrombocytopenia. J. Thromb. Haemost. *13*, 1285–1292.

Liu, J., Kang, H., Raab, M., da Silva, A.J., Kraeft, S.-K., and Rudd, C.E. (1998). FYB (FYN binding protein) serves as a binding partner for lymphoid protein and FYN kinase substrate SKAP55 and a SKAP55-related protein in T cells. Proc. Natl. Acad. Sci. U. S. A. *95*, 8779–8784.

Lub, M., van Kooyk, Y., van Vliet, S.J., and Figdor, C.G. (1997). Dual role of the actin cytoskeleton in regulating cell adhesion mediated by the integrin lymphocyte function-associated molecule-1. Mol. Biol. Cell *8*, 341–351.

Malinin, N.L., Zhang, L., Choi, J., Ciocea, A., Razorenova, O., Ma, Y.-Q., Podrez, E.A., Tosi, M., Lennon, D.P., Caplan, A.I., et al. (2009). A point mutation in KINDLIN3 ablates activation of three integrin subfamilies in humans. Nat. Med. *15*, 313–318.

Malinin, N.L., Plow, E.F., and Byzova, T. V. (2010). Kindlins in FERM adhesion. Blood *115*, 4011–4017.

Manevich, E., Grabovsky, V., Feigelson, S.W., and Alon, R. (2007). Talin 1 and Paxillin facilitate distinct steps in rapid VLA-4-mediated adhesion strengthening to vascular cell adhesion molecule 1 *. J. Biol. Chem. *282*, 25338–25348.

Marelli-Berg, F.M., Cannella, L., Dazzi, F., and Mirenda, V. (2008). The highway code of T cell trafficking. J. Pathol. *214*, 179–189.

Marie-Cardine, A., Hendricks-Taylor, L.R., Boerth, N.J., Zhao, H., Schraven, B., and Koretzky, G.A. (1998a). Molecular Interaction between the Fyn-associated Protein SKAP55 and the SLP-76-associated Phosphoprotein SLAP-130 *. J. Biol. Chem. *273*, 25789–25795.

Marie-Cardine, A., Verhagen, A.M., Eckerskorn, C., and Schraven, B. (1998b). SKAP-HOM , a novel adaptor protein homologous to the FYN-associated protein SKAP55. FEBS Lett. *435*, 55–60.

Massberg, S., Gru, S., Konrad, I., Arguinzonis, M.I.G., Eigenthaler, M., Hemler, K., Kersting, J., Schulz, C., Mu, I., Besta, F., et al. (2004). Enhanced in vivo platelet adhesion in vasodilator-stimulated phosphoprotein (VASP)–deficient mice. Hemostasis, Thromb. Vasc. Biol. *103*, 136–142.

Medeiros, R.B., Burbach, B.J., Mueller, K.L., Srivastava, R., Moon, J.J., Highfill, S., Peterson, E.J., and Shimizu, Y. (2007). Regulation of NF-kB Activation in T cells via Association of the Adapter Proteins ADAP and CARMA1. Science (80-.). *316*, 754–758.

Ménasché, G., Kliche, S., Chen, E.J.H., Stradal, T.E.B., Schraven, B., and Koretzky, G. (2007). RIAM links the ADAP/SKAP-55 signaling module to Rap1, facilitating T-cell-receptor-mediated integrin activation. Mol. Cell. Biol. *27*, 4070–4081.

Mitchell, J.S., Burbach, B.J., Srivastava, R., Fife, B.T., and Shimizu, Y. (2013). Multistage T cell-dendritic cell interactions control optimal CD4 T cell activation through the ADAP-SKAP55-signaling module. J. Immunol. *191*, 2372–2383.

Monkley, S.J., Pritchard, C.A., and Critchley, D.R. (2001). Analysis of the mammalian talin2 gene TLN2. Biochem. Biophys. Res. Commun. *286*, 880–885.

Moretti, F.A., Moser, M., Lyck, R., Abadier, M., Ruppert, R., Engelhardt, B., and Fässler, R. (2013). Kindlin-3 regulates integrin activation and adhesion reinforcement of effector T cells. Proc. Natl. Acad. Sci. *110*, 17005–17010.

Morrison, V.L., MacPherson, M., Savinko, T., San Lek, H., Prescott, A., and Fagerholm, S.C. (2013). The beta2 integrin-kindlin-3 interaction is essential for T cell homing but dispensable for T cell activation in vivo. Blood *122*, 1428–1437.

Mory, A., Feigelson, S.W., Yarali, N., Kilic, S.S., Bayhan, G.I., Gershoni-Baruch, R., Etzioni, A., and Alon, R. (2008). Kindlin-3: A new gene involved in the pathogenesis of LAD-III. Blood *112*, 2591.

Moser, M., Nieswandt, B., Ussar, S., Pozgajova, M., and Fässler, R. (2008). Kindlin-3 is essential for integrin activation and platelet aggregation. Nat. Med. *14*, 325–330.

Moser, M., Bauer, M., Schmid, S., Ruppert, R., Schmidt, S., Sixt, M., Wang, H.-V., Sperandio, M., and Fässler, R. (2009). Kindlin-3 is required for beta2 integrin-mediated leukocyte adhesion to endothelial cells. Nat. Med. *15*, 300–305.

Mould, A.P., Barton, S.J., Askari, J.A., McEwan, P.A., Buckley, P.A., Craig, S.E., and Humphries, M.J. (2003). Conformational changes in the integrin βA domain provide a mechanism for signal transduction via hybrid domain movement. J. Biol. Chem. *278*, 17028–17035.

Mueller, K.L., Thomas, M.S., Burbach, B.J., Peterson, E.J., and Shimizu, Y. (2007). Adhesin and Degranulation-Promoting Adapter Protein (ADAP) positively regulates T cell sensitivity to antigen and T cell survival. J. Immunol. *179*, 3559–3569.

Mun, H., and Jeon, T.J. (2012). Regulation of actin cytoskeleton by Rap1 binding to RacGEF1. Mol. Cells *34*, 71–76.

Musci, M.A., Hendricks-Taylor, L.R., Motto, D.G., Paskind, M., Kamens, J., Turck, C.W., and Koretzky, G.A. (1997). Molecular Cloning of SLAP-130, an SLP-76-associated Substrate of the T Cell Antigen Receptor-stimulated Protein Tyrosine Kinases. J. Biol. Chem. *272*, 11674–11677.

Nguyen, K., Sylvain, N.R., and Bunnell, S.C. (2008). T cell costimulation via the integrin VLA-4 inhibits the actin-dependent centralization of signaling microclusters containing the adaptor SLP-76. Immunity *28*, 810–821.

Niebuhr, K., Ebel, F., Frank, R., Reinhard, M., Domann, E., Carl, U.D., Walter, U., Gertler, F.B., Wehland, J., and Chakraborty, T. (1997). A novel proline-rich motif present in ActA of Listeria monocytogenes and cytoskeletal proteins is the ligand for the EVH1 domain, a protein module present in the Ena/VASP family. EMBO J. *16*, 5433–5444.

Nolte, M.A., Hamann, A., Kraal, G., and Mebius, R.E. (2002). The strict regulation of lymphocyte migration to splenic white pulp does not involve common homing receptors. Immunology *106*, 299–307.

Nolz, J.C., Gomez, T.S., Zhu, P., Li, S., Medeiros, R.B., Shimizu, Y., Burkhardt, J.K., Freedman, B.D., and Billadeau, D.D. (2006). The WAVE2 complex regulates actin cytoskeletal reorganization and CRAC-mediated calcium entry during T cell activation. Curr. Biol. *16*, 24–34.

Nolz, J.C., Medeiros, R.B., Mitchell, J.S., Zhu, P., Freedman, B.D., Shimizu, Y., and Billadeau, D.D. (2007). WAVE2 regulates high-affinity integrin binding by recruiting vinculin and talin to the immunological synapse. Mol. Cell. Biol. *27*, 5986–6000.

Nolz, J.C., Nacusi, L.P., Segovis, C.M., Medeiros, R.B., Mitchell, J.S., Shimizu, Y., and Billadeau, D.D. (2008). The WAVE2 complex regulates T cell receptor signaling to integrins via Abl- and CrkL-C3G-mediated activation of Rap1. J. Cell Biol. *182*, 1231–1244.

Obergfell, A., Judd, B.A., del Pozo, M.A., Schwartz, M.A., Koretzky, G.A., and Shattil, S.J. (2001). The molecular adapter SLP-76 relays signals from platelet integrin αIIbβ3 to the actin cytoskeleton. J. Biol. Chem. *276*, 5916–5923.

Ohkura, N., Kitagawa, Y., and Sakaguchi, S. (2013). Development and maintenance of regulatory T cells. Immunity *38*, 414–423.

Parzmair, G.P., Gereke, M., Haberkorn, O., Annemann, M., Podlasly, L., Kliche, S., Reinhold, A., Schraven, B., and Bruder, D. (2017). ADAP plays a pivotal role in CD4+ T cell activation but is only marginally involved in CD8+ T cell activation, differentiation, and immunity to pathogens. J. Leukoc. Biol. *101*, 1–13.

Pauker, M.H., Reicher, B., Fried, S., Perl, O., and Barda-Saad, M. (2011). Functional cooperation between the proteins Nck and ADAP is fundamental for actin reorganization. Mol. Cell. Biol. *31*, 2653–2666.

Peterson, E.J., Woods, M.L., Dmowski, S.A., Derimanov, G., Jordan, M.S., Wu, J.N., Myung, P.S., Liu, Q.-H., Pribila, J.T., Freedman, B.D., et al. (2001). Coupling of the TCR to integrin activation by Slap-130/Fyb. Science (80-.). *293*, 2263–2265.

Pollard, T.D., and Borisy, G.G. (2003). Cellular motility driven by assembly and disassembly of actin filaments. Cell *112*, 453–465.

Potsch, C., Vöhringer, D., and Pircher, H. (1999). Distinct migration patterns of naive and effector CD8 T cells in the spleen: Correlation with CCR7 receptor expression and chemokine reactivity. Eur. J. Immunol. *29*, 3562–3570.

Raab, M., Kang, H., da Silva, A., Zhu, X., and Rudd, C.E. (1999). FYN-T-FYB-SLP-76 interactions define a T-cell receptor / CD3-mediated tyrosine phosphorylation pathway that up-regulates Interleukin 2 transcription in T-cells *. J. Biol. Chem. *274*, 21170–21179.

Raab, M., Wang, H., Lu, Y., Smith, X., Wu, Z., Strebhardt, K., Ladbury, J.E., and Rudd, C.E. (2010). T cell receptor “inside-out” pathway via signaling module SKAP1-RapL regulates T cell motility and interactions in lymph nodes. Immunity *32*, 541–556.

Reichardt, P., Patzak, I., Jones, K., Etemire, E., Gunzer, M., and Hogg, N. (2013). A role for LFA-1 in delaying T-lymphocyte egress from lymph nodes. EMBO J. *32*, 829–843.

Reinhard, M., Halbrügge, M., Scheer, U., Wiegand, C., Jockusch, B.M., and Walter, U. (1992). The 46/50 kDa phosphopotein VASP purified fromhuman platelets is a novel protein associated with actin filaments and focal contacts. EMBO J. *1*, 2063–2070.

Reinhard, M., Giehl, K., Abel, K., Haffner, C., Jarchau, T., Hoppe, V., Jockusch, B.M., and Walter, U. (1995). The proline-rich focal adhesion and microfilament protein VASP is a ligand for profilins. EMBO J. *14*, 1583–1589.

Reinhard, M., Jarchau, T., and Walter, U. (2001). Actin-based motility: Stop and go with Ena/VASP proteins. Trends Biochem. Sci. *26*, 243–249.

Riedl, J., Crevenna, A.H., Kessenbrock, K., Yu, J.H., Neukirchen, D., Bradke, F., Jenne, D., Holak, T.A., Werb, Z., Sixt, M., et al. (2008). Lifeact : a versatile marker to visualize F-actin. Nat. Methods *5*, 605–607.

Riquelme, D.N., Meyer, A.S., Barzik, M., Keating, A., and Gertler, F.B. (2015). Selectivity in subunit composition of Ena/VASP tetramers. Biosci. Rep. *35*, e00246–e00246.

Rottner, K., and Stradal, T.E.B. (2011). Actin dynamics and turnover in cell motility. Curr. Opin. Cell Biol. *23*, 569–578.

Rottner, K., Krause, M., Gimona, M., Small, J.V., and Wehland, J. (2001). Zyxin is not colocalized with Vasodilator-stimulated Phosphoprotein (VASP) at lamellipodial tips and exhibits different dynamics to Vinculin, Paxillin, and VASP in focal adhesions. Mol. Biol. Cell *12*, 3103–3113.

Samstag, Y., Eibert, S.M., Klemke, M., and Wabnitz, G.H. (2003). Actin cytoskeletal dynamics in T lymphocyte activation and migration. J. Leukoc. Biol. *73*, 30–48.

San Lek, H., Morrison, V.L., Conneely, M., Campbell, P.A., McGloin, D., Kliche, S., Watts, C., Prescott, A., and Fagerholm, S.C. (2013). The spontaneously adhesive leukocyte function-associated antigen-1 (LFA-1) integrin in

effector T cells mediates rapid actin- and calmodulin-dependent adhesion strengthening to ligand under shear flow. J. Biol. Chem. *288*, 14698–14708.

Sanger, F., Nicklen, S., and Coulson, A.R. (1977). Adherence with adjuvant hormonal therapy for breast cancer. Proc. Natl. Acad. Sci. *74*, 5463–5467.

Schlegel, N., and Waschke, J. (2009). VASP is involved in cAMP-mediated Rac 1 activation in microvascular endothelial cells. Am. J. Physiol. Physiol. *296*, C453-62.

Schmidt, S., Moser, M., and Sperandio, M. (2012). The molecular basis of leukocyte recruitment and its deficiencies. Mol. Immunol. *55*, 49–58.

Sebzda, E., Bracke, M., Tugal, T., Hogg, N., and Cantrell, D.A. (2002). Rap1A positively regulates T cells via integrin activation rather than inhibiting lymphocyte signaling. Nat. Immunol. *3*, 251–258.

Senetar, M.A., Foster, S.J., and McCann, R.O. (2004). Intrasteric inhibition mediates the interaction of the I / LWEQ module proteins Talin1, Talin2, Hip1, and Hip12 with actin. Biochemistry *43*, 15418–15428.

Shimonaka, M., Katagiri, K., Nakayama, T., Fujita, N., Tsuruo, T., Yoshie, O., and Kinashi, T. (2003). Rap1 translates chemokine signals to integrin activation, cell polarization, and motility across vascular endothelium under flow. J. Cell Biol. *161*, 417–427.

Siegel, D.H., Ashton, G.H.S., Penagos, H.G., Lee, J. V., Feiler, H.S., Wilhelmsen, K.C., South, A.P., Smith, F.J.D., Prescott, A.R., Wessagowit, V., et al. (2003). Loss of Kindlin-1 , a Human Homolog of the Caenorhabditis elegans Actin – Extracellular-Matrix Linker Protein UNC-112 , Causes Kindler Syndrome. Am. Soc. Hum. Genet. *73*, 174–187.

da Silva, A.J., Rosenfield, J.M., Mueller, I., Bouton, A., Hirai, H., and Rudd, C.E. (1997). Biochemical Analysis of pl20/130. J. Immunol. *158*, 2007–2016.

Simonson, W.T.N., Franco, S.J., and Huttenlocher, A. (2006). Talin1 regulates TCR-mediated LFA-1 function. J. Immunol. *177*, 7707–7714.

Sims, T.N., and Dustin, M.L. (2002). The immunological synapse: integrins take the stage. Immunol. Rev. *186*, 100–117.

Smith, S.J., and McCann, R.O. (2007). A C-terminal dimerization motif is required for focal adhesion targeting of Talin1 and the interaction of the Talin1 I / LWEQ module with F-actin. Biochemistry *46*, 10886–10898.

Smith, A., Carrasco, Y.R., Stanley, P., Kieffer, N., Batista, F.D., and Hogg, N. (2005). A talin-dependent LFA-1 focal zone is formed by rapidly migrating T lymphocytes. J. Cell Biol. *170*, 141–151.

Soriano, S.F., Hons, M., Schumann, K., Kumar, V., Dennier, T.J., Lyck, R., Sixt, M., and Stein, J. V. (2011). In vivo analysis of uropod function during physiological T cell trafficking. J. Immunol. *187*, 2356–2364.

Srivastava, R., Burbach, B.J., and Shimizu, Y. (2010). NF-κB activation in T cells requires discrete control of IκB kinase α/β (IKKα/β) phosphorylation and IKKγ ubiquitination by the ADAP adapter protein. J. Biol. Chem. *285*, 11100–11105.

Starr, T.K., Jameson, S.C., and Hogquist, K.A. (2003). Positive and negative selection of T cells. Annu. Rev. Immunol. *21*, 139–176.

Steiner, O., Coisne, C., Cecchelli, R., Boscacci, R., Deutsch, U., Engelhardt, B., and Lyck, R. (2010). Differential roles for endothelial ICAM-1, ICAM-2, and VCAM-1 in shear-resistant T cell arrest, polarization, and directed crawling on blood-brain barrier endothelium. J. Immunol. *185*, 4846–4855.

Steiner, O., Coisne, C., Engelhardt, B., and Lyck, R. (2011). Comparison of immortalized bEnd5 and primary mouse brain microvascular endothelial cells as in vitro blood-brain barrier models for the study of T cell extravasation. J. Cereb. Blood Flow Metab. *31*, 315–327.

Stewart, M.P., McDowall, A., and Hogg, N. (1998). LFA-1–mediated adhesion is regulated by cytoskeletal restraint and by a Ca 2+-dependent protease, Calpain. J. Cell Biol. *140*, 699–707.

Stradal, T.E.B., Pusch, R., and Kliche, S. (2006). Molecular regulation of cytoskeletal rearrangements during T cell signalling. Results Probl. Cell Differ. *43*, 219–244.

Su, W., Wynne, J., Pinheiro, E.M., Strazza, M., Mor, A., Montenont, E., Berger, J., Paul, D.S., Bergmeier, W., Gertler, F.B., et al. (2015). Rap1 and its effector riam are required for lymphocyte trafficking. Blood *126*, 2695–2703.

Svensson, L., Howarth, K., McDowall, A., Patzak, I., Evans, R., Ussar, S., Moser, M., Metin, A., Fried, M., Tomlinson, I., et al. (2009). Leukocyte adhesion deficiency-III is caused by mutations in KINDLIN3 affecting integrin activation. Nat. Med. *15*, 306–312.

Sylvester, M., Kliche, S., Lange, S., Geithner, S., Klemm, C., Schlosser, A., Großmann, A., Stelzl, U., Schraven, B., Krause, E., et al. (2010). Adhesion and Degranulation Promoting Adapter Protein (ADAP) is a central hub for phosphotyrosine-mediated interactions in T cells. PLoS One *5*, 1–11.

Tan, S.-M. (2012). The leucocyte β2 (CD18) integrins: the structure, functional regulation and signalling properties. Biosci. Rep. *32*, 241–269.

Togni, M., Lindquist, J., Gerber, A., Kölsch, U., Hamm-Baarke, A., Kliche, S., and Schraven, B. (2004). The role of adaptor proteins in lymphocyte activation. Mol. Immunol. *41*, 615–630.

Togni, M., Swanson, K.D., Reimann, S., Kliche, S., Pearce, A.C., Simeoni, L., Reinhold, D., Wienands, J., Neel, B.G., Schraven, B., et al. (2005). Regulation of in vitro and in vivo immune functions by the cytosolic adaptor protein SKAP-HOM. Mol. Cell. Biol. *25*, 8052–8063.

Ussar, S., Wang, H.-V., Linder, S., Fässler, R., and Moser, M. (2006). The Kindlins : Subcellular localization and expression during murine development. Exp. Cell Res. *2*, 3142–3151.

Veale, M., Raab, M., Li, Z., da Silva, A.J., Kraeft, S.-K., Weremowicz, S., Morton, C.C., and Rudd, C.E. (1999). Novel isoform of lymphoid adaptor FYN-T-binding protein (FYB-130) interacts with SLP-76 and up-regulates interleukin 2 production. J. Biol. Chem. *274*, 28427–28435.

Walders-Harbeck, B., Khaitlina, S.Y., Hinssen, H., Jockusch, B.M., and Illenberger, S. (2002). The vasodilator-stimulated phosphoprotein promotes actin polymerisation through direct binding to monomeric actin. FEBS Lett. *529*, 275–280.

Wang, H., Moon, E.-Y., Azouz, A., Wu, X., Smith, A., Schneider, H., Hogg, N., and Rudd, C.E. (2003). SKAP-55 regulates integrin adhesion and formation of T cell-APC conjugates. Nat. Immunol. *4*, 366–374.

Wang, H., McCann, F.E., Gordan, J.D., Wu, X., Raab, M., Malik, T.H., Davis, D.M., and Rudd, C.E. (2004). ADAP-SLP-76 binding differentially regulates supramolecular activation cluster (SMAC) formation relative to T cell-APC conjugation. J. Exp. Med. *200*, 1063–1074.

Wang, H., Liu, H., Lu, Y., Lovatt, M., Wei, B., and Rudd, C.E. (2007). Functional defects of SKAP-55-deficient T cells identify a regulatory role for the adaptor in LFA-1 adhesion. Mol. Cell. Biol. *27*, 6863–6875.

Wang, H., Wei, B., Bismuth, G., and Rudd, C.E. (2009). SLP-76-ADAP adaptor module regulates LFA-1 mediated costimulation and T cell motility. Proc. Natl. Acad. Sci. U. S. A. *106*, 12436–12441.

Wang, H., Lu, Y., and Rudd, C.E. (2010). SKAP1 is dispensable for chemokine-induced migration of primary T-cells. Immunol. Lett. *128*, 148–153.

Ward, S.G., and Marelli-Berg, F.M. (2009). Mechanisms of chemokine and antigen-dependent T-lymphocyte navigation. Biochem. J. *418*, 13–27.

Watanabe, T., Dohgu, S., Takata, F., Nishioku, T., Nakashima, A., Futagami, K., Yamauchi, A., and Kataoka, Y. (2013). Paracellular barrier and tight junction protein expression in the immortalized brain endothelial cell lines bEND.3, bEND.5 and mouse brain endothelial cell 4. Biol. Pharm. Bull. *36*, 492–495.

Wernimont, S.A., Wiemer, A.J., Bennin, D.A., Monkley, S.J., Ludwig, T., Critchley, D.R., and Huttenlocher, A. (2011). Contact-dependent T cell activation and T cell stopping require talin1. J. Immunol. *187*, 6256–6267.

Winder, S.J., and Ayscough, K.R. (2005). Actin-binding proteins. J. Cell Sci. *118*, 651–654.

Witte, A., Degen, J., Baumgart, K., Waldt, N., Kuropka, B., Freund, C., Schraven, B., and Kliche, S. (2012). Emerging Roles of ADAP, SKAP55, and SKAP-HOM for integrin and NF-κB signaling in T cells. J. Clin. Cell. Immunol. *01*, 1–8.

Worbs, T., Bernhardt, G., and Förster, R. (2008). Factors governing the intranodal migration behavior of T lymphocytes. Immunol. Rev. *221*, 44–63.

Wu, J.N., Gheith, S., Bezman, N.A., Liu, Q.-H., Fostel, L. V., Swanson, A.M., Freedman, B.D., Koretzky, G.A., and Peterson, E.J. (2006). Adhesion and Degranulation-promoting adapter protein required for efficient thymocyte development and selection. J. Immunol. *176*, 6681–6689.

Yang, G.X., and Hagmann, W.K. (2003). VLA-4 antagonists: Potent inhibitors of lymphocyte migration. Med. Res. Rev. *23*, 369–392.

Yi, J., Wu, X.S., Crites, T., and Hammer, J.A. (2012). Actin retrograde flow and actomyosin II arc contraction drive receptor cluster dynamics at the immunological synapse in Jurkat T cells. Mol. Biol. Cell *23*, 834–852.

Yokosuka, T., and Saito, T. (2010). Immunological Synapse. Cell *340*, 1–7.

Yokosuka, T., Sakata-Sogawa, K., Kobayashi, W., Hiroshima, M., Hashimoto-Tane, A., Tokunaga, M., Dustin, M.L., and Saito, T. (2005). Newly generated T cell receptor microclusters initiate and sustain T cell activation by recruitment of Zap70 and SLP-76. Nat. Immunol. *6*, 1253–1262.

Yu, T., Wu, X., Gupta, K.B., and Kucik, D.F. (2010). Affinity, lateral mobility, and clustering contribute independently to β 2 -integrin-mediated adhesion . Am. J. Physiol. Physiol. *299*, C399–C410.

Zhang, Y., and Wang, H. (2012). Integrin signalling and function in immune cells. Immunology *135*, 268–275.

Zhou, D., Medoff, B.D., Chen, L., Li, L., Zhang, X., Praskova, M., Liu, M., Landry, A., Blumberg, R.S., Boussiotis, V.A., et al. (2008). The Nore1B/Mst1 complex restrains antigen receptor-induced proliferation of naïve T cells. Proc. Natl. Acad. Sci. U. S. A. *105*, 20321–20326.

Zhu, J., and Paul, W.E. (2010). Peripheral CD4 T cell differentiation regulated by networks of cytokines and transcription factors. Immunol. Rev. *238*, 247–262.

Zhu, J., Yamane, H., and Paul, W.E. (2010). Differentiation of effector CD4 T Cell populations*. Annu. Rev. Immunol. *28*, 445–489.

List of Abbreviations

∞	Infinite
°	Grad
°C	Grad Celsius
%	Percent
α	Alpha
β	Beta
Δ	Delta
γ	Gamma
ε	Epsilon
µF	Microfarad
µg	Microgram
µL	Microliter
µM	Micromolar
µm	Micrometer
µm^2	Square micrometer

A	
A	Adenine
A	Alanine
aa	Amino acid
Abs	Antibodies
ADAP	Adhesion and degranulation-promoting adapter protein
ALN	Axillary lymph node
AMP	Adenosine monophosphate
APCs	Antigen-presenting cells
APC	Allophycocyanin
APS	Ammonium persulfate
APZ	Antigen-präsentierende Zelle
Arp	Actin-related protein
ATP	Adenosine triphosphate

B	
*BamH*I	*Bacillus amyloliquefaciens H*
Bcl10	B-cell leukemia 10
*Bgl*II	*Bacillus globigii*
blueCMAC	7-amino-4-chloromethylcoumarin
BM	Bone marrow
bp	Base pair
BSA	Bovine serum albumin

C	
C	Carbon
C	Cytosine
Ca	Calcium
cAMP	Cyclic adenosine monophosphate
Carma	Caspase recruitment domain-containing protein
cc	Coiled coil
CCL	C-C chemokine motif ligand
CCR	C-C chemokine receptor
CD	Cluster of differentiation
CFSE	Carboxyfluorescein succinimidyl ester
cGMP	Cyclic guanidine monophosphate
Cl	Chloride
cm	Centimeter
cm^2	Square centimeter
CMTMR	5-(and-6)-(((4-chloromethyl) benzoyl)amino) tetramethylrhodamine
CMV	Cytomegalovirus
C-terminus	Carboxy-terminus
CXCL	C-X-C chemokine motif ligand
CXCR	C-X-C chemokine receptor
Cy	Cyanine

D	
D	Aspartic acid

D	*Dexter* (Lat.)
DC	Dendritic cell
dd	Double distilled
DEPC	Diethylpyrocarbonate
dko	Double knockout
DM	Dimerization domain
DMEM	Dulbecco's modified eagle's medium
DMSO	Dimethyl sulfoxide
DNA	Deoxyribonucleic acidic
dNTP	Desoxynucleotide triphosphate

E

E	Glutamic acid
E.coli	*Escherichia coli*
EDTA	Ethylenediaminetetraacetic acid
EF	Elongation factor
EGFP	Enhanced green fluorescent protein
ELISA	Enzyme-linked immunosorbent assay
Ena	Enabled
et al.	*Et alii* (Lat.)
EVH	Ena/VASP homology domain
Evl/Evl-l	Ena-VASP-like (-Intron)

F

F	Fluoride
F	Phenylalanine
F-actin	Filamentous actin
F-tag	Flag-tag
FAB	F-actin binding region
FACS	Fluorescence-activated cell sorting
Fc	Fragment crystallizable region
FCS	Fetal calf serum
FERM	Four-point-one/Ezrin/ Radixin/Moesin
Fig	Figure
FITC	Fluorescein isothiocyanate
fMLP	*N*-Formylmethionyl-leucyl-phenylalanine
for	Forward
FOV	Field of view
Fyn	Feline yes-related protein

G

g	Gravity acceleration
g	Gramm
G	Guanidine
G-actin	Globular actin
GAB	G-actin binding region
Gads	GRB2-related adaptor downstream of Shc
GDP	Guanidine diphosphate
GFP	Green fluorescent protein
GRK	Graduiertenkolleg
GST	Glutathione-S-transferase
GTP	Guanosine triphosphate

H

H	Hydrogen
h	Hour
H_2O	Water
HBSS	Hank’s balanced salt solution
HEK	Human embryonic kidney
HEPES	4-(2-hydroxyethyl)-1-piperazineethanesulfonic acid
HEVs	High endothelial venules
HindIII	*Haemophilus influenzae Rd*
HLA	Human leukocyte antigen
HRP	Horseradish peroxidase
hSH3	Helical Src homology domain 3
hTC	Human T cell

I	
I	Isoleucine
ICAM	Intercellular adhesion molecule
IF	Immunofluorescence
IFN	Interferon
Ig	Immunoglobulin
IL	Interleukin
ILN	Inguinal lymph node
IS	Immunological synapse
i.p.	Intraperitoneal
i.v.	Intravenous

J	
JAM	Junctional adhesion molecule

K	
K	Potassium
kDa	Kilo dalton

L	
L	*Laevus* (Lat.)
L	Leucine
L	Liter
LAD	Leukocyte adhesion deficiency
LAT	Linker for activated T cell
LB	Luria broth
LFA	Lymphocyte function-associated antigen
LM	Lauryl maltoside

M	
M	Molar
mA	Milliampere
mAbs	Monoclonal antibodies
MACS	Magnetic cell separation
Malt	Mucosa-associated lymphoid tissue lymphoma translocation protein
Mena	Mammalian ena
Mg	Magnesium
mg	Milligram
MHC	Major histocompatibility complex
min	Minute
mL	Milliliter
MLN	Mesenteric lymph node
*Mlu*I	*Micrococcus luteus*
mm	Millimeter
mM	Millimolar
Mn	Manganese
Mst1	Mammalian Ste20-like kinase
mTC	Mouse T cell

N	
N	Nitrogen
N	Asparagine
n	Number
Na	Sodium
Nck	Non-catalytic region of tyrosine kinase
NFκB	Nuclear factor kappa-light-chain-enhancer of activated B cells
ng	Nanogram
*Nhe*I	*Neisseria mucosa heidelbergensis*
NK cell	Natural killer cell
nm	Nanometer
*Not*I	*Nocardia otitidiscaviarum*
NP-40	Nonidet P-40
N-terminus	Amino-terminus

O	
O	Oxygen
OD	Optical Density

P	
p	Probability
p	Plasmid
P	Proline
PAGE	Polyacrylamide gel electrophoresis
PBMCs	Peripheral blood mononuclear cells
PBS	Phosphate buffered saline
PCR	Polymerase chain Reaction
PEFA	Pefabloc
PFA	Paraformaldehyde
Pfu	*Pyrococcus furiosus*
PH	Pleckstrin homology domain
PKD	Protein kinase D
PLC	Phospholipase C
PMA	Phorbol myristate acetate
pMBMECs	Primary mouse brain microvascular endothelial cells
pMHC	Peptide major histocompatibility complex
PMSF	Phenylmethylsulfonyl fluoride
PNAd	Peripheral lymph node addressin
PRR	Proline-rich region
PS	Penicillin/streptomycin
PTB	Phosphotyrosine binding domain

R	
r	Recombinant
RA	Ras-associated domain
Rac	Ras-related C3 botulinum toxin substrate
Rap1	Ras-proximate-1
RAPL	Regulator of adhesion and polarization enriched in lymphocytes
RBD	Rap1-binding domain
rev	Reverse
RIAM	Rap1 interacting adapter molecule
RNA	Ribonucleic Acid
rpm	Revolutions per minute
RPMI	Roswell park memorial institute
RT	Room temperature

S	
S	Sulfur
S	Serine
SA	Superantigen
*Sal*I	*Streptomyces albus* G
SD	Standard deviation
SDS	Sodium dodecyl sulfate
SEA	Staphylococcal enterotoxin A
sec	Second
SEM	Standard error of the mean
SH	Src homology domain
sh	Short hairpin
si	Small interference
SKAP55	Src kinase-associated adapter protein of 55 kDa
SKAP-HOM	Src kinase-associated adapter protein of 55 kDa-homologue
SLOs	Secondary lymphoid organs
SLP76	Src homology 2 domain-containing leukocyte protein of 76 kDa
SMAC	Supramolecular activation cluster, c (central), p (peripheral), d (distal)
SOC	Super optimal broth with catabolite repression
SV40	Simian virus 40

T	
T	Thymidine
T	Threonine
TB	Talin binding site
TBSM	Tyrosine based signaling motif
TCR	T cell receptor
TEMED	Tetramethylethylenediamine
TH	Helper T cell
TM	Transmembrane
TNF	Tumor necrosis factor
TP	Teilprojekt
Treg	Regulatory T cell
iTreg	Induced regulatory T cell
tTreg	Thymic regulatory T cell
TRITC	Tetramethylrhodamine B isothiocyanate
TZR	T-Zell-Rezeptor
U	
U	Unit
UV	Ultraviolet
V	
V	Volt
V	Vanadium
v/v	Volume per volume
VASP	Vasodilator-stimulated phosphoprotein
VCAM	Vascular adhesion molecule
VLA	Very late antigen
W	
W	Tryptophan
WAS	Wiskott-Aldrich syndrome
WASP	Wiskott-Aldrich syndrome protein
WAVE	WASP- verprolin-homologous protein
WB	Western blot
WIP	WASP-interacting protein
WT	Wild type
w/v	Weight per volume
X	
*Xba*I	*Xanthomonas badrii*
Z	
ZAP-70	Zeta-chain-associated protein kinase of 70 kDa

List of Figures

List of Tables

Ehrenerklärung

Ich versichere hiermit, dass ich die vorliegende Arbeit ohne unzulässige Hilfe Dritter und ohne Benutzung anderer als der angegebenen Hilfsmittel angefertigt habe; verwendete fremde und eigene Quellen sind als solche kenntlich gemacht.

Ich habe insbesondere nicht wissentlich:
• Ergebnisse erfunden oder widersprüchliche Ergebnisse verschwiegen,
• statistische Verfahren absichtlich missbraucht, um Daten in ungerechtfertigter Weise zu interpretieren,
• fremde Ergebnisse oder Veröffentlichungen plagiiert,
• fremde Forschungsergebnisse verzerrt wiedergegeben.

Mir ist bekannt, dass Verstöße gegen das Urheberrecht Unterlassungs- und Schadensersatzansprüche des Urhebers sowie eine strafrechtliche Ahndung durch die Strafverfolgungsbehörden begründen kann.

Ich erkläre mich damit einverstanden, dass die Arbeit ggf. mit Mitteln der elektronischen Datenverarbeitung auf Plagiate überprüft werden kann.

Die Arbeit wurde bisher weder im Inland noch im Ausland in gleicher oder ähnlicher Form als Dissertation eingereicht und ist als Ganzes auch noch nicht veröffentlicht.

Magdeburg, 11.05.2020

Janine Degen